Non-destructive ultrasound thickness characterization of parts additively manufactured by fused filament fabrication

Abdalrahman Abumettleq

Thesis submitted to the Faculty of Engineering
in partial fulfillment of the requirements for the degree of

Master of Applied Science

in Mechanical Engineering

University of Ottawa

Ottawa, Ontario

Abstract

Additive manufacturing is progressively gaining prominence as a manufacturing method within the industrial sector, owing to its distinctive capability to fabricate intricate and complex parts. Fused filament fabrication (FFF) is an extrusion based additive manufacturing method for fabrication of objects by depositing melted polymers layer-by-layer. Non-destructive thickness assessment assumes a pivotal role in ensuring the reliability and suitability of FFF parts, especially if they are exposed to harsher materials such as exposure to corrosive/abrasive chemicals or slurries. A-scan mode or time-amplitude scan ultrasound testing provides a one-dimensional representation of material interfaces. This method uses sound waves and converts them into spikes that correspond with material interfaces, and therefore is commonly used for parts manufactured with conventional manufacturing methods. However, ultrasound assessment of FFF additively manufactured parts can be challenging due to the layer-by-layer nature of the FFF process, which increases the likelihood of subpar interfaces. The goal of this thesis is to evaluate the use of A-scan ultrasound testing for measuring quality-related metrics of objects fabricated by FFF. The effect of different parameters on the ultrasound measurement such as infill patterns, infill densities as well as the presence of the top or bottom layers, are studied. Results show a limited ability of ultrasound to measure thickness beyond 5 mm for a 10 MHz contact ultrasound transducer. In addition, measurements of some infill patterns are sensitive to transducer orientation. However, the ultrasound results for samples fabricated with concentric infill patterns generally better match thickness measurements with calipers and are less sensitive to transducer orientation. Finally, this thesis investigates thickness monitoring of samples in real-time under the effect of simulated erosion to measure thickness reduction.

Table of Contents

List of figures

List of tables

Abbreviations and Definitions

AM: Additive manufacturing

FFF: Fused Filament Fabrication

ASTM: American Society of Testing and Materials

UT: Ultrasound test

PLA: Polylactic acid

Acknowledgments

Praise is to ALLAH who his grace is righteous. I am happy to have had a chance to glorify his name in the sincerest way through this small accomplishment and ask HIM to accept my efforts.

My deepest appreciation and gratitude to my supervisor Drs. Natalie Baddour and Mohammad Rafiee for their time, support, guidance, and encouragement. Without their numerous suggestions and immense knowledge, this thesis would never have been completed.

My deep love goes to my parents, my brothers and sisters for their constant support and encouragement. May ALLAH bless and provide them with health and wellness. My great gratitude goes for my friends especially my best friends and siblings Mohammad and Hanoon, with whom I shared the joy and difficulties during this program.

1. Introduction

1.1 Additive manufacturing

In recent years, there has been a growing emphasis on using additive manufacturing (AM) techniques, positioning them as pivotal contributors to the industrial landscape. This heightened focus is driven by the dual objectives of reducing energy consumption and minimizing material usage in the manufacturing process, thereby conserving resources [1]. As a result of the development and its impact on the industrial field, AM has become an important aspect of the fourth industrial revolution [2], [3]. By 2025 it is expected that the global annual economic impact will be from $200B to $600B [4]. At its essence, AM is a process characterized by an incremental layer-by-layer construction of objects, ultimately culminating in the production of the final product. The initial stage of manufacturing any component involves the creation of a 3D model, which is subsequently transformed into the stereolithography format (STL) for printing purposes. Within the realm of AM, there exist seven primary techniques, each with its unique characteristics and applications as shown in Figure 1.1. In the beginning of AM adoption, 3D printed parts were mainly employed for prototyping purposes, before growing adoption of 3D printed parts in automotive, aerospace, medical and other industrial applications [5]. Based on the application requirements, suitable materials and techniques need to be selected. AM components are capable of impressive mechanical strength, often coupled with a remarkable lightweight nature [1], [6]. Furthermore, 3D printing technology may facilitate the design and production of intricate parts utilizing a variety of materials, all within a reasonable timeframe, while fully optimizing material utilization [6].

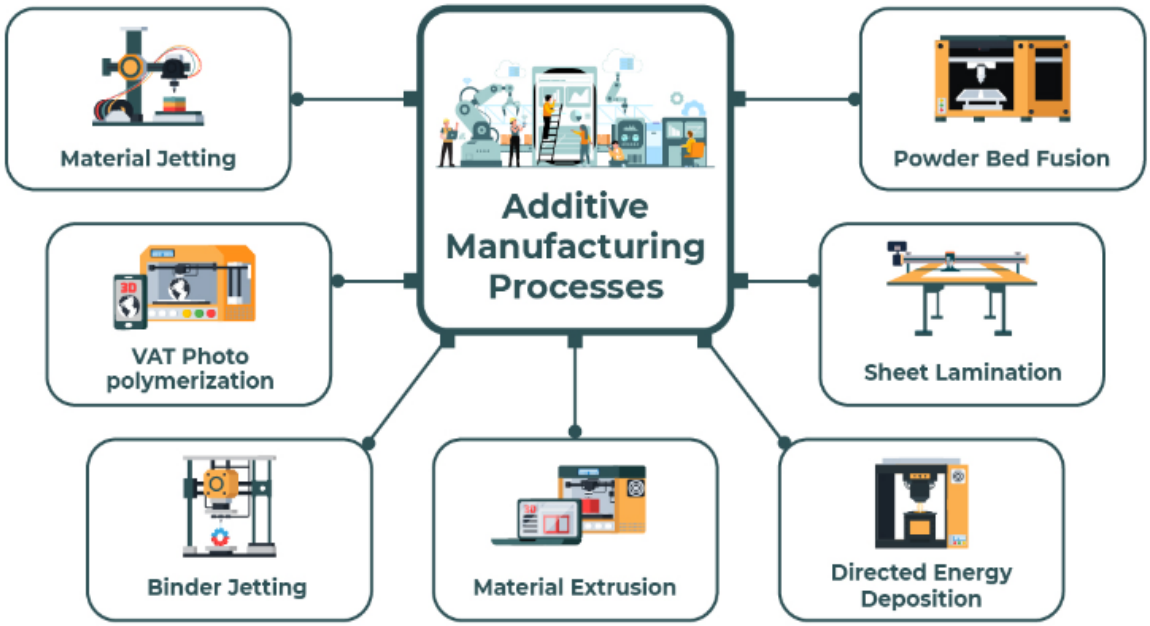

Figure 1.1 American Society for Testing and Materials classification (ASTM) of additively manufacturing techniques (seven categories) [7].

1.1.1. Fused Filament Fabrication

Fused filament fabrication (FFF) is a popular AM method, primarily due to its exceptional material suitability and cost-effectiveness compared to other approaches [8], [9]. The use of FFF moved beyond prototyping applications to usage for the manufacture of high-performance functional parts. Despite some challenges with poor mechanical strength, geometrical fits, poor finish, and printing errors, it still yielded reliable parts that could be used in many mechanical applications [8], [9]. Furthermore, it plays a pivotal role in increasing the flexibility of the supply chain in industry [10]. FFF is a process by which material is heated and extruded through a nozzle. The choice of the nozzle diameter depends on the required features of the printed parts. In addition, the heating temperature needs to be adjusted to align with the chosen material since every polymer has a distinct heating temperature where it transitions from solid to semi-solid to liquid for printing. Many types of polymers can be accommodated with the FFF technique and filaments of other polymers can also be added to improve mechanical properties. The polymer filaments usually have diameter ranges between 1.75 mm and 3 mm and are put through a melting extrusion process driven by a motor. FFF gained significant popularity in many domains, with one of the most important fields being the medical field, where it can be used to cater to custom patient needs [11], [12].

1.1.2. The effect of different parameters on parts printed by fused filament fabrication

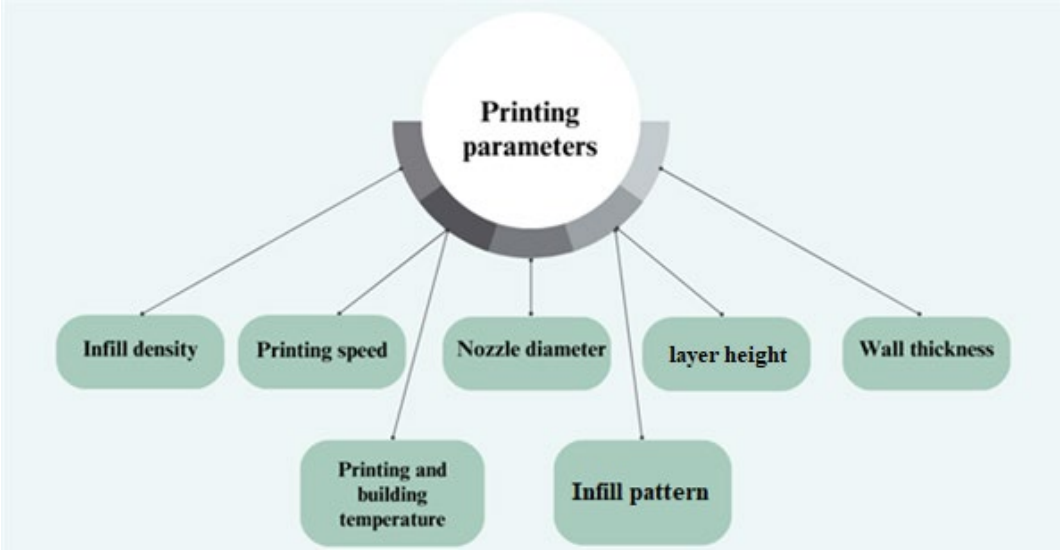

Figure 1.2 Different printing parameters of FFF impacted on the quality on the printed part.

There are several printing parameters that can be selected as part of the printing process, Figure 1.2. These parameters include infill density, printing speed, nozzle diameter, layer height, temperature, infill pattern, and wall thickness. Mechanical properties of printed samples can be adjusted by changing printing parameters. While the infill density undeniably holds a prominent position as one of the most pivotal factors [13], directly correlating with mechanical properties, other parameters could be significant contributors, as shown in Figure 1.2.

1.2 Ultrasound testing

Ultrasound testing is one of several non-destructive testing (NDT) methods employed to ensure product quality without causing damage and is a desirable approach to monitor quality of products. In essence, ultrasound tests utilize a high frequency acoustic wave to conduct an inspection of different materials such as cast materials, composite materials, and polymers. The heart of ultrasonic testing system relies on a piezoelectric element, which is the main part of the ultrasonic transducer. This element is responsible for converting electrical energy to mechanical energy and vice versa. The transducer can act as an emitting and receiving device. Similar to light waves, ultrasonic waves can be reflected, refracted, and focused. As the ultrasound wave propagates through the tested part, it will encounter surfaces leading to a partial reflection of the wave and the rest will be transmitted.

Sound is a vibration that propagates as an acoustic wave through a transmission medium such as a gas, liquid or solid. Sound can be categorised into three main types of sound. The first type is infrasound which is less than 20 Hz, the second is sound between 20 Hz and 20 kHz, the range of human hearing, and the last type is ultrasound (>20 Hz). Every sound wave possesses the following properties [14]:

- Frequency: usually measured in Hertz and represents the number of oscillations per second.
- Amplitude: measures the intensity of the wave.
- Wavelength: measures the distance between two successful peaks, measured in an appropriate unit of length.
- Speed: the distance travelled by the wave per unit time, which varies from material to material.

Ultrasound testing includes three main testing techniques [15], [16]. These are:

- A-Scan: the basic technique which is used to test at a single point. The received signal is plotted as a function of time as shown in Figure 1.3 .
- B-Scan: represents a cross sectional scan of the tested sample, formed by combining a set of A-Scans as shown in Figure 1.3.
- C-Scan: represents a top or bottom view of the tested sample, formed by combining a set of B-Scans as shown in Figure 1.3.

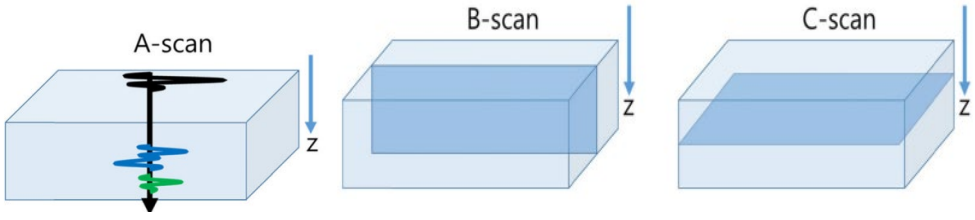

Figure 1.3 Ultrasound testing techniques [17].

Analyzing the received wave and its transit time could be useful to detect desired features such as

thickness [18]–[20]. The transducer can act as emitter and receiver at the same time - this method of measurement is called Pulse-Echo mode (See Figure 1.4(a)). Alternatively, in Transmission mode, one transducer can act as an emitter and another transducer as a receiver, Figure 1.4(b). The pulse echo mode can be further classified based on the angle of transducer with respect to the tested sample (for example, parallel or perpendicular to a certain axis). The transducer could be placed directly in contact with the surface of the sample (Figure 1.5), which is preferable for minimizing test set-up especially for field-testing, or by using an immersion tank as shown in Figure 1.6 (b) [21]. By analyzing data collected by the ultrasonic transducers, it becomes possible to determine the thickness of various materials. This is achievable as each material has its own speed of sound. In addition, interior defects could be detected [22].

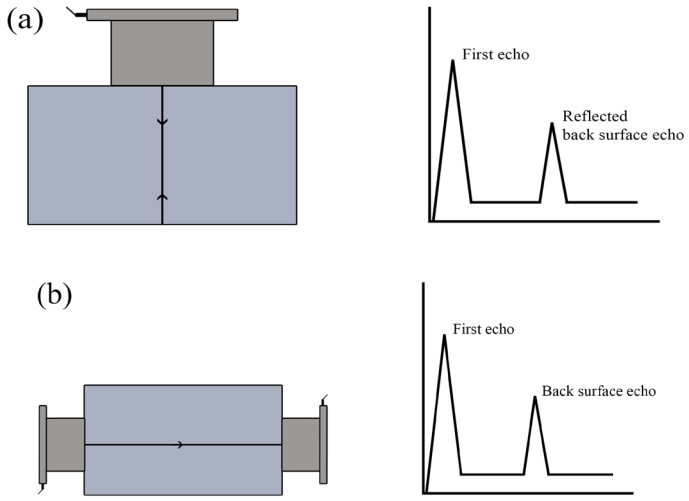

Figure 1.4 (a) Schematic of ultrasonic transducer used in pulse-echo mode; (b) Schematic of ultrasonic transducers in transmission mode.

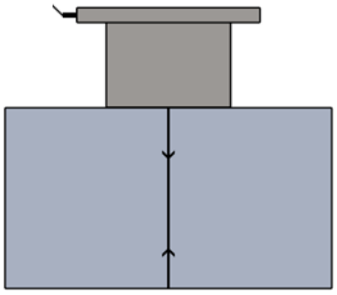

Figure 1.5 Schematic of transducer placed normal to the tested sample.

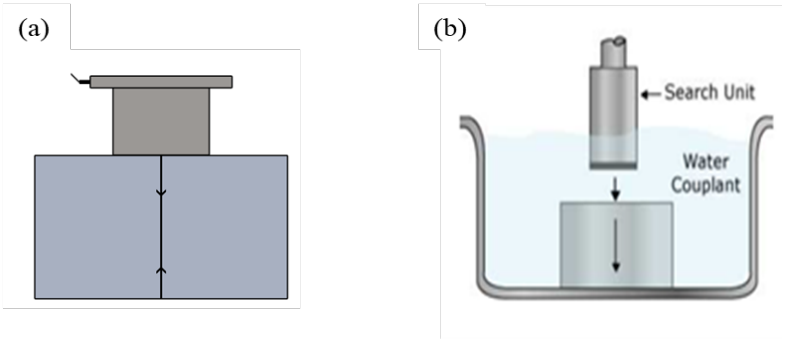

Figure 1.6 (a) Direct contact ultrasonic testing technique; (b) Water immersion ultrasonic testing technique [23].

1.2.1. Pulse echo mode

Pulse echo mode is widely used compared to other ultrasonic transducer modes [21], partly since the transducer can serve dual roles of emitting and receiving waves. The ultrasonic wave is generated by applying an electrical charge to excite the piezoelectrical material based on one of two main elements, polyvinylidene fluoride (PVDF)-film or lead zirconate titanate (PZT)-elements. The transducer performance is directly influenced by prevailing mechanical and electrical conditions during operation [21]. The piezoelectric material has low symmetrical atomic structure, which results in generation of electrical signals by applying mechanical pressure. In this project, a US key will be used, which is an ultrasonic device connected to a transducer. The primary piezoelectric material employed is based on lead zirconate titanate (PZT) supplemented by other supporting materials as shown in Figure 1.7 [24].

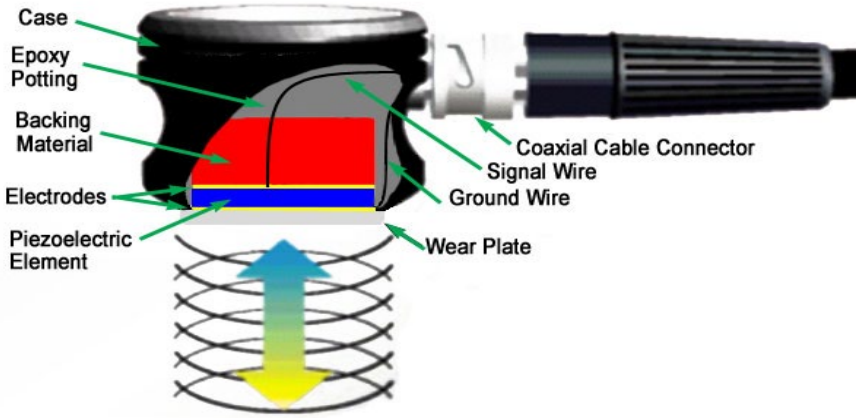

Figure 1.7 A typical configuration for different components of a transducer [24].

In all experiments in this thesis, the A-Scan technique is employed as a fundamental approach. This technique uses a pulse echo mode to extract information from the reflected wave, which can be used to measure the thickness or the depth of a defect by using equation 1.1.

$$\text{Thickness} = \text{speed of sound in the material} \times \left(\frac{\text{Time difference between peaks}}{2}\right) \qquad (1.1)$$

Thickness can be calculated from the time difference between the reflected wave from the contact surface and the back surface of the tested material. As the thickness of the sample increases, the time difference between echoes will increase, as shown in Figure 1.8 [23].

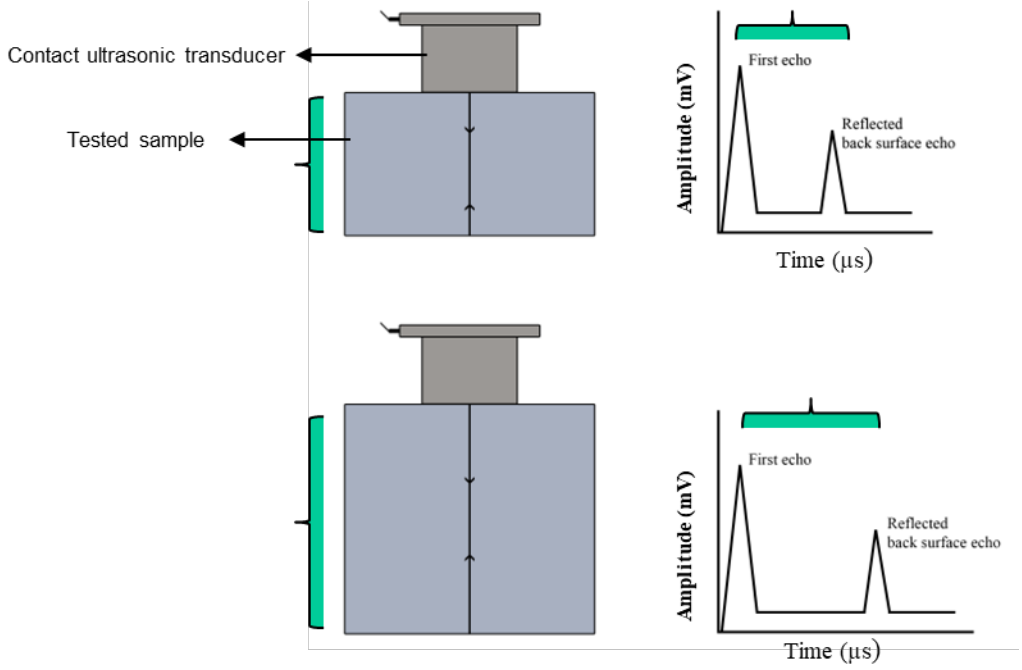

Figure 1.8 Schematic of thickness measurement using an ultrasonic transducer in pulse echo mode.

Every material has its own properties, implying a direct influence on the speed of the ultrasound wave. In general, as molecules become more tightly interconnected, the speed of ultrasonic waves (the speed of sound in the material) increases. Table 1.1 shows the speed of sound in different materials [14].

Table 1.1 Speed of sound in different materials [14].

Material	speed of sound (m/sec)
Dry air	331
Water	1540
Aluminum	6320
Gold	3240
Polylactic acid (PLA)	2100-2246

As shown in Table 1.1, air has the smallest speed of sound as the molecules are separated from each other, but aluminum has a much higher speed of sound as molecules are closer to each other.

1.3 Erosion

Erosion can be defined as a gradual loss of material due to direct friction between two or more objects over time. Erosion can take many forms [25]–[27]:

- Water erosion: gradual material loss over time due to the movement of water over an object. This could be continuous movement such as a river or not continuous movement such as droplets of rain.
- Wind erosion: gradual material loss over time due to the interaction between the object and particles in the wind such as sand.
- Coastal erosion: formation of shores due to waves and tides.

Industrial environments often involve extensive interactions between liquids and various objects, including pipes and equipment which can be subject to erosion and/or corrosion. Monitoring the condition and performance of these assets is of paramount importance for several reasons [28]–[30], including maintenance, efficiency, safety and controlling costs. Maintenance of equipment is critical; equipment such as pumps, pipes, and turbines serve in critical areas such as oil and gas fields, as well as in power generation. Assessing and monitoring this equipment is important to give a timeline for preventive maintenance and replacement to avoid breakdowns. Monitoring equipment to ensure process efficiency is also important. Certain flow optimization systems achieve improved efficiency when operating within specific dimensional parameters. Monitoring

the condition of equipment and ensuring that it operates within these optimal dimensions is essential to maintaining process efficiency. Equipment monitoring is also important for safety. Over time, wear and tear can lead to a reduction in material thickness of components, increasing the risk of leaks and other potential safety hazards. Monitoring equipment conditions helps identify and mitigate these risks, ensuring a safe working environment. Monitoring is also important for controlling costs. The loss of a substantial amount of material due to erosion or wear can significantly impact operational costs of systems. By monitoring equipment conditions, it is possible to optimize maintenance schedules and reduce material losses, contributing to cost efficiency.

There are several techniques that can be used to monitor erosion of equipment over time [28]–[30]. These techniques include visual inspection, which is the monitoring and observation of pits on the surface of the material. Vibration inspection can also be used to compare vibrations under normal conditions of operation and under damaged conditions. Erosion modeling can be used. In this approach, the equipment is designed by using a computational model and applying simulated operation conditions to simulate and predict erosion. Non-destructive approaches, of which ultrasound testing is one possible approach, can also be used.

In this thesis, we are specifically interested in the ability of ultrasound to monitor (simulated) erosion for FFF printed parts.

1.4 Thesis Objectives

The goal of this thesis is to assess the use of ultrasound testing for quality metric measurements of AM printed parts, specifically the use of the A-Scan technique for FFF printed parts. This evaluation of the abilities of ultrasound testing is applied to 3D printed products printed with Polylactic acid (PLA) material using the FFF method with different printing parameters and testing positions. Specifically, the goals are to:

- Evaluate the effect of the thickness of the 3D printed products on the ultrasound measurement.
- Investigate the effect on the ultrasound measurement of using multiple printing patterns in the same sample by using line patterns in the top/bottom layers with other infill patterns.

- Evaluate the effect on the ultrasound measurement of the orientation of the transducer with respect to the printing axis.
- Assess the effect of the infill printing pattern and density on the ultrasound measurements.
- Investigate real time measurement of erosion of materials under the effect of a simulated erosion test.
- Asses the use of ultrasound thickness measurement for industrial applications.

1.5 Outline of the thesis

A brief outline of the thesis is as follows. Chapter one introduces the context of additive manufacturing and FFF, as well as the specific interest of using ultrasound techniques. In chapter two, a literature review is presented to give an overview of FFF and ultrasound measurements in the industrial field and erosion monitoring. In chapter three, the methodology to accomplish the goals of the work is presented. Results are presented and discussed in chapter four for flat samples printed using different printing parameters. Chapter five presented the results of using ultrasound to monitor simulated erosion of a flat printed sample. Chapter six discusses using ultrasound to monitor the thickness of some industrial applications. Finally, chapter seven summarizes and concludes the work in the thesis.

2. Literature review

Within this chapter, a brief introduction and review of literature is given for the proposed nondestructive ultrasound characterization of additively manufactured parts by fused filament fabrication.

2.1. Additive manufacturing

Additive manufacturing (AM) has ignited a transformative phase within the industrial landscape, expanding its role beyond prototyping. This technology has empowered the creation of intricate components of significant quality, utilizing a diverse array of materials, including polymers, metals, ceramics, and composite materials, through various techniques. The initial step of printing any part is designing the 3D models of the product, followed by saving the model to stereolithography format (STL). Subsequently, this model is printed in one of any of various techniques [31], [32]. AM plays a critical role within the context of the fourth industrial revolution to minimize production time and decentralize production processes. Accuracy of AM has become one of its most important features and there are active efforts aiming to enhance AM, emphasizing the layer-by-layer construction approach since all production techniques are computer controlled [33]–[35].

Mehrpouya et al [36] conclude that one of the foremost advantages afforded by AM is the ability to fabricate a highly customized product while reducing the amount of waste material compared with conventional methods by up to 40%. Additionally, in some cases [36] from 95% to 98% of the left-over material can be recycled. In recent years, there has been a notable surge in government and federal organizations interest in AM. As well, this heightened attention coincides with a substantial increase in investments directed towards material, equipment, and services of AM, globally reaching around $21B in 2020 [36], with expectations to reach up to $550B by 2025 [37]. Consequently, organizations worldwide are directing their efforts towards integration of modern manufacturing technologies and information systems to optimize material use and energy [38]. Scott et al [39] reports that the presence of AM has become pivotal in many global events. Consequently, there has been a notable surge in efforts aimed at enhancing the standards governing AM practices. In 2009, through the American Society of Testing and Materials (ASTM) and International F42 committee, four standards were produced in partnership with the International Standard Organization (ISO) regarding materials and processes, terminology, design and data

formats, and test methods. Using suitable AM methods and materials potentially provides advantages to products over others manufactured with conventional methods [40], [41]. This is especially evident in medical applications, where customization to individual patients becomes feasible. Furthermore, in the aerospace and automotive sectors, AM contributes to enhanced fuel efficiency, superior product quality, and lends itself well to conducting comprehensive Strengths, Weaknesses, Opportunities, and Threats (SWOT) analyses [40], [41].

2.2. Fused Filament Fabrication (FFF)

Material extrusion is one of the seven different groups of AM technologies according to ASTM [39]. Fused filament Fabrication (FFF) is a material extrusion technique [41] that has gained popularity and application in various industries. Printing any part by FFF follows the same process as other techniques, namely designing the 3D model of the desired part and producing it in a readable format such as stereolithography (STL). Subsequently, the entire part is sliced into multiple layers, each of which is assigned its specific G code, a programming language used to control 3D printers. During printing, the material is extruded through a nozzle to build the object layer by layer, finally achieving the final product [42]–[46] . Dey et al [42] showed that utilization of FFF provides the ability to build prototypes and complex shapes. FFF has made substantial contributions to the advancement of the manufacturing sector, notably in the medical field. This includes the rapid production of critical medical equipment during the COVID-19 pandemic and the creation of custom medical equipment, as evidenced in reference [47]. Moreover, FFF has contributed to the automotive and aerospace industries via the use of high-quality materials and low weight to reduce fuel consumption, resulting in substantial fuel savings. Aircraft applications alone have yielded annual savings of up to 2.5 million dollars [47]. However, there are challenges to the improvement of FFF, including poor finish in some products and limited mechanical strength [42], [48]. The integrity of interlayer bonding plays a pivotal role in determining the mechanical properties of additively manufactured parts. Moreover, the type of filament material significantly influences the mechanical properties of the final product. There are three main parameters that affect surface roughness, accuracy, and mechanical properties. These are slicing parameters, orientation parameters and temperature conditions [42]. To overcome limited mechanical proprieties, researchers have focused on improving the quality of the filament, including introducing reinforced filaments. Extensive research efforts are being dedicated to minimizing the

printing time and increasing the printing scale [46]. At the same time, improvements in accuracy are being made; Gai et al [45] concluded that the dimensional accuracy of FFF parts could reach up to 100 μm.

2.3. Importance of quality control

It is known that additively manufactured parts have become important contributors in different industrial fields. The pivotal factor driving this adoption is the improved quality of the printed components, which stands as the primary determinant for the transition from conventional to modern manufacturing methods [49]–[51]. Concerns regarding AM products are represented in their mechanical proprieties, surface finish and measurement accuracy. To help address this, a bimodal powder which helps combine different size particles is used to give a finer surface finish and minimize post processing techniques. Also using updated technology such as high-resolution printers has helped to improve the accuracy of 3D printed products. However, achieving a balance between light weight and superior mechanical proprieties in automotive and aerospace applications is still the focus before moving towards replacing conventionally manufactured parts with 3D printed parts. Many factors affect the mechanical quality of the product, such as filament types, extrusion nozzle, set-up of printers, infill density and print orientation. The parameter with the largest effect is thought to be the infill density [49], [52].

Hisham et al [53] showed that quality control monitoring of 3D printed parts is crucial during the printing process, from the initial printed layer up to the last one. To address this, they introduced a geometrical defect camera to monitor the dimensions of the 3D printed part to provide early defect detection. In addition, to overcome warping caused by temperature changes, a layer defect monitoring system was employed to detect faults during printing. Other research has shown that techniques could be developed to monitor surface defects using artificial intelligence [54] [55].

2.4.2. Non-Destructive Testing

Non-destructive Testing (NDT) is defined as examining materials or samples without damaging the material. There are various NDT techniques, some of the most prominent ones include ultrasonic testing, eddy current testing, magnetic-particle testing, liquid penetrant testing, radiographic testing, and visual testing. Ensuring the quality of the product is the foundation for

making any product reliable. As additively manufactured parts become more popular and useful, quality assurance is important for products used in critical functions in industries such as the aerospace and automotive industries [55]. In contrast to mass production of products, additively manufactured parts are easily customized products and built layer by layer. NDT is an efficient way to ensure quality of products and give an indication of mechanical proprieties [18].

Butt et al [56] confirmed that NDT can be used to study the effect of nozzle temperature, printing speed and bed temperature to estimate the mechanical proprieties of a product without any deformation by using ultrasound and identification hardness testing. They compared the NDT results with destructive testing measurements. Both NDT approaches did not show any changes due to changes in printing speed but could be used to correlate with results of the destructive testing for changes in nozzle bed temperatures. NDT can help understand the interior structure, as well as detect interlayers and defects which can have adverse effects on mechanical properties. Furthermore, the interior structure of 3D printed products, even when made from the same material, is highly dependent on various printing parameters, including printing speed, bed temperature, infill pattern, infill percentage, and nozzle diameter.

The use of ultrasonic testing, regarded as one of the most prevalent non-destructive techniques, can play a pivotal role in accurately identifying the positions of cracks and interlayer failures, as outlined in [57]. Peng et al [58] showed that an ultrasonic guided wave, characterized by its high sensitivity, can be used to detect cracking in threaded steel rods used in engineering structures. In addition, ultrasound NDT is considered one of the most useful techniques for investigating composite materials using longitudinal and shear waves. Through analyzing data of the pulse-echo received wave, interior structural defects can be located with precision and can be used to produce an ultrasound scan photo [57]. Ultrasound testing has also been conducted on ice samples, including glaze and rim ice samples. The results show that rim samples have more gaps as the attenuation coefficient is higher than for glaze samples. This can be used to correlate the slope of the attenuation coefficient-frequency graph to the existence of voids [59].

Ultrasound can be used to measure different thicknesses for various materials, as well as to detect any interlayers or defects in the tested parts. The tested material can be a single material like lubricant film or steel or can be a multilateral like a composite material or reinforced concrete for safety purposes [57], [60]–[62].

Ultrasound transducers with different frequencies can be used with a US key to measure sample thickness of different materials such as aluminum, plastic, rubber, and wood. This key is a device that acts as transmitter and receiver. It is connected to a laptop to analyze the results using software such as LabView or MATLAB [14].

Additively manufactured parts by fused deposition modeling are investigated by nondestructive ultrasonic testing techniques to evaluate the effective density within the part [63]. It was found that the ultrasound could probe into the additively manufactured object and was effective at density characterization when applied axially.

In another application, samples were prepared from Graphite-enhanced Polylactic acid (PLA) and tested by destructive and NDT techniques. The correlation between techniques concluded that high strength samples showed lower gaps and higher adhesion interfaces [56].

2.5. Erosion

Erosion is defined as the gradual loss of material due to the interaction between external particles and the object over time [64], [65]. This loss of material could have a negative effect on the shape of components, and can affect other performance metrics, for example the efficiency of a turbine blade [64], [65]. For this reason, Oka et al [62] recommended that materials such as ceramics and composites be used in applications like pumps to reduce erosion and wear, thereby extending the lifespan and efficiency of components. There are several environment factors that could lead to erosion of structural material over time such as wind, water flow, rain droplets, snow, and/or other chemical components [65]. The erosion of material depends on several factors, one of the most important being the elasticity of the material, which in turn affects the impact of absorption of falling water on the material. Furthermore, the contact angle between the material and the water is also important. As the angle of incidence approaches normal or near normal, the rate of erosion tends to minimize. When the impinging water molecules strike the surface at a shallow angle, they tend to have a more glancing effect and can move material sideways, potentially increasing erosion. However, when they strike the surface at a near-normal angle, the energy is directed more vertically, leading to less lateral movement of material, which tends to reduce erosion rates. Moreover, water pressure and water speed have a significant effect on material removal; the rate of material loss can be accelerated if the water is mixed with another material such as sand [66].

2.5.1. Erosion forms

Eroded surfaces are easily discernible due to the visible damage they exhibit, and such damage can arise from various underlying causes [65]:

- Solid particles: particles can be mixed with different types of gases such as in a gas turbine.
- Slurry erosion: particles mixed with liquids such as river water mixed with sand. This is also present in oil and gas pipes.
- Impingement erosion: occurs when a liquid impacts an object, resulting in potential fracture and damage. This type of erosion is often associated with the corrosion of pipes, particularly in applications involving the transportation of chemical substances.
- Droplet erosion: material loss due to frequent droplets such as rain droplets on aircraft.
- Cavitation erosion: this happens due to mixing bubbles in a liquid, especially in a pumped liquid.

The selection of materials for industrial components is typically driven by the specific application, with erosion resistance being an important consideration. The aim is to minimize the adverse consequences of material loss during operations, which can include environmental impacts and cost considerations. By choosing erosion-resistant materials tailored to the application, these negative effects can be mitigated.

2.5.2. Simulation of erosion

The waterjet is one of several techniques employed to gradually remove material from objects and as such, can be used to simulate erosion. In this process, the jet delivers water, or water mixed with another material, through a fixed diameter nozzle for a specific duration. The duration can be from 2 minutes to 60 minutes. The mass difference is then recorded before and after running the waterjet. The work in [67] utilized a 1.2 mm nozzle diameter and a 65 mm standoff distance to test the erosion behavior of a Ti-Ni binary alloy. In addition, Hloch et al [68] showed that erosion can be simulated using a waterjet moving 5 mm/sec over a step stair as the standoff distance starts from 100 mm and reaches 5 mm. This test was conducted to observe the effect of distance between the sample and the fixed 1.19 mm nozzle. Different pressures in the range between 100 to 40 MPa

were used. Additionally, to simulate erosion resulting from rain droplets or other similar environmental factors, a rotating disc can be employed. This disc, equipped with specific hole diameters, rotates after the pump nozzle to deliver water droplets onto the tested sample, thus replicating erosion conditions commonly encountered in applications like turbine blades [69].

2.5.3. Detecting erosion by ultrasound

Ultrasound testing can be used to measure the thickness of objects. As a potential application, high pressure headers are used to collect crude oil and over time, the thickness of the header decreases because of high-pressure flow as well as the presence of other materials such as sand in the oil. Therefore, analyzing data received from ultrasound could help identify the thickness of industrial components which might erode over time. This approach can be used to monitor critical components to avoid reaching their minimum allowable thickness. Ultrasound testing technology can help minimize breakdown and leakage from these inspected components [70].

Based on the literature review of previous research, there is a lack of research in the domain of quality monitoring for components manufactured using fused filament fabrication (FFF). Given that FFF often involves customized products, destructive testing is impractical. NDT emerges as the preferred approach for 3D printed products compared to destructive tests. Among NDT methods, the pulse-echo mode of ultrasonic testing is widely employed for monitoring thicknesses in various materials, including steel and multilayer materials such as composites. Each echo received during ultrasonic testing provides valuable data for understanding the interior structures of printed components. Consequently, it is hypothesized that this technique can be used to assess the accuracy of product dimensions for FFF components. This could help in optimizing the 3D printing parameters and monitoring the quality of printed parts. Additionally, there is a lack of published research in monitoring the erosion rate of components fabricated using FFF technology. Addressing this gap could contribute to a better understanding of the long-term durability and performance of 3D printed parts in various applications.

3. Methodology

The goal of this thesis is to study the effects of different 3D printing parameters on ultrasound measurements, including sample thickness, presence of a top or bottom solid layer, transducer orientation with respect to the side wall, infill percentage, infill patterns, erosion, and functional parts. For this purpose, step gauges are 3D printed for parametric study and flat samples are 3D printed for the erosion test that will be discussed later in this section. Each step gauge sample is printed with specific printing parameters to study the capability of a contact ultrasound transducer to measure the thickness of the samples. In addition, an erosion test will be set up in order to simulate real-time thickness measurement for 3D printed parts exposed to an erosive environment. Flat plates are printed, and the erosion rate is measured during the test. Finally, to demonstrate the effectiveness of the contact ultrasound measurement, some functional parts with different surfaces, such as flat or curved surfaces which are used in industry, are printed and tested. To find the differences between the ultrasound measurement and the ground truth measurement, a digital caliper with a resolution of 0.01 mm is used to verify the measurements.

3.1. Sample preparation and testing

Two step gauges are designed using Solidworks software, ensuring that each possess an identical testing surface measuring 20×20 mm^2 with different thicknesses 2.5, 5,10, and 20 mm, Figure 3.1. To study the effect of the transducer orientation, two samples from each group are printed. One of the samples is printed to be tested with transducer oriented parallel to the printing axis and the other is printed to be tested with transducer oriented perpendicular to the printing axis. Figure 3.1 shows the sensor placement on the sample and the printing axis.

The samples shown in Figure 3.1(b) have sidewalls. The sidewalls are parallel to the printing axis but represent top/bottom interfaces with respect to the ultrasound measurement (since the transducer is oriented perpendicular to the printing axis, see Figure 3.1 (b)). Although these side walls will become top/bottom interfaces for the ultrasound, they will be referred to as ‘sidewalls’ in the rest of the thesis to distinguish them from the interfaces that are top/bottom interfaces for *both* printing and ultrasound. The design is sliced by Ultimaker Cura 5.2.1 to give the G-code of the samples, and the general printing parameters are given in Table 3.1.

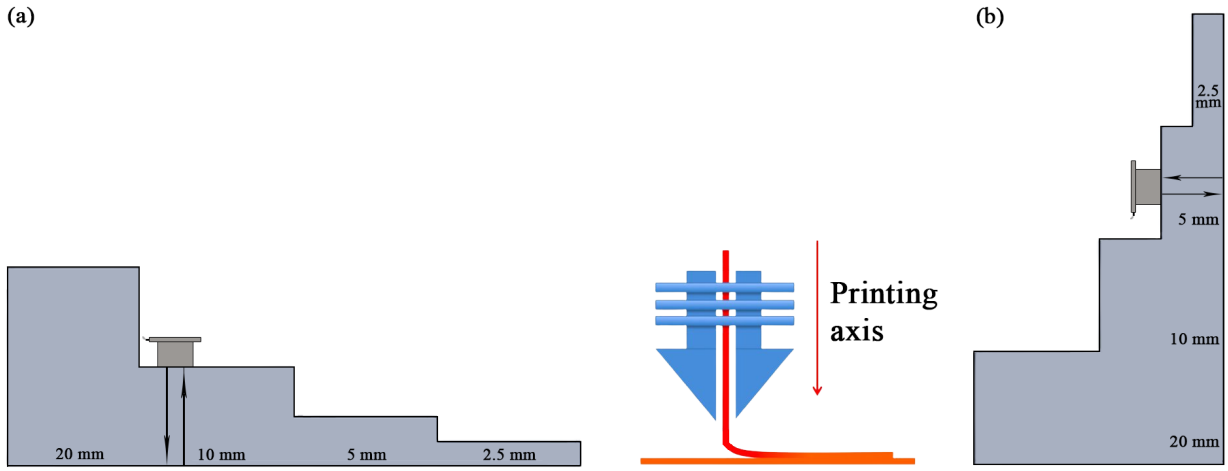

Figure 3.1 (a) Schematic of placing ultrasonic transducer parallel to the printing axis; (b) Schematic of placing ultrasonic transducer perpendicular to the printing axis.

Table 3.1 General print settings for all printed samples.

Printing parameters	Specification
Filaments (Ø 2.85 mm)	PLA
3D printer	Ultimaker 2+
Build plate	Glass
Infill printing speed	30 mm/s
Wall printing speed	26 mm/s
Infill layer thickness	0.1 mm

3.1.1. Material selection

PLA emerges as a material of importance in FFF because of its availability and low price, while also possessing reasonably good mechanical properties. PLA is used in many different industrial parts either for prototyping or as a functional material, as shown in Figure 3.2. Functional 3D printed parts can replace conventional parts to minimize weight, minimize manufacturing cost, or to permit design modification to a complex part [71]. The PLA may not always be the best choice; however it gives good mechanical properties compared with its price. The PLA used for all the printed samples in this thesis is PLA 3D850 from Voxel.

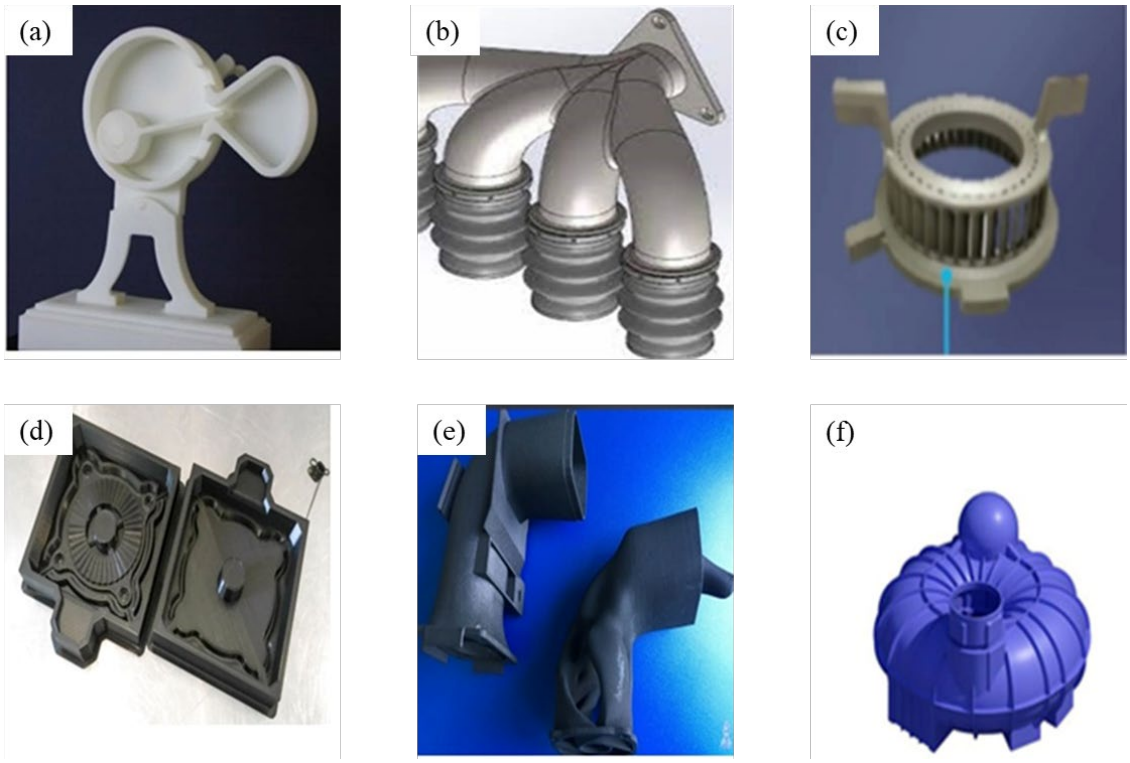

Figure 3.2 (a) Prototyping of double-chamber leaf pump; (b) Four port to one port duct assembly; (c) 3D printed combustion chamber; (d) 3D FFF printed gear mold; (e) 3D FFF printed flow optimizer; (f) 3D printed tank [71], [72].

3.1.2. Nozzle diameter

In the realm of 3D printing, the selection of nozzle diameter emerges as a pivotal factor in the manufacturing process. The two most common nozzle diameters are 0.4 mm and 0.6 mm, which offer reasonable printing times with relative high resolution. A smaller 0.25 mm nozzle diameter will take more time, although it will yield excellent resolution. Conversely, a 0.8 mm nozzle diameter may negatively affect geometric accuracy or resolution of the product [73]. Hence, in this thesis, the selected nozzle diameter for all samples is 0.4 mm, chosen to reflect the most common nozzle diameter. It is expected to give good resolution with reasonable printing time. The printer selected for all samples is the ulimaker2+ [74].

3.1.3. Infill pattern

Infill density is the most crucial factor affecting 3D printed part strength, which could be enhanced by using an appropriate infill pattern. However, part strength is also influenced by layer thickness;

layer thickness has an inverse relationship with strength of the printed part [75], [76]. Different infill patterns will be printed and assessed to compare the effect of infill pattern on the ultrasound tests. The selected infill patterns are shown in Figure 3.3. These are concentric, line, grid, triangle, and zig zag infill patterns. Every infill pattern is characterized by its own advantages, which could be mechanical properties or could be other characteristics such as surface finish [77], [78]. Different infill patterns will be printed and investigated as given in Table 3.2.

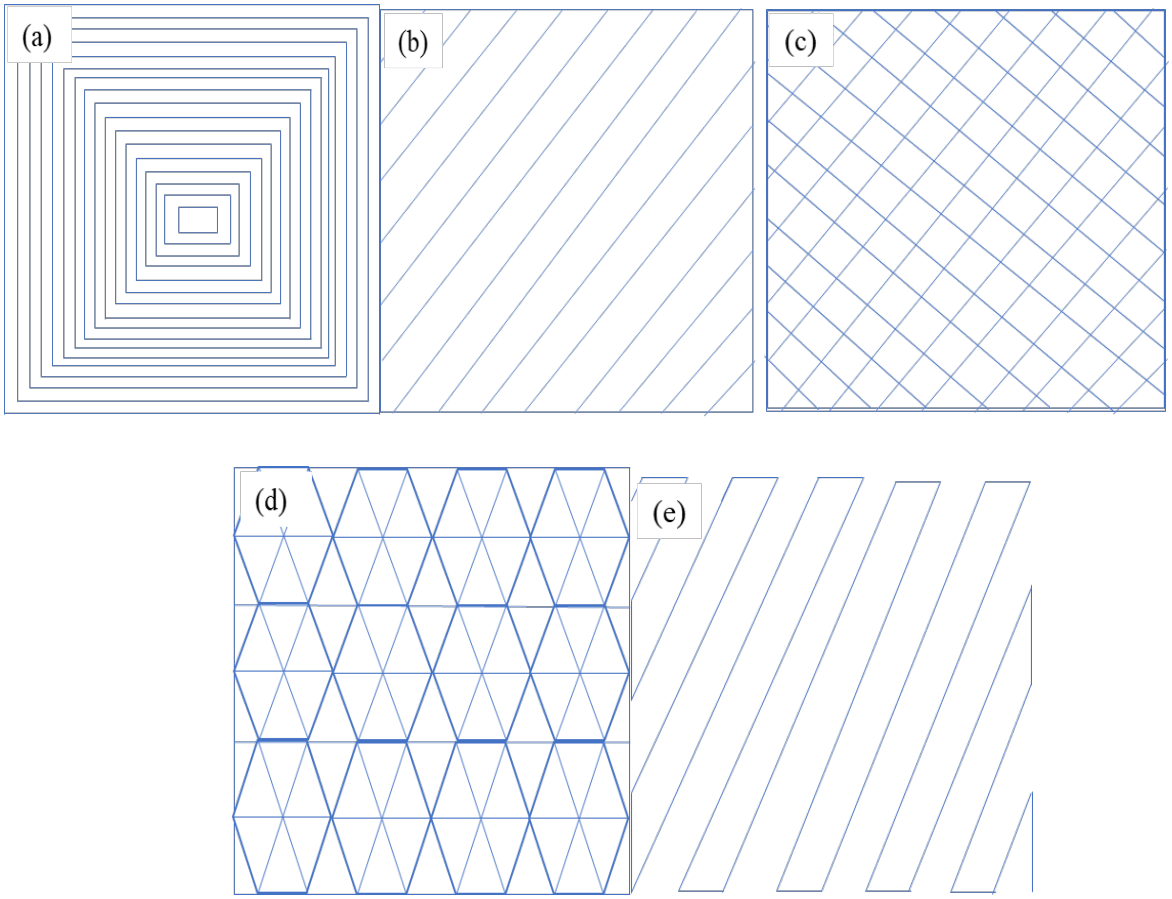

Figure 3.3 (a) Schematic of concentric infill pattern; (b) Schematic of line infill pattern; (c) Schematic of grid infill pattern; (d) Schematic of triangle infill pattern; (e) Schematic of zig zag infill pattern.

Table 3.2 General printing parameters of the printed samples.

Number of group samples	Nozzle diameter (mm)	Material	Infill pattern
12	0.4	PLA	Concentric
4	0.4	PLA	Zig zag
4	0.4	PLA	Triangle
4	0.4	PLA	Grid
2	0.4	PLA	Line

3.1.4. Notation

To give the specifics of each sample based on infill pattern and infill percentage, this thesis will use the following shorthand notation: [A:X/Y% I/X] to indicate every category. Specifically,

A: the symbol that replaces placeholder A indicates the orientation of the ultrasound transducer. Specifically, testing is performed with the transducer oriented parallel (∥) or perpendicular (⊥) to the printing axis.

X: indicates the thickness of solid top or bottom layer, measured in millimeters.

Y: indicates the infill percentage.

I: indicates the infill pattern, which can be Concentric (C), Triangle (T), Zigzag (Z), Grid (G), or Line (L).

As an example: [∥ : 1/100%C/1] means that the sample is printed with 100% concentric infill, with presence of 1 mm top/bottom layer and the transducer is placed parallel to the printing axis.

3.1.5. Transducer orientation

Testing of 3D printed parts in the industrial field could occur with the transducer oriented either parallel or perpendicular to the printing axis. For example, in Figure 3.4 the side wall would be tested by placing the transducer perpendicular to the printing axis, whereas the bottom of the base would be tested with transducer parallel to the printing axis. For this reason, studying the effect of sensor placement is important. Two group samples from each category will be printed to investigate transducer orientation parallel/perpendicular to the printing axis.

Figure 3.4 3D printed part which could be tested in parallel or in perpendicular to the printing axis [79] .

To clarify, parallel to the printing axis means that the transducer will be placed in parallel or aligned to the printing axis (with or without the presence of top/bottom layers). For the second test, perpendicular to the printing axis means the transducer will be placed perpendicular to the printing axis (with or without a side walls). Side solid walls with respect to the printing axis will act as top / bottom layers with respect to the ultrasound transducer measurement axis, as shown in Figure 3.5. The symbols will be added with the descriptive name of the samples. For notation purposes, ∥ indicates that the transducer is placed parallel to the printing axis. The symbol ⊥ indicates that the transducer is placed perpendicular to the printing axis, for example as would occur when placing a transducer on a pipe.

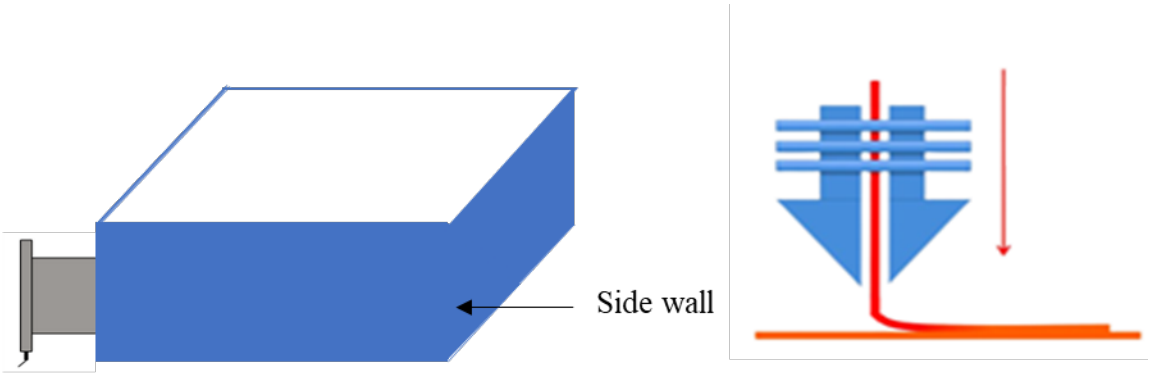

Figure 3.5 Schematic of transducer oriented perpendicular to the printing axis, with (printing) side wall acting as a (ultrasound) top and bottom layer.

3.1.6. Sample selection

In the first step, 12 group samples with five samples in each group will be printed with the concentric infill pattern since it provides the best mechanical properties amongst all the infill patterns [75]. The samples will be printed with different infill percentages and different printing parameters, as shown in Table 3.3. Two group samples (5 samples per group) for each category will be printed and tested for transducer orientation parallel and perpendicular to the printing axis. The samples will be tested and compared to evaluate the effect of infill percentage on the measurement and the effect of the presence of top and bottom layers, as well as the difference between parallel and perpendicular tests. Another 14 group samples will be printed with line, grid, triangle, and zig zag infill patterns. Two groups will be printed for each category - for parallel and one for perpendicular tests, as shown in Table 3.3.

Table 3.3 Number of printed samples with different printing parameters used for ultrasound testing.

Infill pattern (Printed sample)	Sample Specification
Concentric (2 groups, 5 samples per group)	[∥ or ⊥ : 1/100% C/1]
Concentric (2 groups, 5 samples per group)	[∥ or ⊥ : 0/100% C/0]
Concentric (4 groups, 5 samples per group)	[∥ or ⊥ : 1/95% or 90% C/1]
Concentric (4 groups, 5 samples per group)	[∥ or ⊥ : 0/95% or 90% C/0]
Line (2 groups, 5 samples per group)	[∥ or ⊥ : 0/100% L/0]
Grid (2 groups, 5 samples per group)	[∥ or ⊥ : 1/100% G/1]
Grid (2 groups, 5 samples per group)	[∥ or ⊥ : 0/100% G/0]
Triangle (2 groups, 5 samples per group)	[∥ or ⊥ :1/100% T/1]
Triangle (2 groups, 5 samples per group)	[∥ or ⊥ :0/100% T/0]
Zig zag (2 groups, 5 samples per group)	[∥ or ⊥ :1/100% Z/1]
Zig zag (2 groups, 5 samples per group)	[∥ or ⊥ :0/100% Z/0]

All samples will be evaluated using a sample holder, and the results will be compared to the concentric infill samples.

3.2. Ultrasound measurement setup

3.2.1. Pulse echo mode

In the context of 3D printed products used in industrial applications, the choice of transducer frequency depends on the thickness of the material to be investigated. A 10 MHz transducer is typically sufficient for examining materials up to 10 mm in thickness. In this thesis, a US Key manufactured by LeCoeur Electronique was selected. Although a transducer of 5 MHz could penetrate further, a 10 MHz transducer offers better resolution. The 3D printed products are built from layers and the interior structure is complex, hence resolution is important. Furthermore, thickness of 3D printed products such as pipes is not high, further justifying the 5 MHz choice. The transducer is BCRM-74-6, manufactured by Olympus. The selection of the transducer frequency needs to be based on the inspection requirements, and the desired balance between penetration depth and image clarity [16], [80]. A high frequency transducer can be used alone or combined with other visible LED lights which can help with proper positioning and alignment during the test. By utilizing these instruments, it becomes possible to gain an understanding of the interior structure of the material, which is vital for assessing overall quality and assuring dimensional accuracy [17], [80], [81]. Many types of transducers for pulse echo mode are available for NDT purposes, but using high frequency transducers enables easy analysis of received data. In addition, the use of pulse-echo techniques offers significant advantages when it comes to scanning and examining materials with varying shapes. These transducers enable NDT and evaluation without the need for extensive pre-setup procedures, such as immersion in a water tank [82], [83].

3.2.2. Coupling agent

In ultrasonic testing, there are typically two common methods for ensuring effective coupling between the transducer and the tested material. One approach is using a gel agent, while the other is immersing the test piece in a water tank. Without using a coupling agent, the ultrasound wave might not transmit from the transducer to the tested part, and hence may not reach the tested part [84]–[87].

Indeed, while water immersion can be effective for ultrasonic testing, it may not always be the most practical method, especially due to the challenges associated with tank size and sample handling

logistics. On the other hand, the direct contact approach using a coupling agent like a gel, or a similar substance offers more convenience and flexibility, making it suitable for various testing scenarios. In all the experiments for this thesis, a gel agent will be used because of ease of use and low preparation. The type of gel chosen for this work is Ultragel II (Ultrasonic Couplant Acoplante). It is important to note that the effectiveness of this method can be sensitive to the pressure applied to the transducer. Maintaining consistent and controlled pressure is crucial to ensuring reliable and accurate ultrasonic inspections [84].

3.2.3. Transducer holder

To address concerns related to excessive pressure and vibration during ultrasonic testing, Mostavi et al [88] recommend designing a transducer holder that can maintain a consistent pressure for all samples [83]. Using SolidWorks, a clamp design was prepared and transferred to Ultimaker Cura to be sliced for printing. The nozzle diameter was selected as 0.8 mm and printing speed as 50 mm/sec with 60% zig zag infill pattern. The complete experimental setup is shown in Figure 3.6. The pressure applied on the transducer is the weight from the upper part of the holder, which serves to maintain the same pressure for all samples.

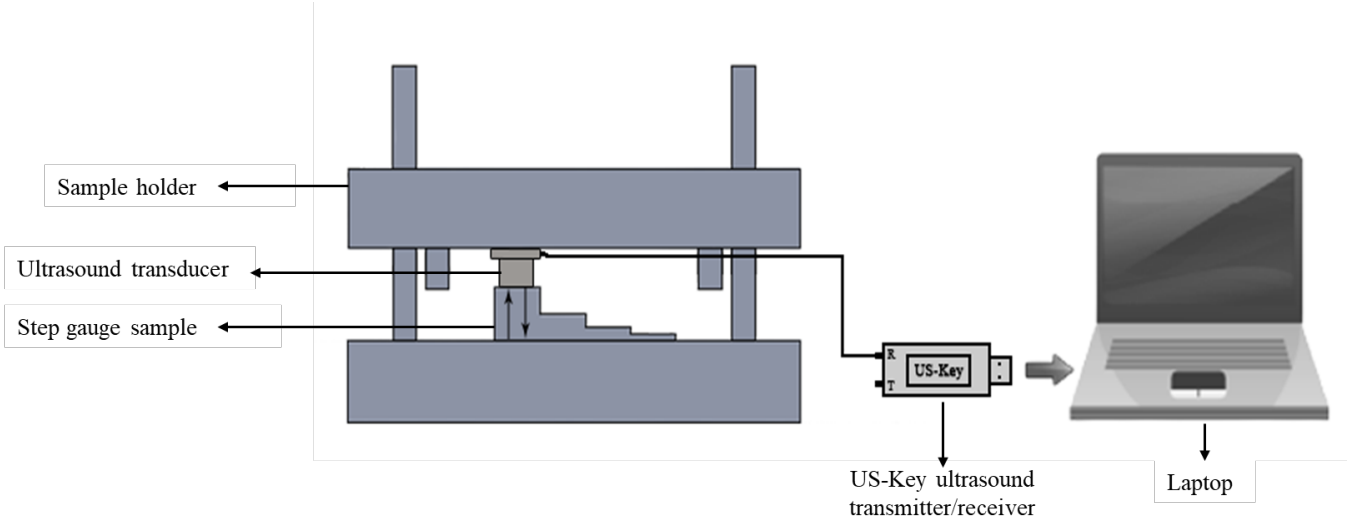

Figure 3.6 Schematic of a transducer holder used to maintain the pressure on the transducer during ultrasound testing. The holder has two parts, upper and lower parts with identical face of 30x200 mm and thickness of 20 mm.

3.3. Transducer calibration

The calibration process is implemented by measurement of an aluminum cube with specific side dimensions of 15 mm using a digital caliper. Aluminum is a well-known material with specific speed of sound, meaning highly reliable results. The digital caliper has a resolution of 0.01 mm. The measurements obtained from the caliper are considered to be ground truth and are compared to the results obtained with the ultrasound transducer. The ultrasonic measurement is obtained by multiplying half the time difference between peaks with the speed of sound in aluminum (6320 m/s). One additional aluminum cube with holes drilled 7 mm away from the surface was also used to validate the measurements returned by the transducer. The data received from the transducer was analyzed and compared with the dimensions obtained with the digital caliper.

For each test configuration, each test is repeated five times for each sample. It was found that the maximum variation among the five measurements is within ± 0.1 μs.

In the LabVIEW software, a digital filter was used to eliminate noises (high frequency or low frequency) from the window. This enables improved selection of peaks, which in turn is reflected in the repeatability of the measurements.

Based on several experiments conducted through this thesis, the speed of sound in PLA varies based on the color of the PLA. The speed of sound in each color of PLA is determined by printing twenty-four samples with different colors and comparing digital caliper measurements with ultrasound measurements. The speeds of sound determined with this approach are shown in Table 3.4 .

Table 3.4 Speed of sound in different color of PLA

PLA color	speed of sound ± 10 (m/s)
White	2100
Blue	2100
Pink	2100
Black	2150
Red	2200
Orange	2246

The speed of sound which is used in the calculations will be based on the color of the PLA used for the sample.

All sample measurements utilize a sampling frequency of 160 MHz. The uncertainty of the location of a given peak is thus ±0.003 μs, from the sampling rate. Repeating measurements on a given sample and averaging multiple measurements gives a margin of uncertainty of ± 0.10 μs, suggesting a potential uncertainty in the calculated speed of sound of 10 m/sec. The average of these five sample measurements is computed and displayed in Table 3.4. It's important to note that this uncertainty persists throughout all measurements discussed in the results section, particularly impacting higher thickness measurements. The speed of sound referenced in Table 3.4 is utilized, and errors in the results section are assessed accordingly based on the table.

3.4. Transducer selection

There are several factors that affect the choice of transducer. Acoustic impedance is a material parameter defined as product of the mean density of the material and the speed of sound within that material. That is, $z = C \times \rho$ where z is acoustic impedance, c is speed of sound in the material and ρ is the material density. When an acoustic wave travels between different mediums, it undergoes partial reflection and partial transmission, depending on the acoustic impedance mismatch between the materials. As the acoustic impedance match between the materials increases, the percentage of wave reflection will decrease, and a larger percentage of the incident wave will be transmitted. The percentage of reflected waves can be calculated according to the reflection coefficient given in equation (3.1). Table 3.5 shows acoustic impedance values of various materials.

Table 3.5 Acoustic impedance of different materials

Medium	Acoustic impedance Z (MRayls)
Air	0.0004
Water	1.48
Aluminum	17.33
Ultrasound coupling	2.42
PLA	2.68

The reflection coefficient R is given by

$$R = \frac{(z_2 - z_1)^2}{(z_2 + z_1)^2} \times 100\% \qquad (3.1)$$

where z_i is acoustic impedance of each material.

The acoustic impedance of PLA is given by $C \times \rho$ = 2150× 1250= 2.68 MRayls.

The reflection coefficient from the coupling agent to PLA boundaries is given by

$\frac{(2.42\text{-}2.68)^2}{(2.42+ 2.68)^2} \times 100\% = 0.26\%$.

The frequency of the ultrasound wave is controlled by the transducer and plays a crucial role in ultrasonic testing. A high frequency transducer offers a high resolution, but limited penetrate depth, while a low frequency transducer can penetrate deeper but offers lower resolution. However, it is important to know every material has a recommended transducer frequency. For polymers, the recommended range is typically between 5 to 10 MHz [14].

The US key serves as a tool to transmit a pulse via an ultrasound transducer and subsequently plot the received wave. This functionality can be harnessed in conjunction with various software platforms, including LabView and MATLAB, to facilitate data acquisition and analysis [14].

3.5. Sources of errors

In any experimental process, it is acknowledged that errors can arise, but rigorous efforts are made to minimize them by adhering to proper procedures and techniques. Potential sources of measurement error include:

- Over pressure: the pressure applied on the transducer has a significant effect on the amplitude of the received data and could hence affect the detection of echoes. To eliminate this source of error, the transducer is clamped to ensure consistent pressure for all samples [88].
- Vibration: testing materials under vibration will affect penetration and may lead to incorrect results [89].

3.6. Sample testing

The printed samples were investigated separately five times using pulse echo with A-scan mode via a LabView program. The samples were printed according to the specified printing parameters. These samples were used to determine the maximum thickness which can be (sufficiently) accurately measured by ultrasound. In the next step, two groups of samples were printed using the same printing pattern without any top/bottom layer to assess the effect of the presence of these layers on ultrasonic testing. The tests were done with transducer oriented in parallel and perpendicular to the printing axis. To evaluate the effect of transducer orientation with presence of a side wall, the same printing parameters were used to print another five samples to be tested perpendicular to the printing axis. Then, groups of non-solid (less than 100% infill) samples were printed to study the effect on the ultrasound, with or without solid top/bottom layer and in both axis orientations.

In the next step, the samples were printed using only the pattern which is used for the top/bottom layer (line pattern) and tested in parallel and perpendicular to the printing axis. Some solid samples were printed with infill patterns, with and without top/bottom layers, and tested in parallel and perpendicular to the printing axis. Then, to evaluate the ability of ultrasound to monitor erosion rates, samples were printed and fixed over the transducer. The erosion rate (rate of material loss) was monitored during the test. Finally, some functional parts were printed and tested to demonstrate the efficacy of ultrasound testing in industrial applications.

3.7. Erosion

For the erosion tests, rectangular samples of 50× 120 mm with thicknesses of 6 mm and 5 mm were designed and printed according to the specifications shown in Table 3.6. The printing parameters

are based on the results of chapter 4, where it is concluded that the best results are obtained from concentric infill patterns without any solid top and bottom layer [0/100%C/0].

Table 3.6 Printing parameter for erosion test sample.

Material	PLA
Printer	Ulitimaker 2+
Nozzle diameter	0.4 mm
Infill printing speed	30 mm/s
Wall printing speed	26 mm/s
Infill layer thickness	0.1 mm
Infill pattern	Concentric
Solid top / bottom thickness	0 mm

Most of the applications of FFF products will be vulnerable to material loss if interacting with a liquid for a long time, such as in pipes. To simulate erosion, a waterjet (model Flow Mach 2 1313b) capable of 60 kPsi and minimum of 5 kPsi was used to apply a jet of water mixed with a garnet (a silicate material).

Several waterjet parameters were attempted to determine suitable parameters that would enable monitoring time within the order of several minutes. To start, the pressure was 10 kPsi mixed with garnet pointed to specific point in the 3D printed flat sample. The sample lost 2.5 mm of its thickness within 30 seconds, which would not give any chance to monitor the erosion rate. To overcome this problem, the pressure was decreased to 5 kPsi. After two minutes of pointing the nozzle at a specific point, the sample lost 2 mm of thickness. Therefore, to increase the monitoring time, the nozzle was moved along a line forward and backwards. To remove 1.5 to 2 mm, the test was performed for six minutes according to Table 3.7. For all tests, more than 60% of the material must remain to protect the transducer from the water pressure.

Table 3.7 Parameters of erosion experiment set up.

Experiment parameters	Specification
Pressure	5000 Psi
Slurry material	Garnet
Traveling speed	20 mm/s
Standoff distance	125 mm
Nozzle diameter	1 mm

To fix the transducer under the sample, a holder was designed and printed with a cavity for the sensor. The holder holds the sensor firmly in place under the sample to avoid any sliding under the path of the nozzle, as shown in Figure 3.7. Using SolidWorks, the clamp design was prepared and

transferred to the Ultimaker Cura to be printed. The nozzle diameter was 0.8 and the printing speed was 50 m/sec with a zig zag infill pattern and 60% infill.

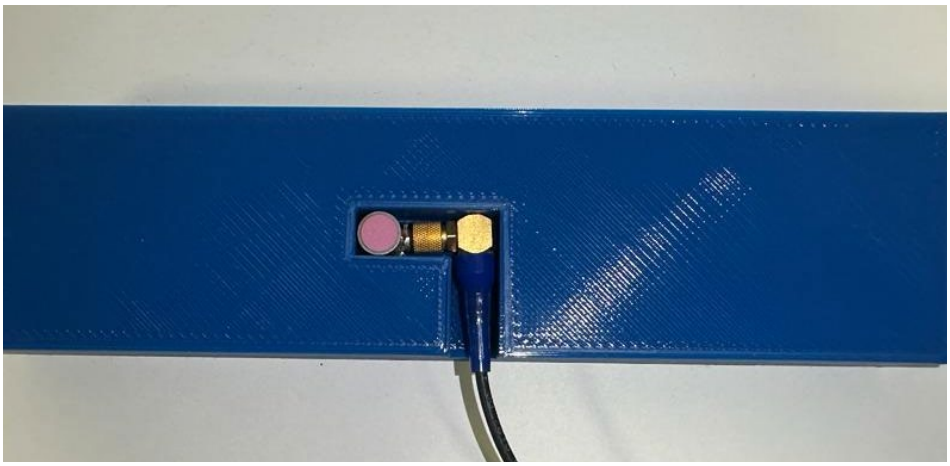

Figure 3.7 Printed holder with a slot to place the transducer underneath the sample during real-time erosion test.

The transducer was placed in the groove and the sample clamped over it to fix sample and holder to the waterjet table using mechanical clamps (Figure 3.8). The coupling agent was placed between the sample and transducer prior to clamping.

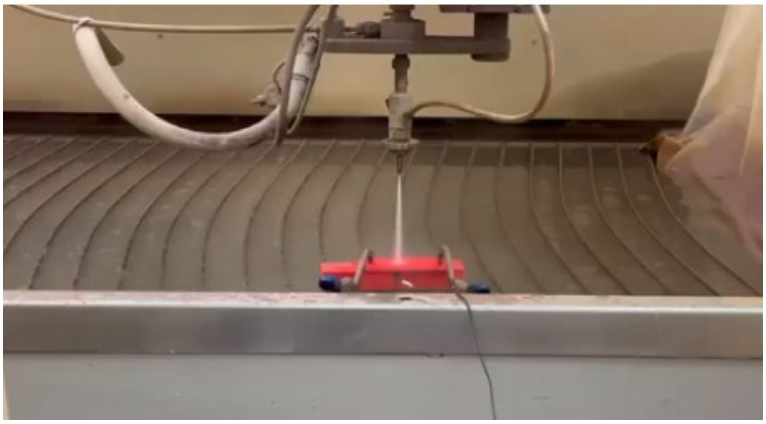

Figure 3.8 Experimental set up of erosion shows the holder, ultrasound transducer.

The jet was started, and the duration of the test was set to six minutes. Data were exported every minute. Figure 3.9 shows the damage caused by the erosion test.

Figure 3.9 image of the sample after erosion test.

4. Results of characterization test

In this chapter, the effect of overall sample thickness on the ultrasound results is studied. Additionally, the effects of the presence of top/bottom/side wall layers and infill percentages are also investigated. The ultrasound transducer PZT is excited with a voltage of 30 volts, and the amplitude gain is set to 35, with a sampling frequency of 160 MHz. To ensure consistency and reliability in the testing process, all samples are secured in a sample holder. This holder maintains a uniform and constant pressure on the sensor throughout testing across different test scenarios.

4.1. Effect of sample thickness

The step gauge of [‖ : 1/100%C/1] was investigated to determine the maximum thickness that could be measured by a 10 MHz transducer. We define maximum measurable thickness as the largest sample thickness where first and last echoes can be detected, as was shown in Figure 3.3. In these tests, the transducer is placed in parallel to the printing axis, as was shown in Figure 3.1. Concentric infill, one of the most common infill patterns, provides the best mechanical properties compared with other infill patterns [75] and hence was selected for the first test. The first and last ultrasound echoes could be detected for the 2.5, 5, and 10 mm thicknesses, as shown in Figure 4.1. However, the pulse echo return corresponding to the 20 mm thick sample could not be detected and hence is not shown.

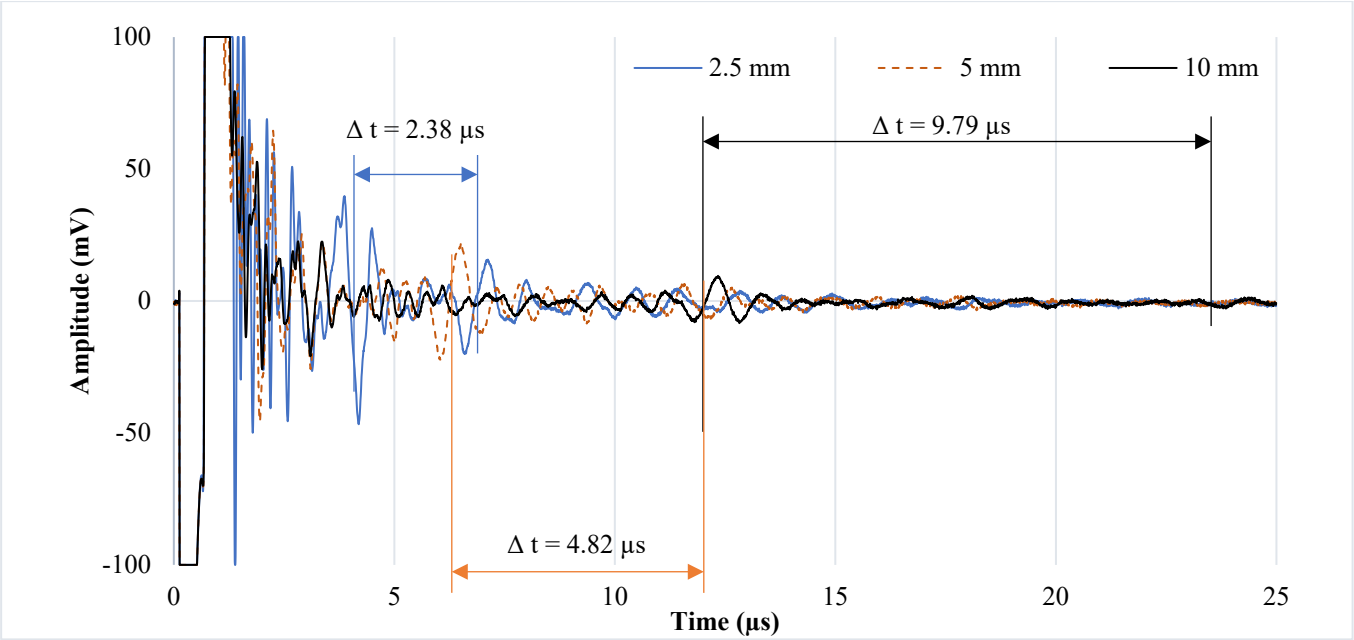

Figure 4.1 Time history of [‖ : 1/100%C/1] test of different thicknesses of 2.5, 5, and 10 mm. The time differences are used to calculate the thickness of the tested sample.

The sample thickness is estimated by multiplying half of the time difference (Δt) by the speed of sound (2100 m/sec) of blue PLA. Results are shown in Table 4.1.

Table 4.1 Experimental calculation based on the time differences of [‖ : 1/100%C/1] test for different thicknesses.

Sample measurement	Sample thickness (mm)		
	2.5	5	10
Experimental thickness calculation (mm)	2.49	5.06	10.28
Caliper reading (mm)	2.49	4.98	9.97
Difference between caliper and experimental (mm) [%]	0[0%]	0.08[-1.5%]	0.31[-3.02%]

[%] = [(Caliper- Experimental)/Caliper × 100%]

The caliper reading of the sample matches the experimental calculation at 2.5 mm thickness. Meanwhile, for the 5 mm thickness, there is a small difference between the caliper reading and experimental calculation. The difference becomes more significant with the 10 mm thickness measurement. The increasing error with increasing thickness is likely due to the loss of wave energy and reduced clarity of the echo peaks. This implies larger errors (and hence reduced accuracy) are to be expected when measuring the thickness of thicker samples using the same ultrasonic testing method.

4.2. Effect of top/bottom solid layer

Outer solid top and bottom solid layers are often printed to give the structure a good surface finish and to minimize material usage [90]. To investigate the effect of this layer, another two groups of samples were printed without any top and bottom solid layer and without side wall. That is, the samples were printed completely with concentric infill, as illustrated in Figure 4.2(a). Two samples were printed to test the effect of the transducer orientation with respect to the printing axis.

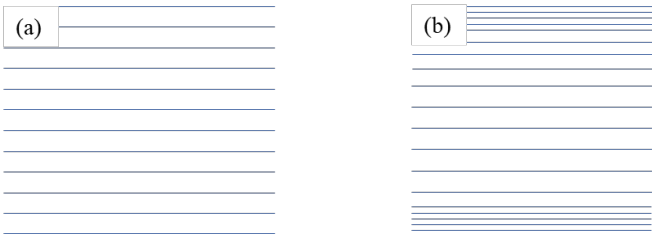

Figure 4.2 Schematic showing the difference with/without the presence of a solid top and bottom layer (a) Schematic of [0/100%C/0]; (b) Schematic of [1/100%C/1].

Test results are shown in Figure 4.3. The first and last echoes can be identified up to 10 mm thickness in both parallel and perpendicular tests.

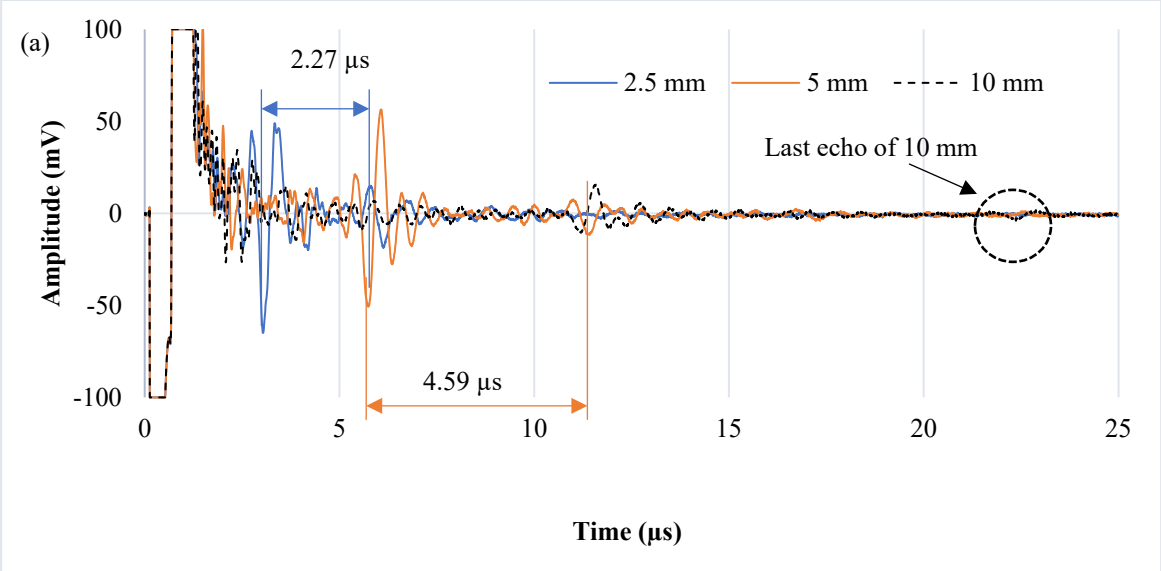

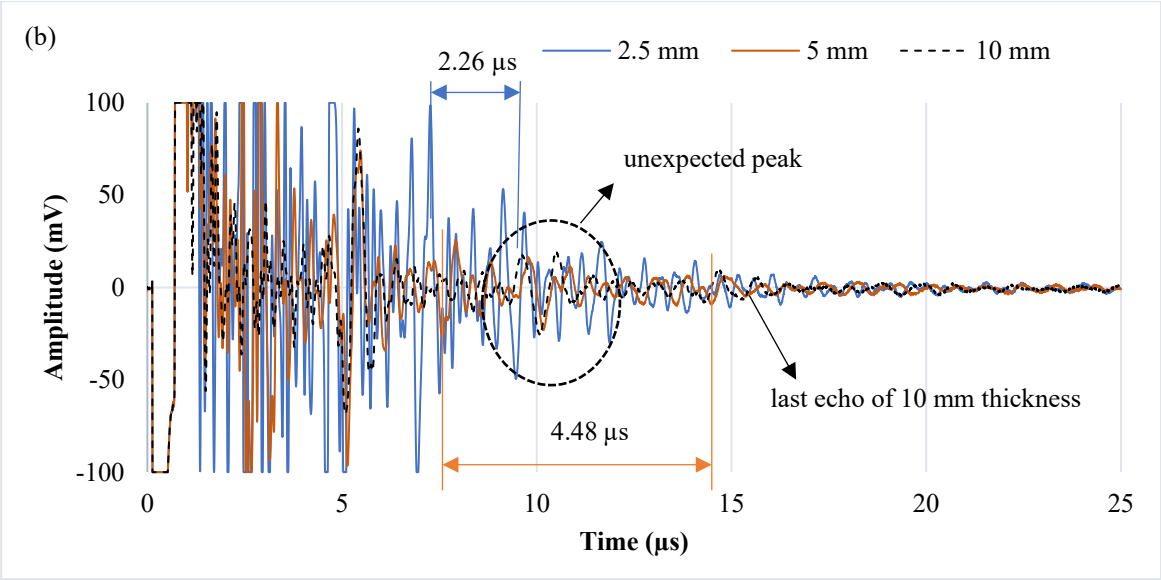

Figure 4.3 (a) Time history of [∥ : 0/100%C/0] test of different thicknesses of 2.5, 5, and 10 mm. The time differences were used to calculate the thickness of the sample; (b) Time history of [⊥ 0/100%C/0] test of different thicknesses of 2.5, 5, and 10 mm. The time differences were used to calculate the thickness of the sample.

The sample thickness can be calculated by multiplying half the transit time by the speed of sound in the red material, given by 2200 m/sec. Results are shown in Table 4.2. It is expected that by increasing the thickness, the difference between the caliper reading and experimental calculation becomes more significant. At 5 mm, there is an unexpected peak present between the first and last echoes. The calculation shows that the unexpected peak corresponds to a depth of 2.5 mm, which is half of 5 mm. The same is true for the 10 mm thickness sample; there is an unexpected peak corresponding to a depth of 5mm. It is conjectured that the reason for this unexpected peak is that the step sample is printed in various thicknesses, starting with the thinner layers followed by the printing of thicker layers. This likely results in the creation of interlayers.

Table 4.2 Experimental calculation based on the transit times of [∥ and ⊥ : 0/100%C/0] tests of different thicknesses.

Transducer position in respect to the printing axis	Parallel to printing axis			Perpendicular to printing axis		
Sample thickness(mm)	2.5	5	10	2.5	5	10
Time difference (microseconds)	2.27	4.59	10.60	2.26	4.48	9.11
Experimental thickness calculation (mm)	2.50	5.05	11.66	2.49	4.93	10.21
Caliper reading (mm)	2.50	5.00	9.95	2.49	4.97	9.96
Difference between caliper and experimental (mm) [%]	0[0%]	0.05[-0.9%]	1.71[-14%]	0[0%]	0.04[0.8%]	0.25[-2.4%]

[%] = [(Caliper- Experimental)/Caliper × 100%]

In the parallel test, the echoes for [∥ : 0/100%C/0] can be detected up to 10 mm same as [∥ 1/100%C/1]. Meanwhile, for the perpendicular test the echoes can be detected up to 10 mm thickness for [⊥ : 0/100%C/0]. It is hypothesized that the improved result follows from using the same pattern without side walls, which leads to less interlayers and less energy dissipation.

4.3. Effect of measurement axis with respect to printing direction (side wall)

In some applications, the test is expected to be conducted perpendicular to the printing axis, such as when testing printed pipes or tanks. To compare the effects of transducer orientation, another test was conducted with the transducer placed perpendicular to the printing axis, as was illustrated in Figure 3.1. However, with this orientation, the material discontinuity is larger since printing is performed layer by layer from the outer border of the object towards the core. In addition, the side walls are printed in a different way, and the pattern in between is concentric. Hence, it is expected that a lot of energy is dissipated as the wave propagates from one pattern to another. Indeed, no first and last echoes were identified at all thicknesses except 2.5 mm. Furthermore, the peaks were found only through use of the digital filter. Results are shown in Figure 4.4.

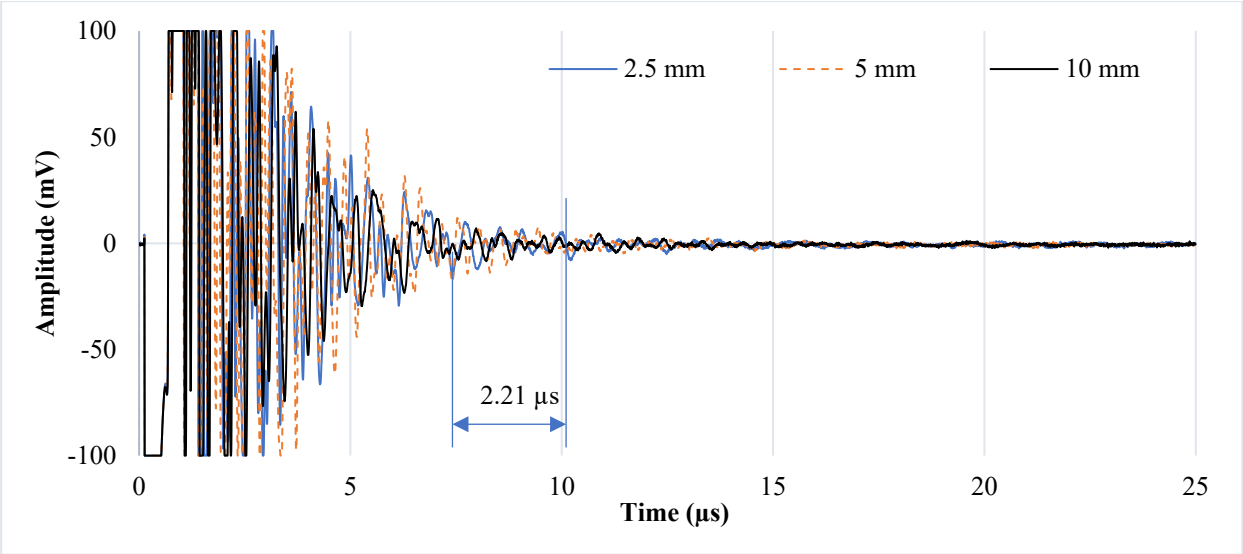

Figure 4.4 Time history of [⊥:1/100%C/1] test of different thicknesses of 2.5, 5, and 10 mm (transducer perpendicular to print axis). No pulse return could be detected for both 5 and 10 mm tests.

It is worth noting that the perpendicular test exhibits more noise compared with the parallel test, as shown in Figure 4.5. Figure 4.5 shows results for the 2.5 mm thickness for both transducer orientations.

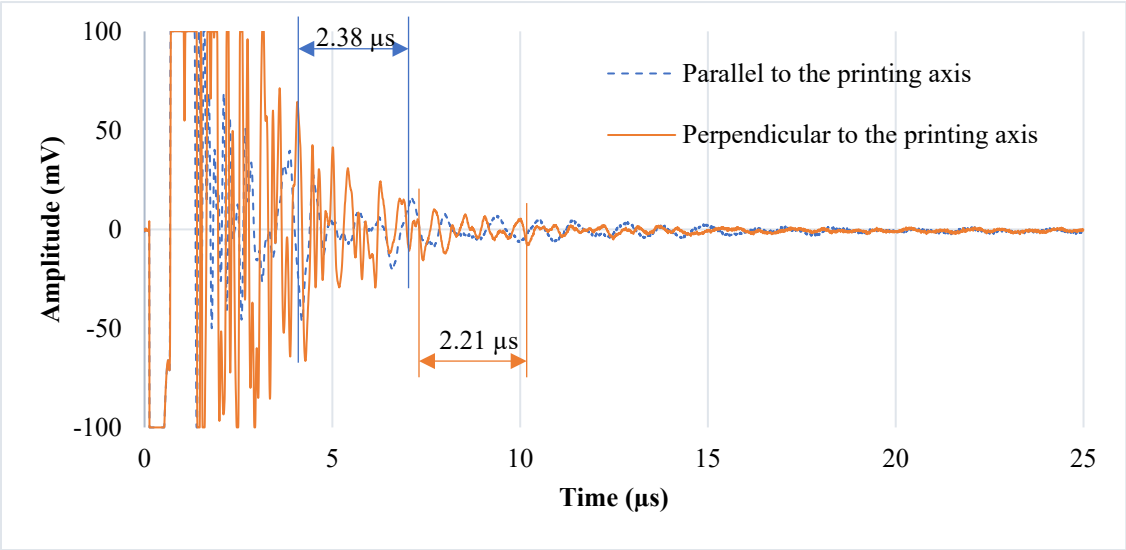

Figure 4.5 Time history graph of response with placing the transducer Parallel vs Perpendicular to the printing axis. The sample was 2.5 mm thick [1/100%C/1].

A similar approach was used to calculate the thickness by multiplying half the transit time and the speed of sound. The peaks were selected via the digital filter, which was used to eliminate higher and lower frequencies and reduce noise. The time difference between peaks is 2.21 µs and the speed

of sound in orange PLA is 2246 m/sec. By multiplying half the transit time with the speed of sound, the thickness is measured at 2.48 mm, which is same as the caliper reading. At 2.5 mm thickness, the experimental calculation is (within measurement uncertainty) the same as the caliper reading of the sample in both parallel/perpendicular configurations with the presence of the solid layer for 2.5 mm thickness. On the other hand, for the perpendicular test the echoes can be detected up to 10 mm thickness for [⊥ : 0/100%C/0], when there are no side walls but were detectable only up to 2.5mm with presence of side wall for [⊥:1/100%C/1]. It is speculated that the reason for this is that the infill in [⊥ : 0/100%C/0] is all concentric without any side walls. This is printed by using only the concentric pattern, which minimizes discontinuities and thus minimizes energy dissipation.

4.4. Effect of infill percentage

Mechanical properties are typically enhanced by increasing the infill percentage. To study the effect of infill percentage, two groups are printed [1/95%C/1] and [1/90%C/1], in addition to the original 100% infill samples. Every group has two samples, one to be tested in parallel to the printing axis and another one for testing perpendicular to the printing axis with presence of side walls which acts as the ultrasound top/bottom solid layer. For all the different infill percentages, the previously observed trend is expected to continue; ultrasound echoes are not expected at 20 mm. As the infill decreases, it is expected that the ultrasound wave energy dissipates more. This explains the observation shown below that echoes can only be identified in samples with 90% infill up to 2.5 mm thickness. However, at 95% infill, the echoes can be identified up to 10 mm, as shown in Figure 4.6.

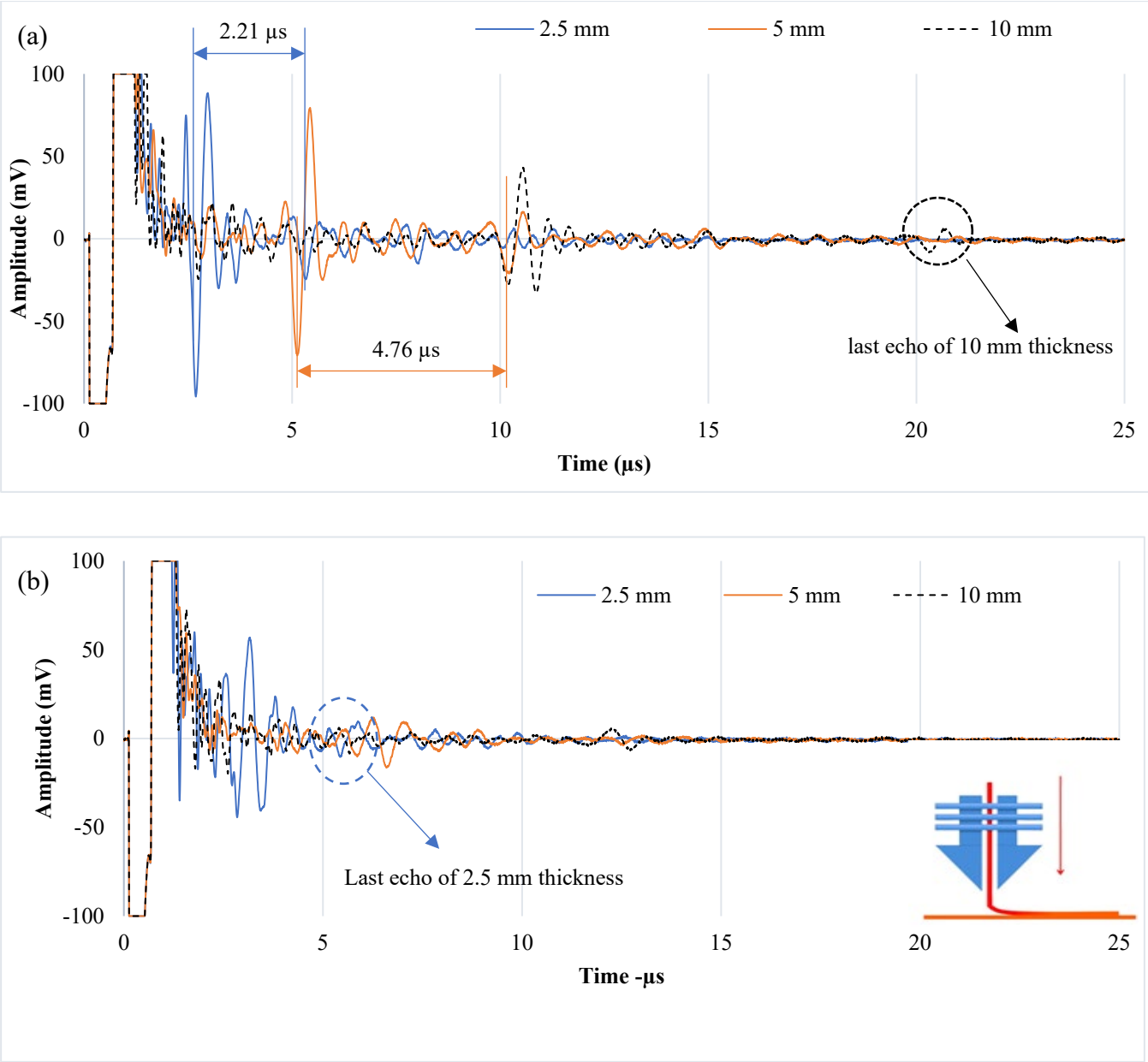

Figure 4.6 (a) Time history of [‖:1/95%C/1] test of different thicknesses of 2.5, 5, and 10 mm.; (b) Time history of [‖:1/90%C/1] test of different thicknesses of 2.5, 5, and 10 mm. Time differences are used to calculate the thickness of the tested sample.

Table 4.3,Table 4.4, and Table 4.5 compare the experimental calculations of different infills at the same thickness. The speed of sound in the orange sample used for 95% infill is 2246 m/sec. For 90% infill, the blue sample has a speed of sound 2100 m/sec.

Table 4.3 Experimental calculation of 2.5 mm test based on the time differences of [‖ :1/100%C/1] Vs [‖ :1/95%C/1] Vs [‖ :1/90%C/1].

Sample specifications	[‖:1/100%C/1]	[‖:1/95%C/1]	[‖:1/90%C/1]
Time difference (microseconds)	2.38	2.21	2.49
Speed of sound (m/sec)	2100	2246	2100
Experimental calculation (mm)	2.50	2.48	2.61
Caliper reading (mm)	2.50	2.48	2.50
Difference between caliper and experimental (mm)	0[0%]	0[0%]	0.11[-4.2%]

[%] = [(Caliper- Experimental)/Caliper × 100%]

The difference between the caliper and experimental calculation in [‖:1/100%C/1] and [‖:1/95%C/1] at 2.5 mm thickness is zero. However, in [‖:1/90%C/1], the 4.2% error implies that by decreasing the infill percentage, the errors become more significant, even at small thicknesses. It is hypothesized that with the lower (90% vs 100%) infill, there are more discontinuities (voids) in the material and hence more energy dissipation.

Table 4.4 Experimental calculation of 5 mm test based on the time differences of [‖ :1/100%C/1] Vs [‖ :1/95%C/1] Vs [‖ :1/90%C/1].

Sample specifications	[‖:1/100%C/1]	[‖:1/95%C/1]	[‖:1/90%C/1]
Time difference (microseconds)	4.82	4.76	No peaks detected
Speed of sound (m/sec)	2100	2246	2100
Experimental calculation (mm)	5.05	5.35	No peaks detected
Caliper reading (mm)	4.98	4.94	4.99
Difference between caliper and experimental (mm)	0.07[-1.4%]	0.41[-7.7%]	No peaks detected

[%] = [(Caliper- Experimental)/Caliper × 100%]

The error between the caliper reading and experimental calculations becomes more pronounced at 5 mm thickness of [‖:1/95%C/1] and reaches 0.41mm (7.7%). This follows due to the lower infill (increased voids in the material) which compounds the energy loss and hence errors as the wave has a longer distance to travel compared with 2.5 mm. On the other hand, at [‖:1/100%C/1], the difference was only 0.07 mm (1.4%). For 90% infill, no peaks in the pulse echo returns could be detected and thus no thickness measurement could be made. It is hypothesized that the lower infill (90%) leads to a larger number of voids in the material and hence greater energy losses in the ultrasound wave, to the point that no pulse echo return could be detected.

Table 4.5 Experimental calculation of 10 mm test based on the time differences of [‖ :1/100%C/1] Vs [‖ :1/95%C/1] Vs [‖ :1/90%C/1].

Sample specifications	[‖:1/100%C/1]	[‖:1/95%C/1]	[‖:1/90%C/1]
Time difference (microseconds)	9.79	9.97	No peaks detected
Speed of sound (m/sec)	2100	2246	2100
Experimental calculation (mm)	10.29	11.2	No peaks detected
Caliper reading (mm)	9.97	9.75	9.89
Difference between caliper and experimental (mm)	0.32[-3.1%]	1.45[-12.9%]	No peaks detected

[%] = [(Caliper- Experimental)/Caliper × 100%]

At 10 mm, the error between the caliper and experimental calculation in [‖:1/95%C/1] becomes more significant than for the sample [‖:1/100%C/1]. For the 90% infill, no peaks in the pulse echo returns could be detected and thus no thickness measurement could be made.

To study the effect of top/bottom or side wall solid layers in the samples with less than 100% infill, another four group samples were printed with all 95% infill density or all 90% infill density (without any top or bottom layer or side walls). Two samples are to be tested in parallel and two to be tested perpendicular to the printing axis.

In the parallel to the printing axis test of [‖: 0/95%C/0], the echoes can be detected only in the 2.5 mm and 5 mm samples. In contrast, no ultrasound return that can be detected in [‖: 0/90%C/0], as shown in Figure 4.7. It is proposed that without outer layers, the roughness of the surface increases with decreasing infill percentage, which in turn dissipates ultrasound wave energy before it penetrates the bulk material. In the perpendicular test for both infill percentages, there were no detectable peaks at all thicknesses, as shown in Figure 4.8.

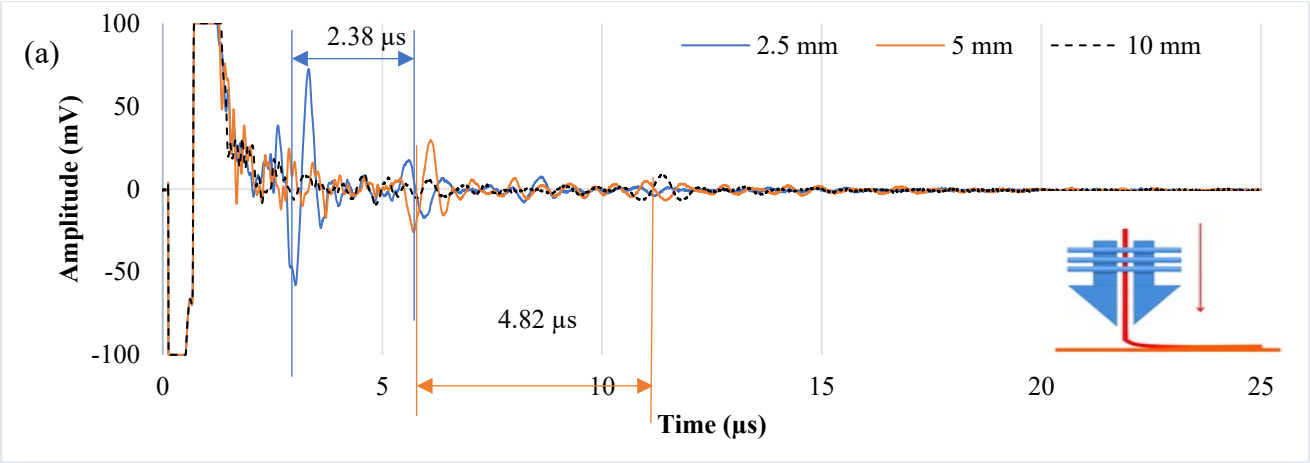

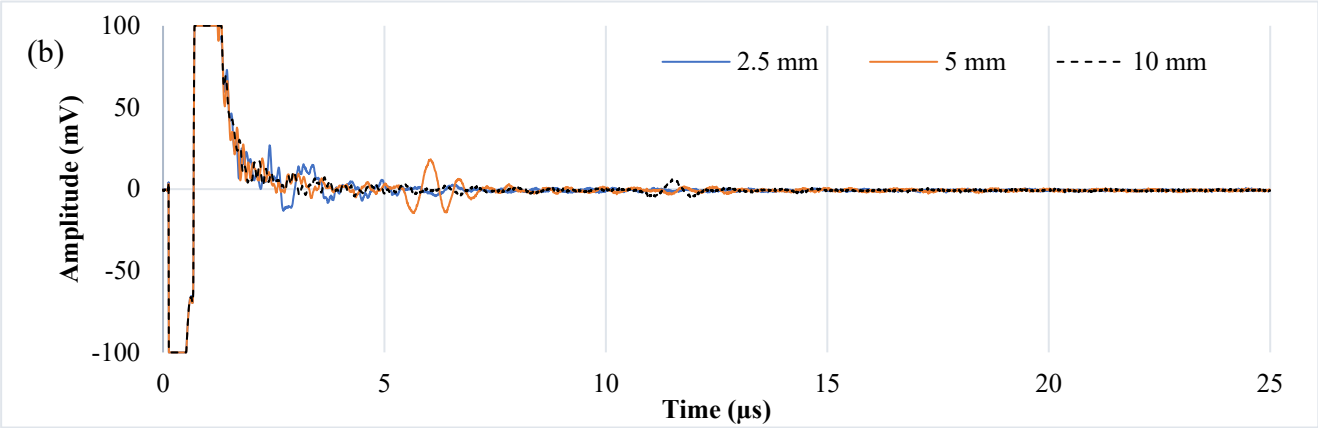

Figure 4.7 (a) Time history of [‖ :0/95%C/0] test of different thicknesses of 2.5, 5, and 10 mm. Time differences are used to calculate the thickness of the tested sample; peaks can be detected only for 2.5 and 5 mm test; (b) Time history of [‖ :0/90%C/0] test of different thicknesses of 2.5, 5, and 10 mm. No peaks can be detected for all thicknesses, implying that thickness cannot be measured.

The thickness of the samples of [‖:0/95%C/0] is calculated by multiplying half the time differences by the speed of sound, which is 2100 m/sec in white PLA as shown in Table 4.6.

Table 4.6 Experimental calculation test based on the time differences of [‖:0/95%C/0] for different thicknesses.

Sample measurement	Sample thickness (mm)		
	2.5	5	10
Experimental calculation (mm)	2.50	5.06	No peaks detected
Caliper reading (mm)	2.49	4.92	9.79
Difference between caliper and experimental (mm)[%]	0.01[-0.4%]	0.14[-2.7%]	No peaks detected

[%] = [(Caliper- Experimental)/Caliper × 100%]

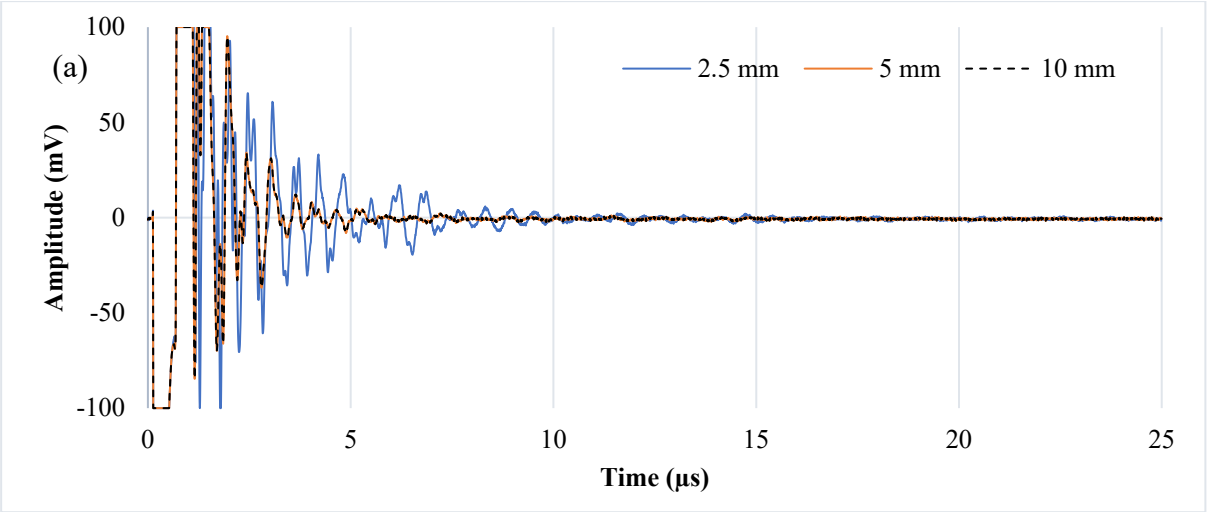

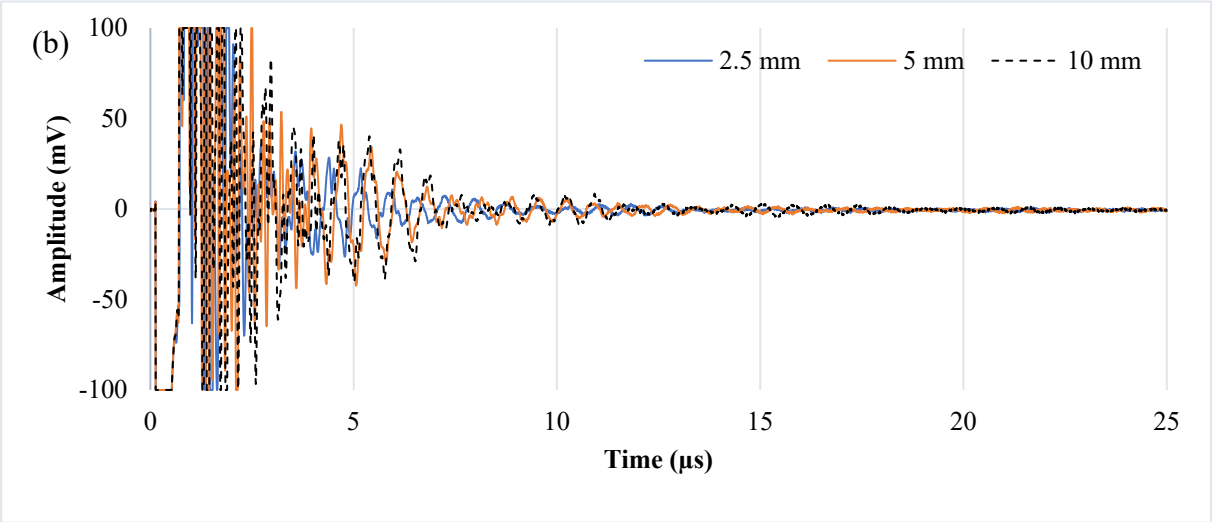

Figure 4.8 (a) Time history of [⊥: 0/95%C/0] test of different thicknesses of 2.5, 5, and 10 mm. No peaks can be detected for all thicknesses, which means thickness cannot be measured; (b) Time history of [⊥ : 0/90%C/0]] test of different thicknesses of 2.5, 5, and 10 mm. No peaks can be detected for all thicknesses, which means thickness cannot be measured.

On the other hand, to study the effect of side walls, two samples of [⊥:1/95%C/1] and [⊥ :1/90%C/1] were printed and investigated with the transducer now perpendicular to the printing axis to study the effect of the side walls on the measurements. The echoes were detectable only by digital filter in 2.5 mm thickness of [⊥ 1/95%C/1], as shown in Figure 4.9. However, no peaks could be detected in the sample of [⊥ 1/90%C/1], and hence no thickness measurement could be made.

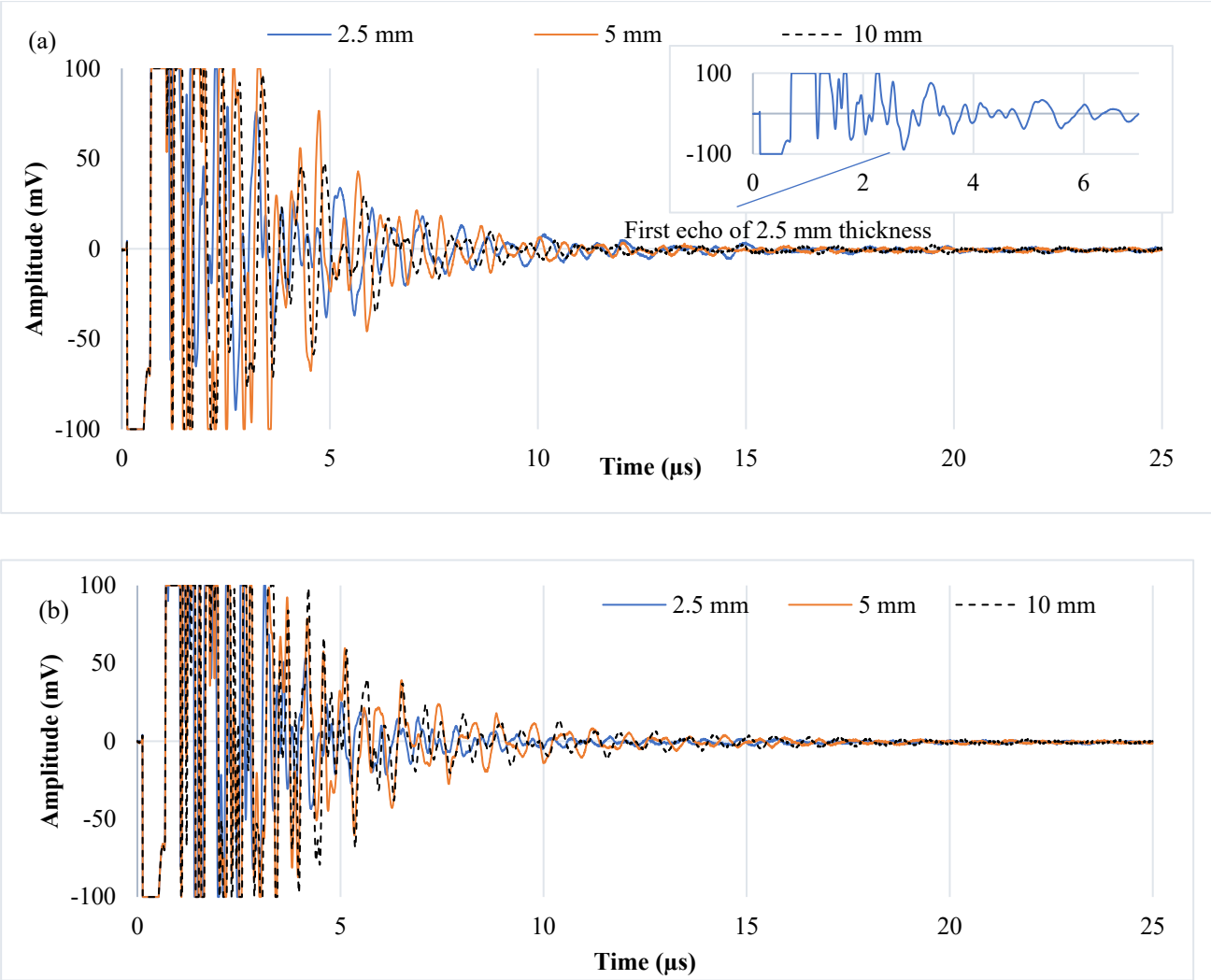

Figure 4.9 (a) Time history of [⊥ :1/95%C/1] test of different thicknesses of 2.5, 5, and 10 mm. Time differences in peaks were used to calculate the thickness of the tested sample at 2.5 mm. No peaks can be detected in all other thicknesses which means thickness cannot be measured; (b) Time history of [⊥: 1/90%C/1] test of different thicknesses of 2.5, 5, and 10 mm. No peaks can be detected in all thicknesses, which means thickness cannot be measured.

The thickness of the 2.5 mm sample of [⊥ :1/95%C/1] is calculated by multiplying the half of time difference between peaks (2.23 µs) by the speed of sound of black PLA (2150 m/sec), and the result is 2.5 mm. The caliper reading matches the experimental calculation, continuing the trend of accurate thickness measurements at 2.5 mm. The reason behind the ability to accurately measure the thickness of the sample is the presence of the 2 mm solid side walls layer. This implies that 80% of the overall thickness is solid.

In all printed samples, no echoes can be identified at 20 mm thickness as the wave cannot penetrate to that thickness. In addition, for all samples where the peaks can be identified, the difference

between caliper reading and experimental calculation increases as the sample thickness increases. The error also increases as the infill percentage decreases. At 90% infill, even the 2.5 mm thickness of [∥:1/90%C/1] displayed a large difference between ultrasound and caliper measurements. At 95% infill, the [∥:1/95%C/1] sample at 5 mm thickness displayed an unacceptable ultrasound measurement compared with the caliper measurement.

For transducer perpendicular to the printing axis test with presence of side wall, the only thickness that returned reasonable thickness measurement results is 2.5 mm – for both [⊥ :1/100%C/1] and [⊥ :1/95%C/1]. Even so, a digital filter was required because of the presence of different infill patterns. Surface roughness is also a critical factor that can significantly influence the measurement process, particularly in the case of porous samples characterized by uneven or rough surfaces. The presence of a rough surface can impede the penetration of ultrasonic waves and results in increased energy dissipation during measurements. Therefore, for [∥:0/95%C/0], the maximum thickness that could be measured was 5 mm and nothing could be measured for [∥:0/90%C/0].

To investigate the interior of the samples, they were sliced on a lathe machine to show the effect of the surface. As shown in Figure 4.10 (a), [∥: 1/100%C/1] test, the face is clear and uniform but in Figure 4.10 (b), [⊥: 1/100%C/1] the surface is not smooth as the side wall layers are present and are not the same pattern as the concentric infill. Consequently, the discontinuity is clear. In Figure 4.10 (c), [∥: 1/90%C/1], after removing the first millimeter of the top solid layer, the gaps in between the printed layers are clear. It is hypothesized that this is the reason for limited penetration.

Figure 4.10 Lathed surfaces of 3D printed samples (a) Cleaned surface of [‖: 1/100%C/1] showing less discontinuity implies ability to measure thicknesses ; (b) Cleaned surface of [⊥: 1/100%C/1] showing discontinuity between the outer layer and the inner infill implying inability to measure thicknesses; (c) Cleaned surface of [‖:1/90%C/1] showing discontinuity through the sample and implying an inability to measure thicknesses.

4.5. Effect of printing patterns

4.5.1 All solid top and bottom layer (Line pattern)

In certain 3D printing applications, factors such as printing time and material usage become critical considerations. To optimize these aspects, the choice of infill pattern becomes pivotal. One effective approach is to employ a line infill pattern, which can help reduce printing time and optimize material usage. Using all solid top and bottom layers can also be a strategic choice in specific scenarios, depending on the desired outcome and the specific requirements of the 3D printed object. The selection of the most suitable infill pattern should be based on a careful assessment of the priorities and constraints of the project [91]. Figure 4.11 illustrates the difference

between samples with no top/bottom layers (a), samples with a solid top/bottom layer (b) and samples that are all solid (c), where the infill is the same as the top/bottom layer. To investigate these differences, two group of samples are printed with all-solid top and bottom layers. The effect of thickness of this sample is investigated, as well as the effect of transducer orientation.

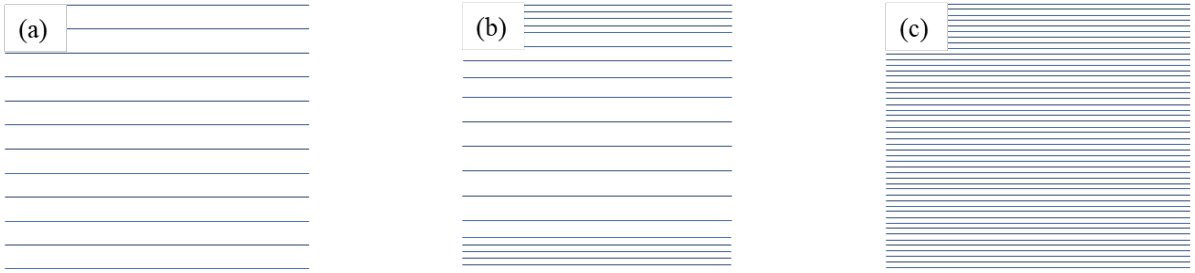

Figure 4.11 Schematic shows the differences between presence of solid top and bottom layer (a) Schematic of [0/100%C/0]; (b) Schematic of [1/100%C/1]; (c) Schematic of [1/100%L/1].

A. Effect of thickness

When the transducer is parallel to the printing axis, the first and last echo can be identified, up to 10 mm sample thickness. The same trend continues as before; at 20 mm as there is no detectable peak in the signal, as shown in Figure 4.12.

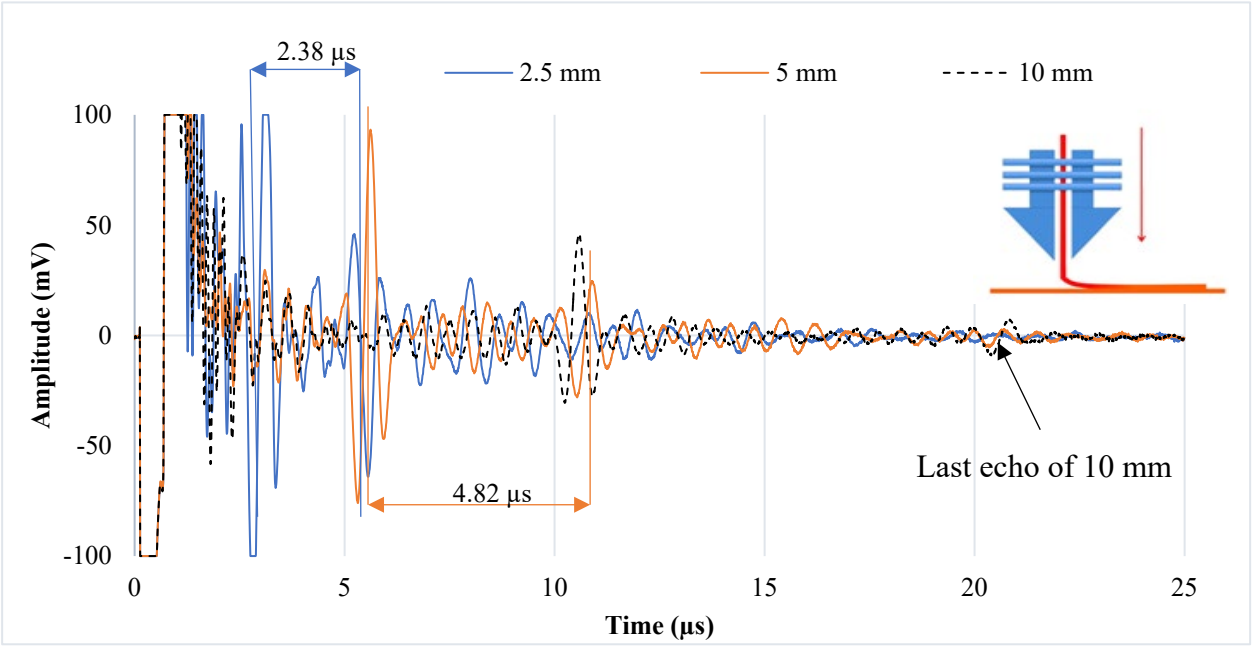

Figure 4.12 Time history of [‖ :0/100%L/] test of thicknesses of 2.5, 5, and 10 mm.

The thickness of each sample is calculated by multiplying half of the time difference with the speed

of sound, (2100 m/sec) in white PLA, as illustrated in Table *4.7* Table 4.7.

Table 4.7 Experimental calculation test based on the time differences of [∥ : 0/100%L/0] test of different thicknesses.

Thickness(mm)	2.5	5	10
Time difference (microseconds)	2.38	4.82	9.79
Experimental calculation (mm)	2.5	5.06	10.28
Caliper reading (mm)	2.5	4.98	9.97
Difference between caliper and experimental (mm) [100%]	0[0%]	0.08[-1.6%]	0.31[-4.0%]

The same trend as previously observed continues. The measurement difference at the 2.5 mm thick sample is zero, while increasing the thickness also increases the difference between the caliper and ultrasound measurements.

B. Effect of measurement axis with respect to printing direction without side wall

Another sample is printed and investigated to compare the results between parallel and perpendicular transducer orientation. In this case, the first and last echoes can be detected up to 10 mm because the same infill pattern is used as in the top and bottom layer, Figure 4.13. The thickness of the sample is calculated by multiplying half the time difference by the speed of sound of orange PLA (2246 m/sec), results are shown in Table 4.8.

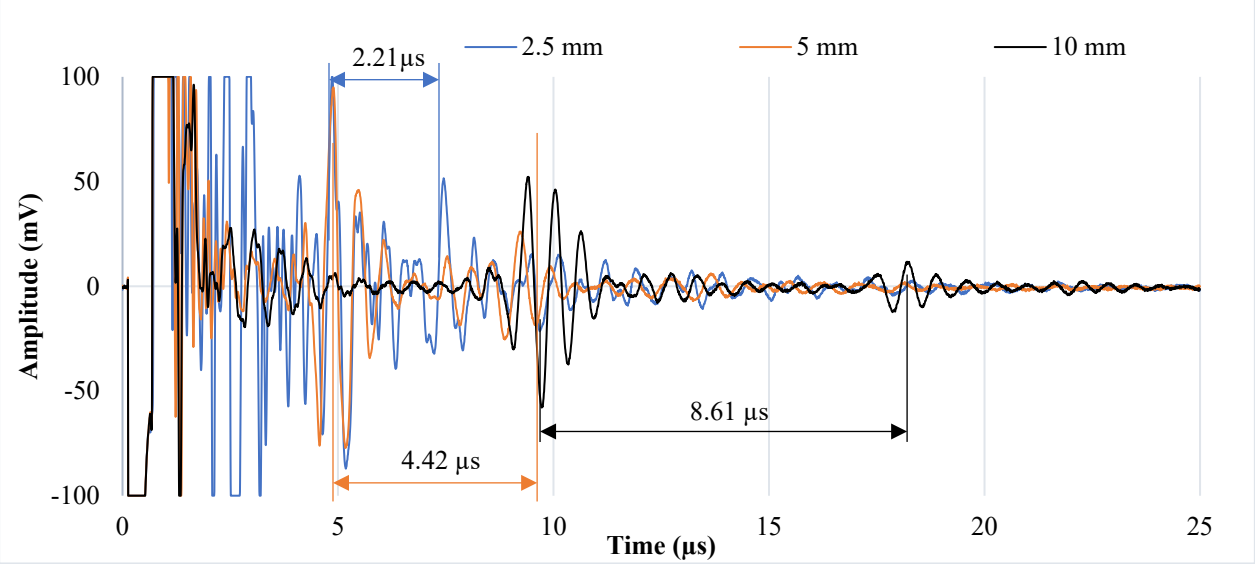

Figure 4.13 Time history of [⊥ : 0/100%L/0] test of different thicknesses of 2.5, 5, and 10 mm.

Table 4.8 Experimental calculation test based on the time differences of [⊥: 0:/100%L/0] test for different thicknesses.

Sample measurement	Sample thickness (mm)		
	2.5	5	10
Experimental calculation (mm)	2.48	4.96	9.68
Caliper reading (mm)	2.48	4.96	9.95
Difference between caliper and experimental (mm) [%]	0[0%]	0[0%]	0.27[-2.7%]

In the sample printed with all solid top and bottom layers, [[‖ :0/100%L/0], the first and last echo can be identified easily, the same as for [‖ :1/100%C/1]. It is proposed that this follows because the layers stick on top of each other due to the heat from printing and this helps the wave to travel for a longer distance. In test of [⊥: 0/100%L/0], even without digital filter the echoes can be identified up to 10 mm, same as for [⊥: 0/100%C/0]. It is proposed that this follows from using the same infill pattern for the entire sample, and also a sufficiently smooth surface finish for the outer layers. On the other hand, for [⊥: 1:/100%C/1], only up to 2.5 mm is measurable as the discontinuity is present. Since there is less discontinuity, the ultrasound is attenuated less, and peaks can be detected to 10mm.

4.5.2. Grid infill pattern

The grid infill pattern, Figure 3.3, has demonstrated an ability to deliver favorable mechanical properties while optimizing material usage. Additionally, it offers the advantage of shorter printing times compared to infill patterns such as the triangle infill pattern [92]. To gain a deeper understanding of the potential benefits of this widely used infill pattern, a study has been undertaken. This study involves printing samples while systematically varying different parameters to evaluate and analyze their effects on the printed objects.

A. Effect of thickness

The samples were first tested with the transducer placed parallel to the printing axis. A similar trend as previous observed continues, where the first and last echoes can be detected in all thicknesses except 20 mm, as shown in Figure 4.14.

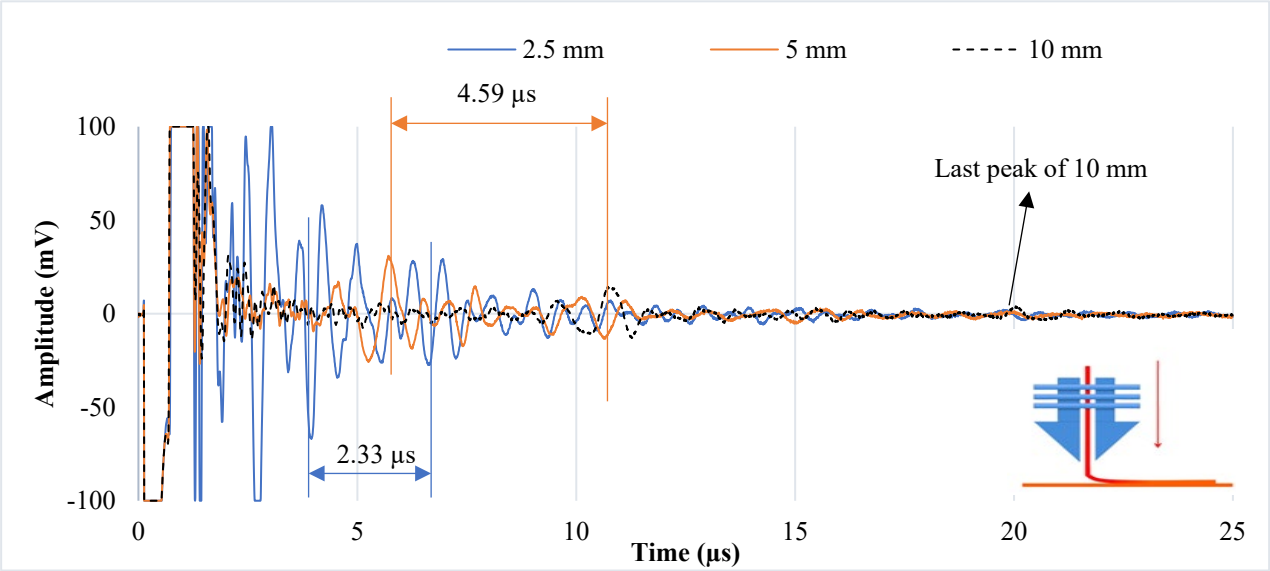

Figure 4.14 Time history of [‖ :1/100%G/1] test of different thicknesses of 2.5, 5, and 10 mm.

The same approach is used to calculate the thickness of the samples, where the half time difference is multiplied by the speed of sound (2150 m/sec) of black PLA, as shown in Table 4.9. Similar to prior tests, the error between the caliper and ultrasound measurements increases as the sample thickness increases.

Table 4.9 Experimental calculation of [‖ :1/100%G/1] test of different thicknesses.

Thickness(mm)	2.5	5	10
Time difference (microseconds)	2.33	4.59	9.29
Experimental calculation (mm)	2.50	4.93	9.99
Caliper reading (mm)	2.50	4.96	9.82
Difference between caliper and experimental (mm) [%]	0[0%]	0.03[0.6%]	0.17[-1.7%]

[%] = [(Caliper- Experimental)/Caliper × 100%]

The same trend continues with the presence of the top layers - the surface finish is smoother, enabling the wave to propagate through the material.

B. Effect of presence of solid top and bottom layers

Another two group samples without top/bottom layers and without side walls are printed to

investigate the effect of presence of outer solid layers, Figure 4.15. One sample is to be tested in parallel to the printing axis and the other sample to be tested in perpendicular to the printing axis. For the case with no top/bottom layers, when tested with transducer in parallel to the printing axis test, the echoes can only be identified at 2.5 mm thickness. However, there are no discernible peaks in the perpendicular test, Figure 4.16.

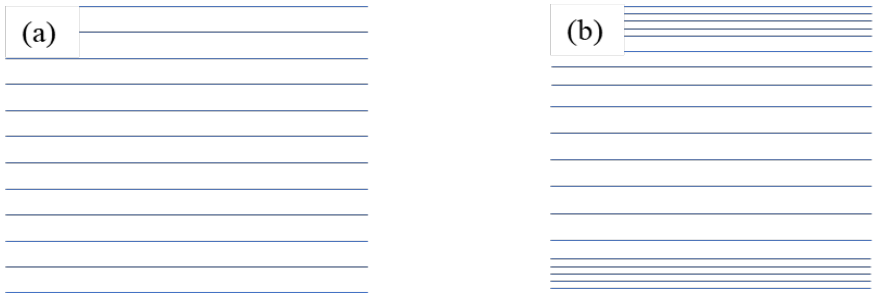

Figure 4.15 Schematic showing the difference between the presence of solid top and bottom layer (a) Schematic with no top/bottom layers [0/100%G/0]; (b) Schematic with top/bottom layers [1/100%G/1].

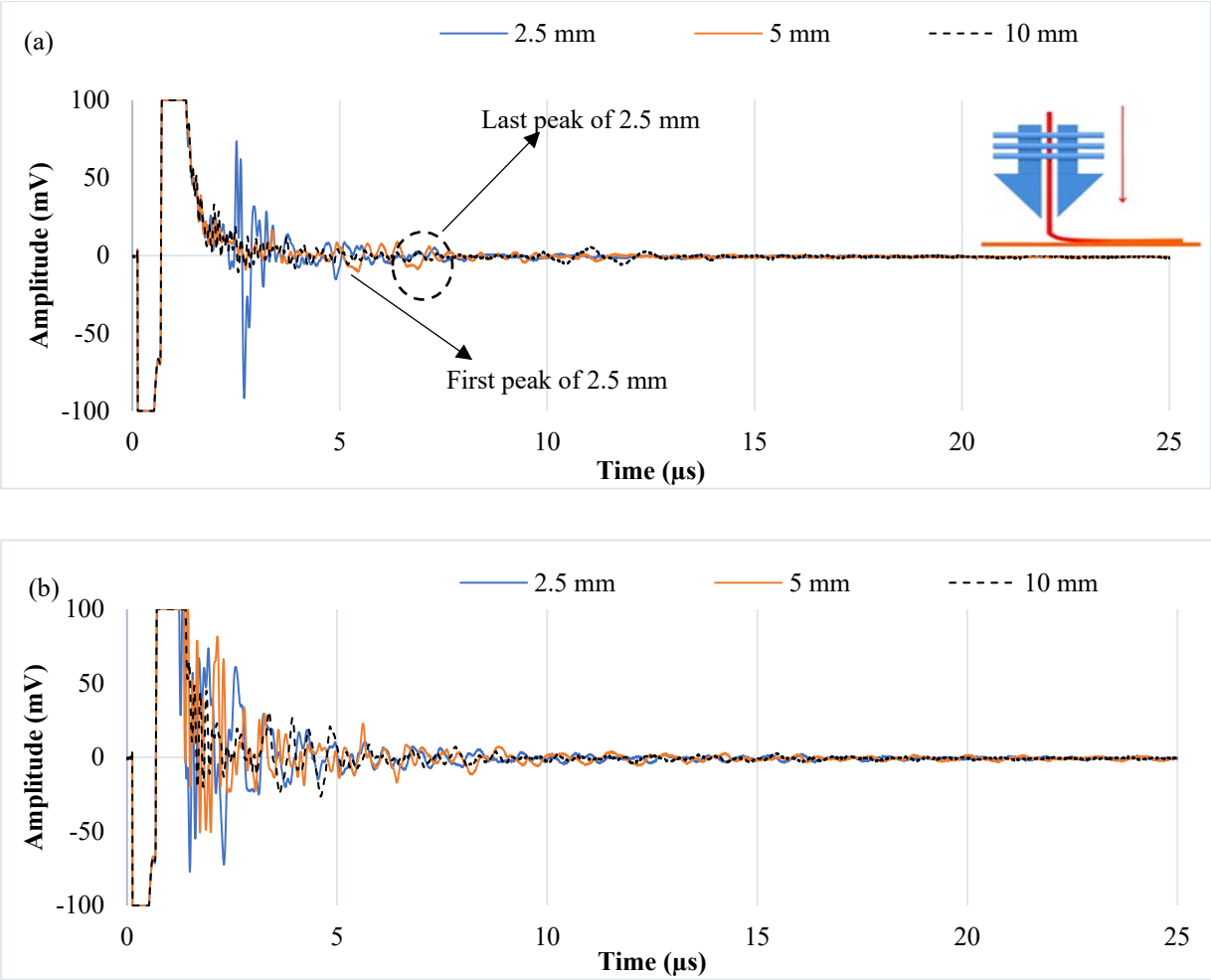

Figure 4.16 (a) Time history of [‖ : 0/100%G/0]test of different thicknesses of 2.5, 5, and 10 mm. No peaks can be detected in all thicknesses other than 2.5mm, which means thickness cannot be measured with ultrasound; (b) Time history of [⊥:0/100%G/0] test of different thicknesses of 2.5, 5, and 10 mm. No peaks can be detected in all thicknesses, which means thickness cannot be measured using ultrasound.

The time difference between the peaks for the parallel test at 2.5 mm is 2.21µs, and the speed of sound in orange PLA is 2246 m/sec. The half transit time and speed of sound yield a thickness measurement 2.49 mm, which is equal to the caliper reading. The roughness of the surface in the samples without top/bottom layers [‖ : 0/100%G/0] is high, which affects propagation of the wave. The same observation can be made for [⊥:0/100%G/0]; the surface finish is rough, and the energy of the wave dissipates before the penetration.

C. Effect of transducer orientation with respect to printing axis (side wall)

To investigate the effect of transducer orientation to the printing axis with presence of the side wall, separate samples are prepared for testing with respect to the orientation. With the transducer

perpendicular to the print axis, echoes can only be detected for the 2.5 mm sample. No clear peaks could be detected for the other sample thicknesses (Figure 4.17).

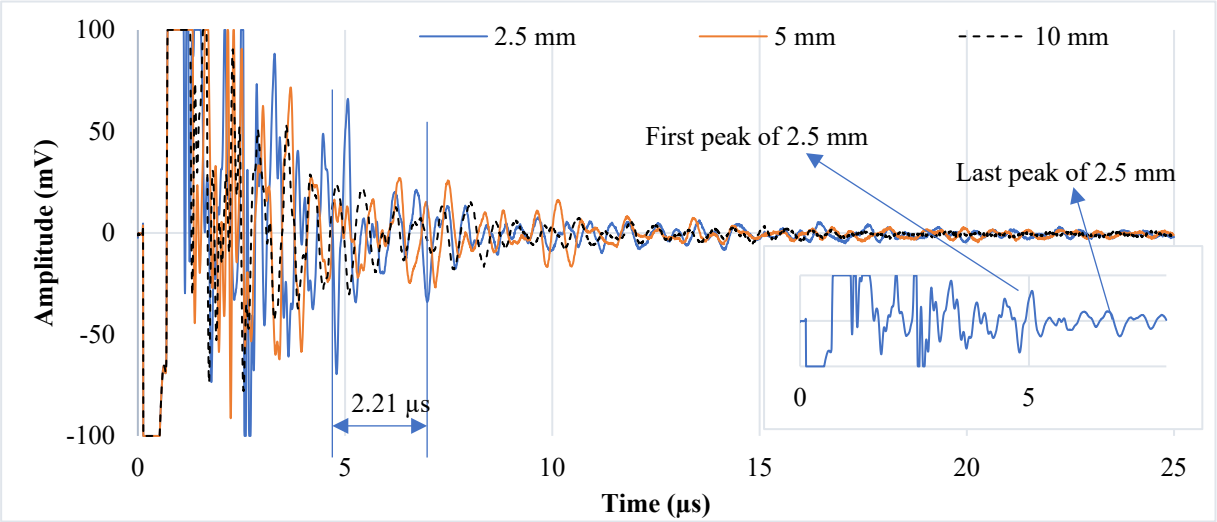

Figure 4.17 Time history of [⊥ : 1/100%G/1] test of different thicknesses of 2.5, 5, and 10 mm. No peaks could be detected for thicknesses other than 2.5 mm, which means thickness cannot be measured using ultrasound.

The same calculation approach is used by multiplying half the time difference (2.21 µs) by the speed of sound of orange PLA (2246 m/sec). The caliper reading is 2.48 mm, which is equal to the calculated value. The reason behind the ability to measure up to 2.5 mm for [⊥ : 1/100%G/1] is the presence of the smooth wall. However, the presence of discontinuities implies that the ultrasound wave loses energy and cannot penetrate further.

Despite using the same gain in both tests, the amplitude in the perpendicular test with side wall is higher than for the parallel test with top/bottom solid layer. In addition, the window of the perpendicular test is noisier since the discontinuity is more pronounced in the perpendicular test.

The same trend continues in the printed samples with grid infill pattern, [∥ :1/100%G/1], parallel to the printing axis. First and last echoes can be detected up to 10 mm thickness, as well in the perpendicular test with presence of side wall [⊥:1/100%G/1] up to 2.5 mm. The surface finish of the grid infill pattern is rough, which explains why in the case of [∥ :0/100%G/0], the only echoes that can be identified in 2.5 mm are for the parallel to the printing axis case. There are no discernible peaks in the perpendicular test at all thicknesses of [⊥:0/100%G/0].

4.5.3. Triangle infill

Triangle infill (Figure 3.3) is one of the most common infill patterns and can provide good strength while also helping to reduce the amount of material consumed [93]. In this section, the effect of several printing parameters will be investigated.

A. Effect of thickness

The test has been done on the sample of [‖ :1/100% T/1] with the transducer placed parallel to the printing axis (Figure 3.1). Similar trends as previous tests were observed; ultrasound echoes can be detected for thicknesses up to 10mm, with no discernible signal at 20mm thickness (Figure 4.18).

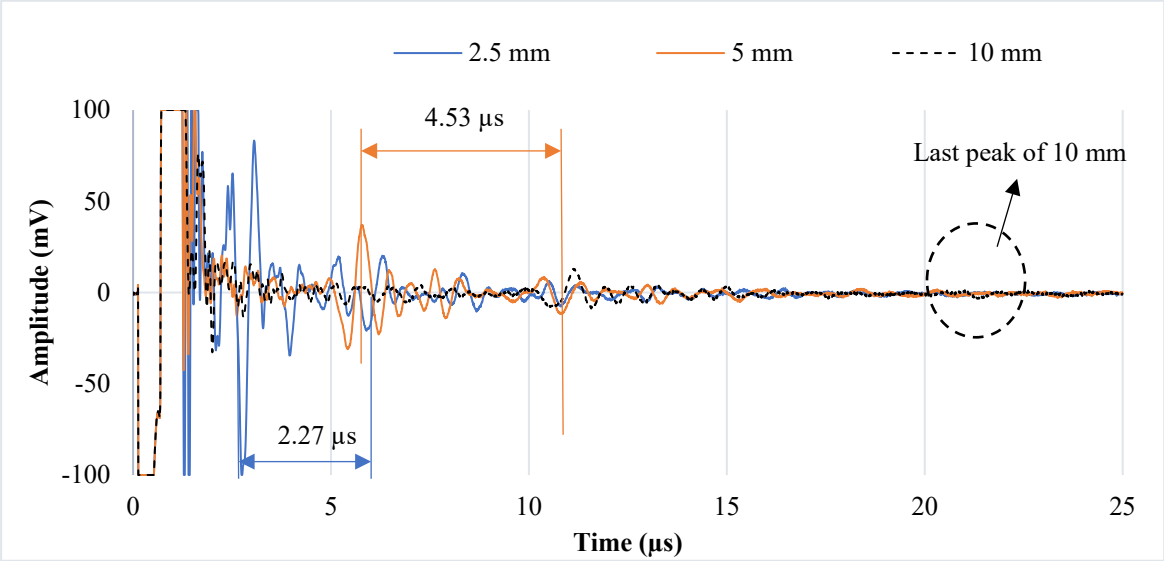

Figure 4.18 Time history of [‖ :1/100%T/1] test of different thicknesses of 2.5, 5, and 10 mm.

The same approach is used to calculate the thickness, by multiplying half of the time difference by the speed of sound in the red material (2200 m/sec) (Table 4.10).

Table 4.10 Experimental calculation test based on the time dime differences of [‖ :1/100%T/1] test of different thicknesses.

Thickness(mm)	2.5	5	10
Time difference (microseconds)	2.27	4.53	10.21
Experimental calculation (mm)	2.50	4.98	11.23
Caliper reading (mm)	2.50	4.97	9.95
Difference between caliper and experimental (mm)[%]	0[0%]	0.01[-0.2%%]	1.28[-11.4%]

[%] = [(Caliper- Experimental)/Caliper × 100%]

As before, increasing differences in the ultrasound thickness measurement are observed with increasing thickness of the sample. As the top/bottom layers are present, the surface finish is smooth enough to enable the wave to penetrate. Furthermore, the discontinuity is smaller since the layers stick to each other because of the heat from the printing process.

B. Effect of presence of solid top and bottom layers

Another two samples were printed without any solid top and bottom layer or side wall (Figure 4.19) to be investigated with the transducer oriented parallel and perpendicular to the printing axis (Figure 3.1). In the parallel test, the peak echoes can be identified only in the 2.5 mm and 5 mm samples. However, no peaks could be identified in the perpendicular test. (Figure 4.20)

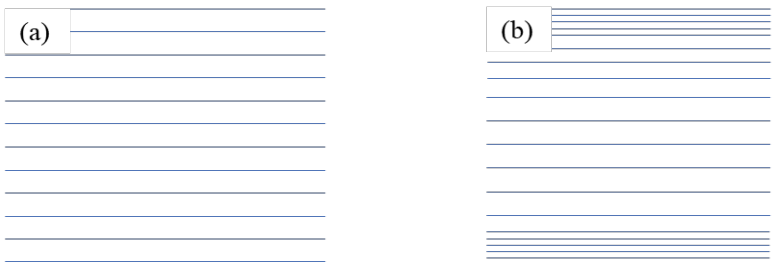

Figure 4.19 Schematic shows the difference between presence solid top and bottom layer (a) Schematic of [0/100%T/0]; (b) Schematic of [1/100%T/1].

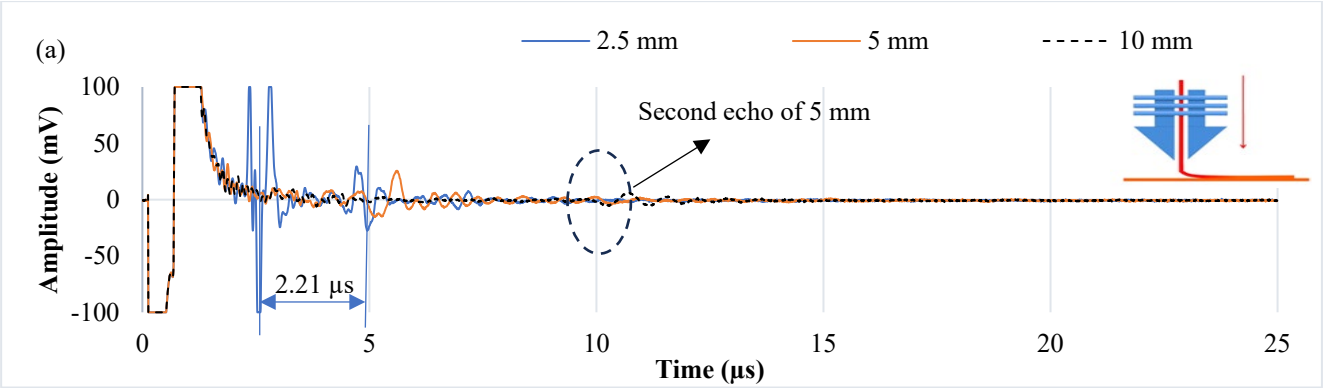

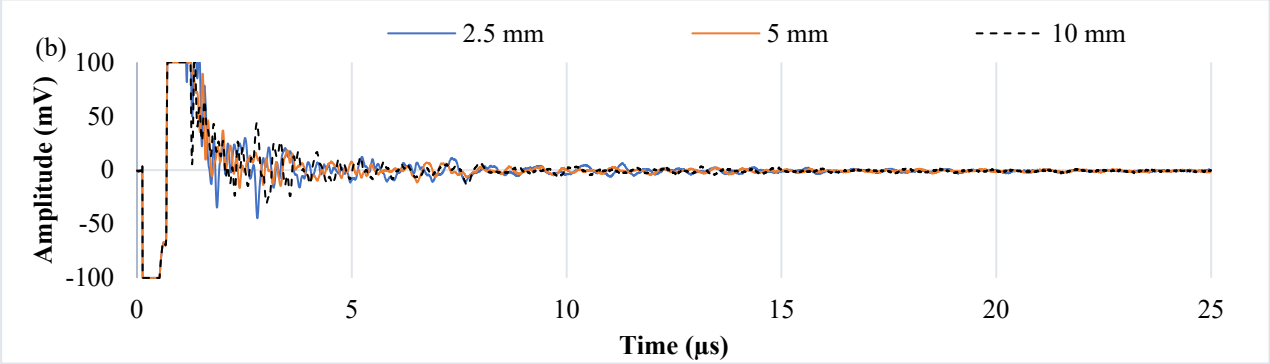

Figure 4.20 (a) Time history of [‖ :0/100%G/0] test of different thicknesses of 2.5, 5, and 10 mm. No peaks can be detected in 10 mm, which means thickness cannot be measured using ultrasound; (b) Time history of [⊥ : 0/100%G/0] test of different thicknesses of 2.5, 5, and 10 mm. No peaks can be detected in all thicknesses which means thickness cannot be measured using ultrasound.

As shown in Table 4.11, the thickness is calculated and compared with caliper reading by multiplying half the time difference by the speed of sound of red PLA which is 2246 m/sec.

Table 4.11 Experimental calculation test based on the time dime differences of [‖ : 0/100%T/0] of different thicknesses.

Thickness(mm)	2.5	5	10
Time difference (microseconds)	2.21	4.59	No peaks detected
Experimental calculation (mm)	2.48	5.15	No peaks detected
Caliper reading (mm)	2.48	4.98	9.90
Difference between caliper and experimental (mm) [%]	0[0%]	0.17[-3.3%]	No peaks detected

[%] = [(Caliper- Experimental)/Caliper × 100%]

The surface finish of the [‖ : 0/100%T/0] is smoother than the surface finish of the [‖ : 0/100%G/0] sample, which is the reason for the ability to measure up to 5 mm. In addition, the surface finish of the [⊥ : 0/100%T/0] is rough, which prevents the ultrasound wave from propagating.

C. Effect of measurement axis with respect to printing axis (side wall)

Another group sample was printed with [1/100% T/1] to investigate the effect of the side wall, now with the transducer perpendicular to the printing axis (Figure 3.1). In this case, no discernible echoes could be detected at any thickness (Figure 4.21). The implication of this is that ultrasound cannot be used for thickness measurements with this configuration (triangle infill and transducer perpendicular to the print axis). The reason behind that is the mismatch in pattern between the outer wall and the infill is high enough to cause energy losses.

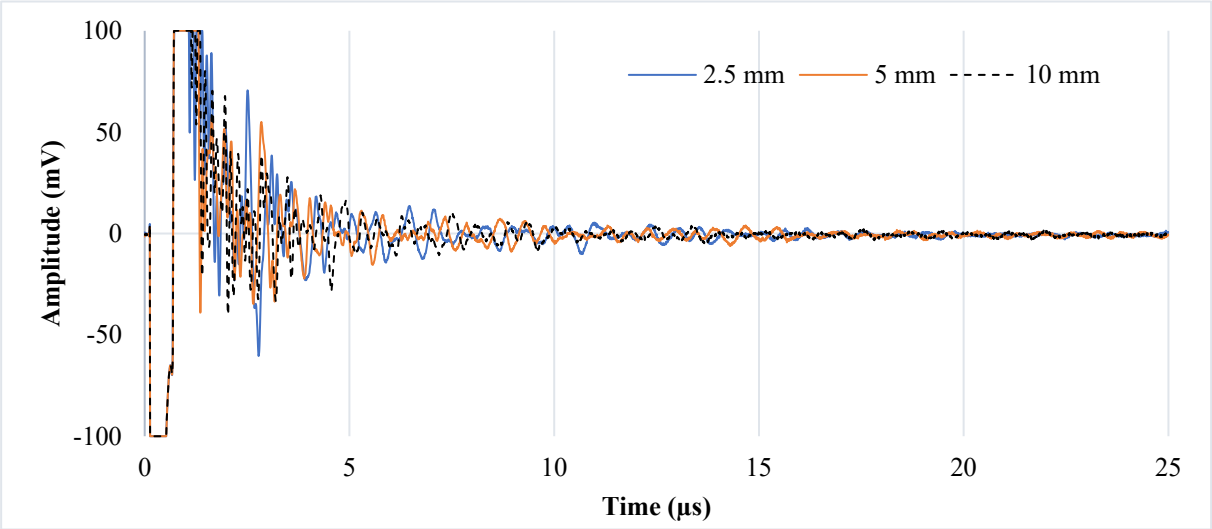

Figure 4.21 Time history of [⊥: 1/100%T/1]test of different thicknesses of 2.5, 5, and 10 mm. No peaks can be observed at all thicknesses.

The trend continues for the [∥:1/100%T/1] sample; the first and last echoes can be identified for all thicknesses of the parallel test, except for the 20 mm sample. On the other hand, nothing can be identified for the perpendicular test in the presence of side wall. This is worse than for the equivalent perpendicular test for the concentric infill, [⊥ : 1/100%C/1]. However, in the sample printed without any solid top and bottom layers [∥: 0/100%T/0], the echoes can be identified only in the 2.5 mm and 5 mm thicknesses, which is better than the equivalent test for the grid infill, [∥: 0/100%G/0]. No discernible peaks could be detected for the perpendicular test without any side wall tests for both triangle [⊥ : 0/100%T/0] and grid [⊥ : 0/100%G/0].

4.5.4. Zig zag infill

Zig zag infill pattern, as illustrated in Figure 3.3, is a widely preferred choice for infilling complex

shapes that do not require exceptionally high mechanical properties, especially when compared to mechanical properties achievable with concentric infill patterns [94]. Additionally, the zigzag pattern offers the advantage of providing a visually pleasing appearance to the printed object, making it an attractive option for applications where aesthetics is important.

A. Effect of thickness

One sample of [‖: 1/100% Z/1] is printed and investigated with transducer oriented parallel to the printing axis (Figure 3.1). First and last echoes can be identified in all thicknesses except for the 20 mm thickness (Figure 4.22).

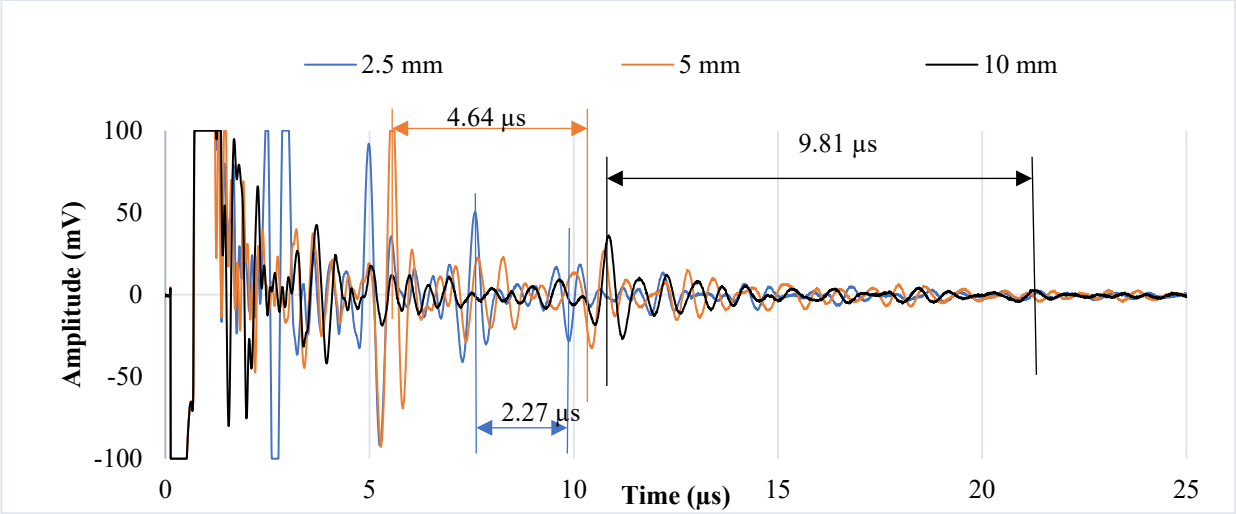

Figure 4.22 Time history of [‖ :1/100%Z/1] test of different thicknesses of 2.5, 5, and 10 mm.

To calculate the thickness of the samples, half the time difference between peaks is multiplied by the speed of sound of red PLA (2200 m/sec) (Table 4.12).

Table 4.12 Experimental calculation test based on the time differences of the [‖: 1/100%Z/1] test with different thicknesses.

Sample measurement	Sample thickness (mm)		
	2.5	5	10
Experimental calculation (mm)	2.50	5.10	10.79
Caliper reading (mm)	2.50	4.96	9.96
Difference between caliper and experimental (mm)[%]	0[0%]	0.14[-2.8%]	0.83[-7.7%]

[%] = [(Caliper- Experimental)/Caliper × 100%]

As before, the differences between caliper and experimental calculations increase as the thickness of the sample increases. However, there is an unexpected peak in the 5 mm window which indicates a 2.5 mm thickness. This is because the step gauge sample is printed with 2.5 mm thickness at the beginning and then another 2.5 mm is added to reach to 5 mm thickness. This has the effect of creating an interlayer in between. The same trend continues as before since top/bottom layers are present; the surface is smooth with low discontinuity which enables propagation up to 10 mm.

B. Effect of presence of solid top and bottom layers

To study the effect of solid top and bottom layers, (Figure 4.23), two samples are printed without top/bottom or side wall layers to be tested in parallel and perpendicular to the printing axis. The first and last echoes in the parallel test can be identified for all thicknesses except for 20 mm, Figure 4.24. However, the only thickness in the perpendicular test where echoes can be identified is 2.5 mm, as shown in Figure 4.25. The same approach is used to calculate the thickness of the samples (Table 4.13).

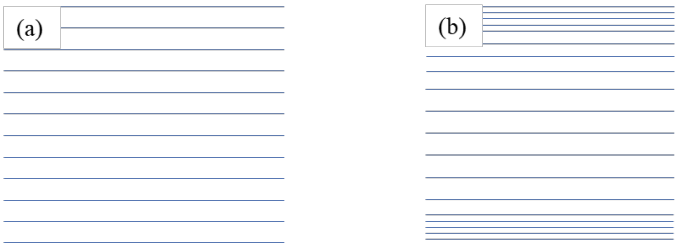

Figure 4.23 Schematic shows the difference between presence solid top and bottom layer (a) Schematic of [0/100%Z/0]; (b) Schematic of [1/100%Z/1].

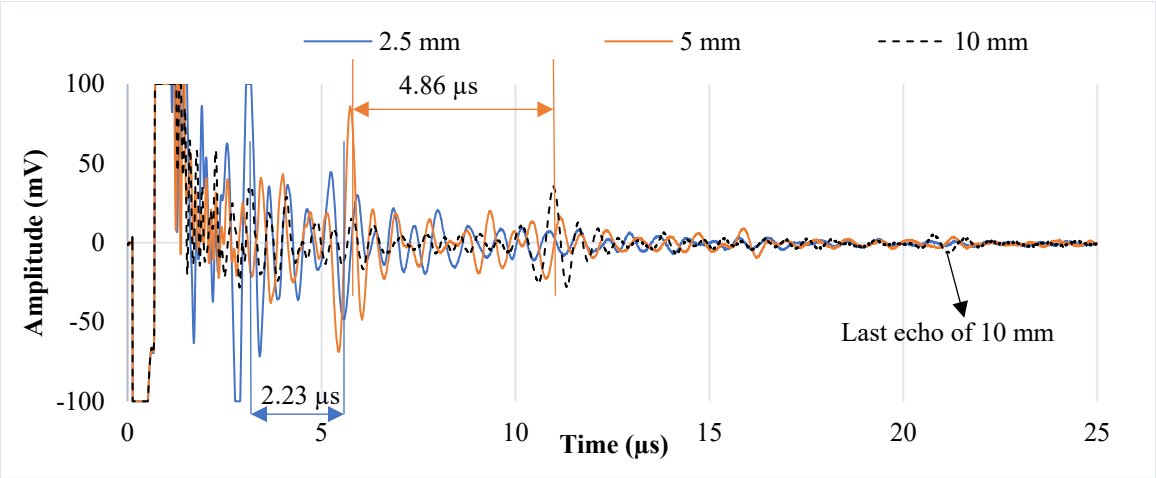

Figure 4.24 Time history of [‖ : 0/100%Z/0] test of different thicknesses of 2.5, 5, and 10 mm.

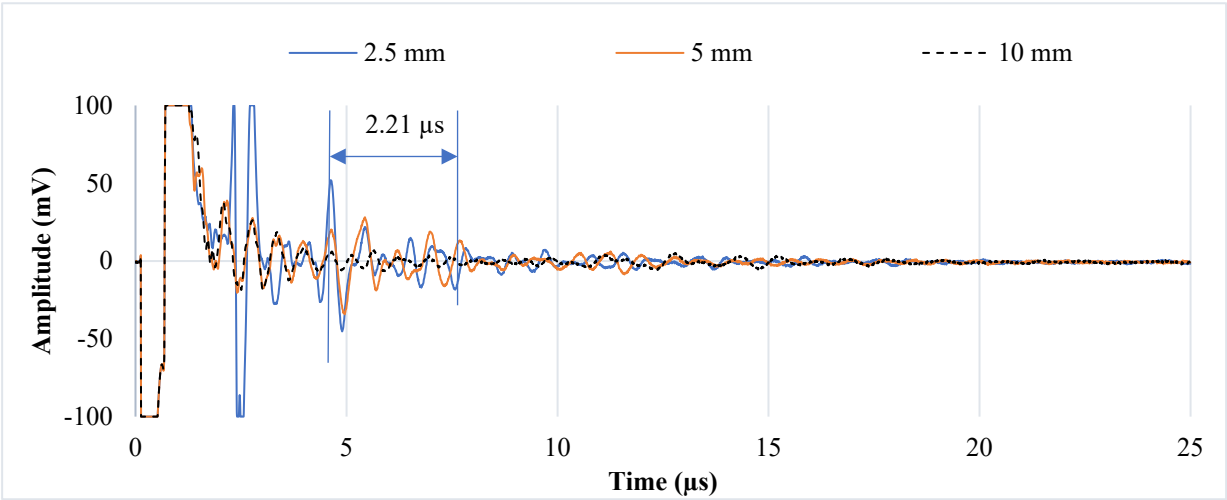

Figure 4.25 Time history of [⊥: 0/100%Z/0] test of different thicknesses of 2.5, 5, and 10 mm. No peaks can be detected in thicknesses other than 2.5mm.

Table 4.13 Experimental calculation test based on the time differences of [∥ and ⊥: 0/100%Z/0] test of different thicknesses.

Transducer position in respect to the printing axis	Parallel to printing axis			Perpendicular to printing axis
Sample Thickness(mm)	2.5	5	10	2.5
Time difference (microseconds)	2.23	4.86	9.86	2.21
Speed of sound (m/sec)	2200	2200	2200	2246
Experimental calculation (mm)	2.45	5.34	10.85	2.48
Caliper reading (mm)	2.47	4.97	9.95	2.48
Difference between caliper and experimental (mm) [%]	0.02[0.7%]	0.37[-3.9%]	0.90[-8.3%]	0[0%]

[%] =[(Caliper- Experimental)/Caliper × 100%]

The surface finish of the of [∥ : 0/100%Z/0] is smooth, the same as of [∥ :0/100%C/0]. This enables propagation up to 10 mm. On the other hand, the surface finish of the sample without side walls of [⊥: 0/100%Z/0] is rougher and it follows that propagation is only up to 2.5 mm.

C. Effect of transducer orientation with respect to the printing axis (side wall)

To study the effect of orientation of the measurement axis, another sample was printed and tested with the transducer oriented perpendicular to the printing axis in present of side wall layers. As shown in Figure 4.26, the echoes can be detected up to 10 mm, which is better than for the comparable case of [⊥: 1/100%C/1].

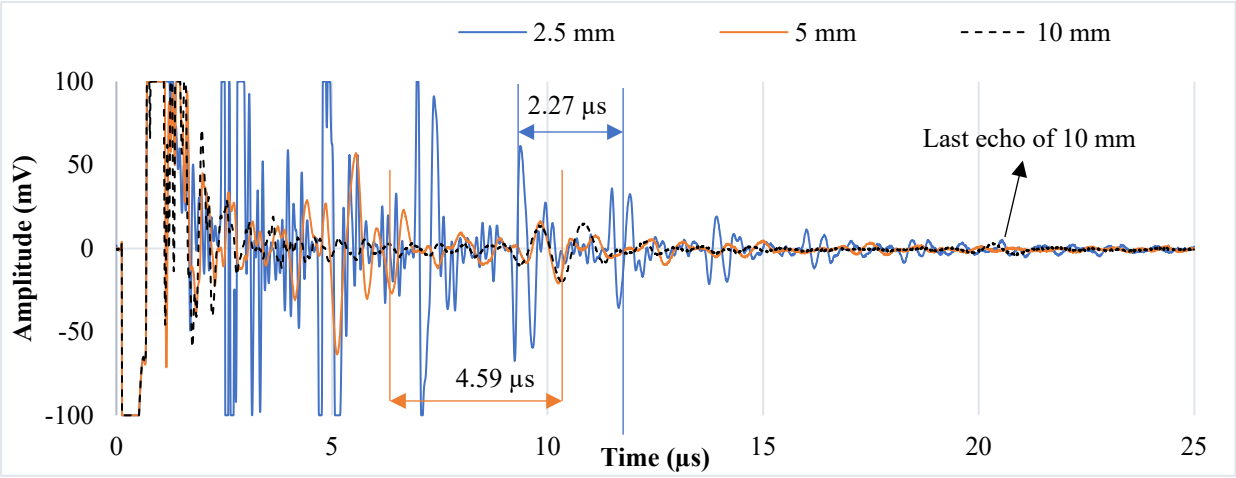

Figure 4.26 Time history of [⊥ : 1/100%Z/1] test of different thicknesses of 2.5, 5, and 10 mm.

The thickness of the sample is calculated by multiplying half the time difference by the speed sound (2200 m/sec) of red PLA, as shown in Table 4.14.

Table 4.14 Experimental calculation test based on the time differences of [⊥ : 1/100%Z/1] test of different thicknesses.

Sample thickness(mm)	2.5	5	10
Time difference (microseconds)	2.27	4.59	9.80
Experimental calculation (mm)	2.50	5.05	10.78
Caliper reading (mm)	2.50	4.96	9.98
Difference between caliper and experimental (mm)	0[0%]	0.09[-1.8%]	0.80[-7.4%]

[%] = [(Caliper- Experimental)/Caliper × 100%]

The echoes are clear and can be detected for samples up to 10 mm thickness, with the presence of side wall layers. The zig zag infill pattern bears a strong resemblance to the side wall printing pattern. Hence, there is little loss of energy at the interface of the top/bottom layers with the infill, contributing to clear echoes.

As with other infill patterns, the echoes are clear in the parallel test, up to the 10 mm thickness. However, the difference between [1/100%Z/1] and [1/100%C/1] is in the perpendicular test. In this case, with the zig zag infill, the wave can penetrate up to 10 mm in the perpendicular test [⊥: 1/100%Z/1. However, for the [⊥: 1/100%C/1] case, the only thickness where the echoes were detected was the 2.5 mm thickness, and even then, only with the use of a digital filter. For the parallel test, the echoes of [‖:0/100%Z/0] are clear and can be detected up to 10 mm, which is the same as for [‖ : 0/100%C/0]. However, for the perpendicular test with the zig zag infill [⊥: 0/100%Z/0], the echoes can be detected only in 2.5 mm, while in [⊥: 0/100%C/0] up to 10 mm thickness.

5. Results of Erosion

In this chapter, the erosion rate monitored by using ultrasound is studied. By using a flat sample with specific thicknesses fixed by 3D printed holder and mechanical holder under the effect of 5000 psi of mixed slurry water, erosion is monitored over a specific time. Samples of 6 and 5 mm thicknesses are tested to verify the results of the erosion test.

Two samples are printed with Ultimaker 2+, then clamped to the printed transducer holder. Underneath the sample in the transducer holder, there is a place for the transducer to be placed, away from the waterjet. Two other mechanical clamps are used to clamp the sample and holder to the waterjet bed table. Data is recorded during the waterjet test. The speed of sound in the pink, and blue PLA of the printed samples is 2100 m/sec. The time differences between the peaks are measured, as shown in Figure 5.1. The thicknesses of all samples are calculated prior to running the jet, Table 5.1.

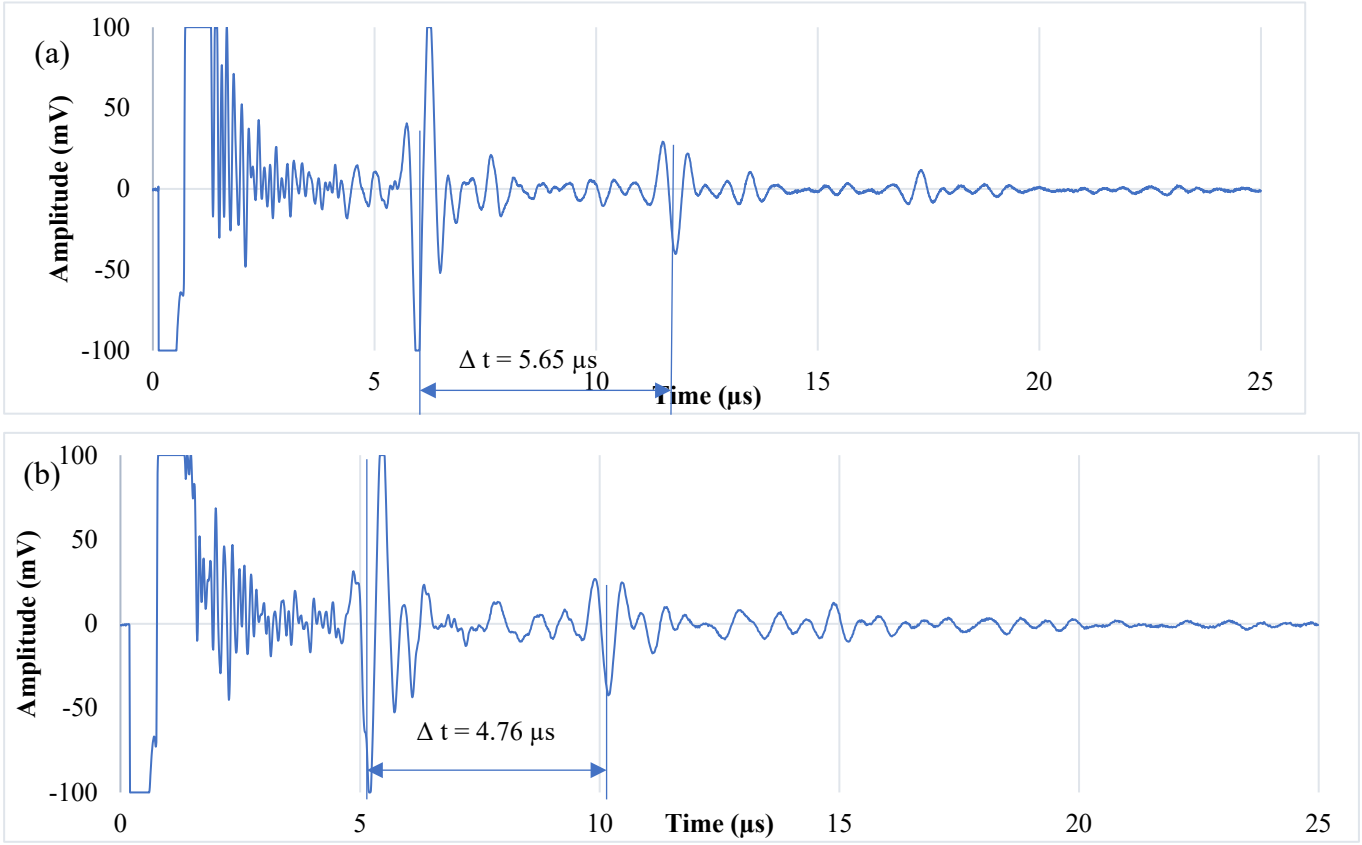

Figure 5.1 Ultrasound response of samples of different thicknesses to show the time differences between peaks to calculate the sample thicknesses (a) Time history of 6 mm sample of [‖ :0/100%C/0] before erosion test; (b) Time history of 5 mm sample of [‖ :0/100%C/0] before erosion test.

Table 5.1 Experimental calculation of [‖: 0/100%C/0] test of different thicknesses before running the water jet.

Sample measurement	Sample thickness (mm)	
	First Sample	Second Sample
Nominal thickness (mm)	6	5
Caliper reading (mm)	5.93	5
Experimental calculation (mm)	5.93	5
Difference between caliper and experimental (mm) [%]	0[0%]	0[0%]

[%] = [(Caliper- Experimental)/Caliper × 100%]

The pump is operated at 5000 psi to deliver slurry water (a mixture of water and garnet) from a nozzle diameter of 1 mm. At the same time, the head of the pump is moved forwards and backwards along a line at 20 mm/sec. At each minute, the data are exported and analyzed. After one minute of the waterjet test, almost nothing has changed; ultrasound time differences extracted are almost the same as at the start of the test, indicating no erosion has taken place. However, the amplitudes of the peaks become lower, and some noise starts to appear. After three minutes of the waterjet test, some material has been removed from the sample and the time difference between the peaks becomes smaller, as shown in Figure 5.2. As illustrated in Figure 5.3, the same trend continues with additional sample material being removed as the waterjet test progresses. After the loss of approximately the first millimeter, the time difference between peaks decreases significantly, indicating significant removal of material. The thickness of the samples and the percentage of material removal are calculated, as shown Table 5.2. After the erosion test is performed, the samples are removed from the holder and the depth of the material removal area is measured and compared with the final calculated values.

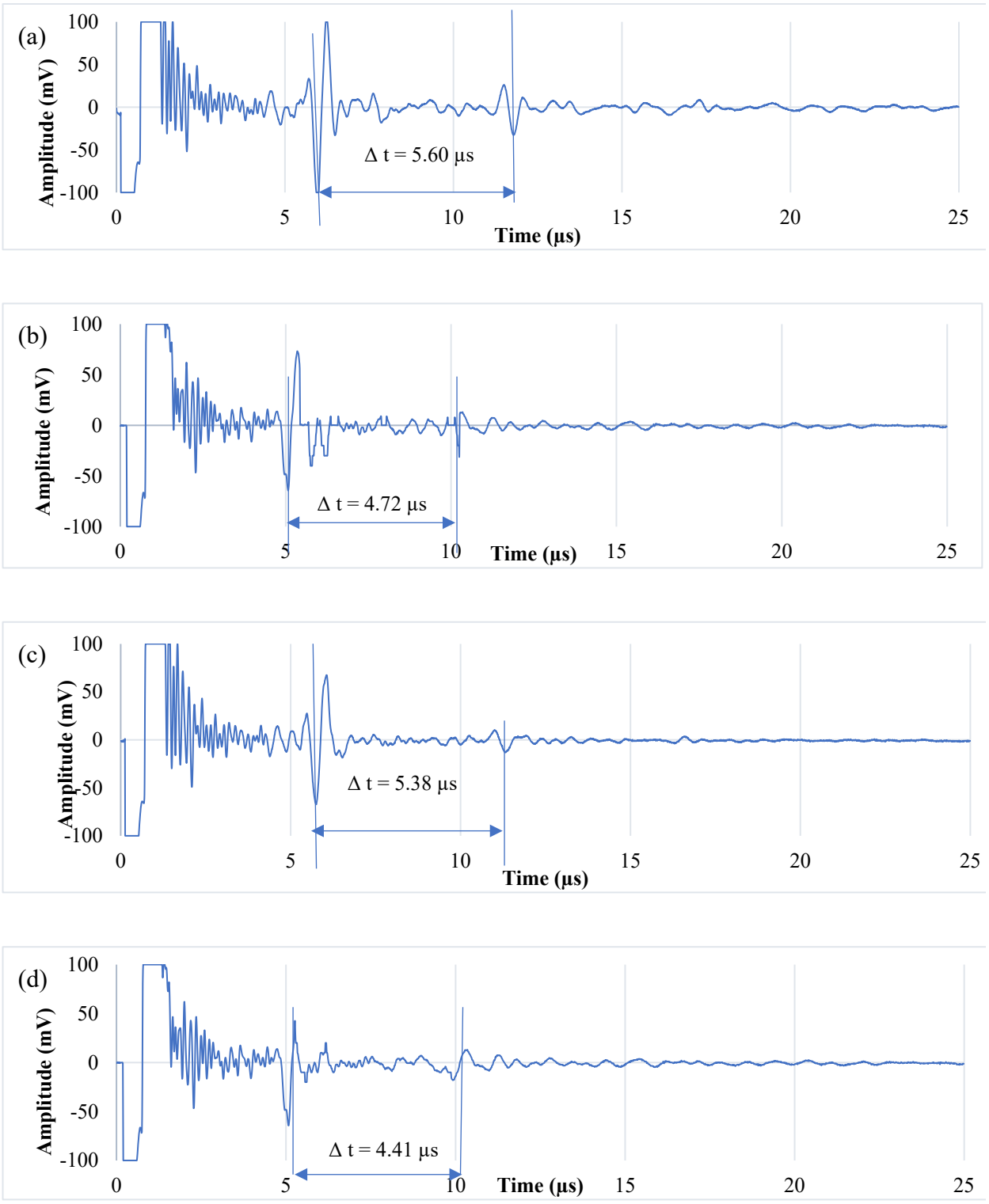

Figure 5.2 Time history of 6 and 5 mm thicknesses to show the time differences between peaks to calculate the sample thicknesses of [‖ :0/100%C/0] (a) after one minute of waterjet test of 6 mm sample; (b) after one minute of waterjet test of 5 mm sample ; (c) after three minutes of waterjet test of 6 mm sample : (d) after three minutes of waterjet test of 5 mm sample

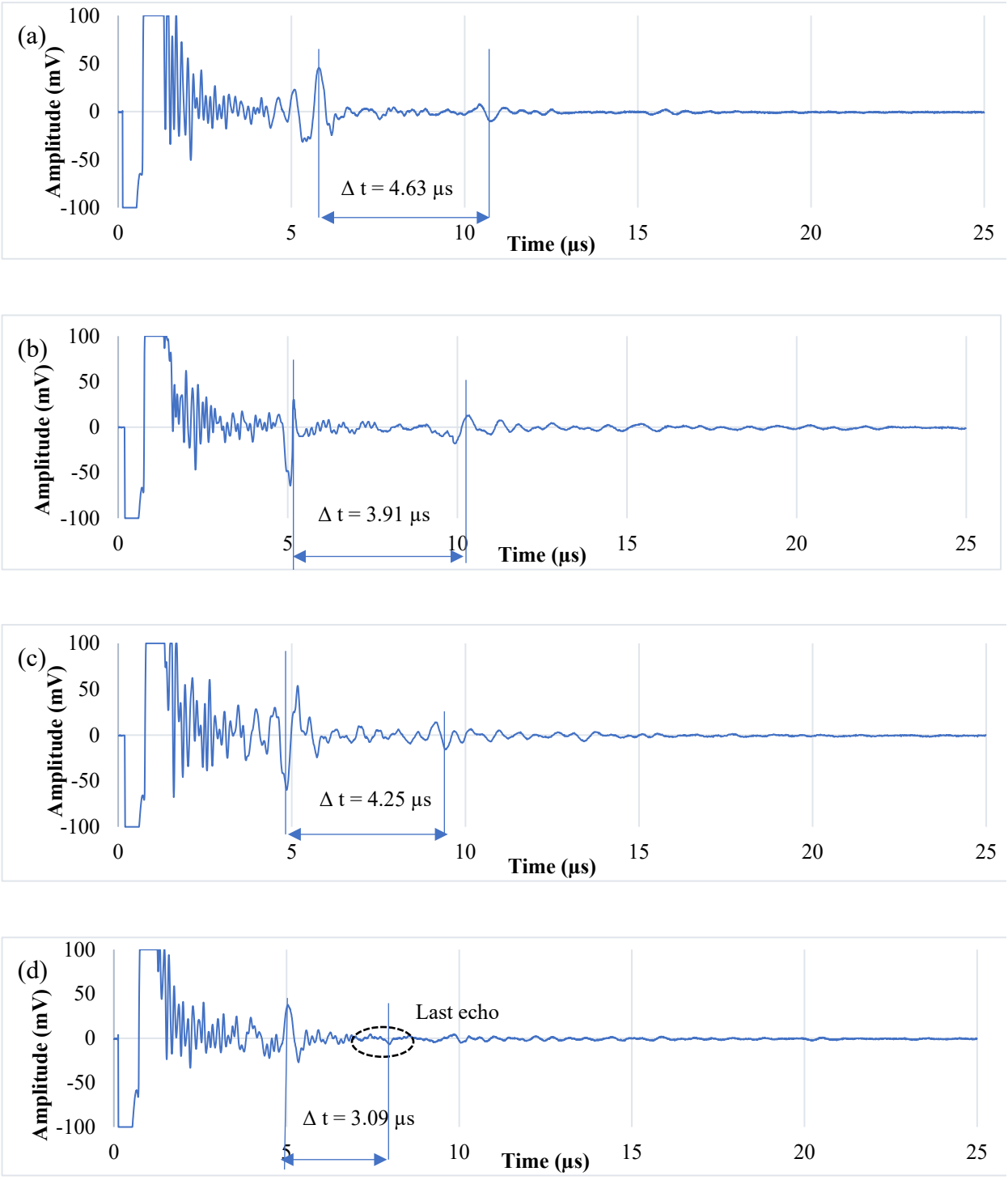

Figure 5.3 Time history of 6 and 5 mm thicknesses to show the time differences between peaks to calculate the sample thicknesses of [‖ :0/100%C/0] (a) after five minutes of waterjet test of 6 mm sample; (b) after five minutes of waterjet test of 5 mm sample; (c) after six minutes of waterjet test of 6 mm sample; (d) after six minutes of waterjet test of 5 mm sample.

Table 5.2 Experimental calculation test based on the time differences of [‖: 0/100%C/0] erosion test of different thicknesses after one minute, three minutes, five minutes, and six minutes.

Sample measurement	Sample thickness (mm)	
	6 mm Sample	5mm Sample
Initial thickness (mm)	5.93	5
Experimental calculation after one minute (mm)	5.88	4.96
Experimental calculation after three minutes (mm)	5.65	4.63
Material removal after three minutes (mm) [%]	0.28[4.7%]	0.37[7.4%]
Experimental calculation after five minutes (mm)	4.86	4.10
Experimental calculation six minutes (mm)	4.46	3.24
Material removal after six minutes (mm) [%]	1.47[24.8%]	1.76[35%]
Caliper reading of depth of removed material (mm) [%]	1.51[25.5%]	1.72[35.2%]

From Table 5.2, it is noted that the thickness drops significantly between the fifth and sixth minutes, especially after losing the first millimeter of material.

As shown in Figure 5.4, the thickness of the sample decreased gradually after the first minute until losing the first millimetre of material. There was a significant drop in overall sample thickness between the fifth and sixth minutes, to approximately 0.9 mm in one minute in the 5mm sample. This indicates that the erosion rate increases after losing the first millimeter. To check the accuracy of the ultrasound testing, a digital caliper was used to validate the ultrasound measurements and the differences between the digital caliper were 0.04 mm.

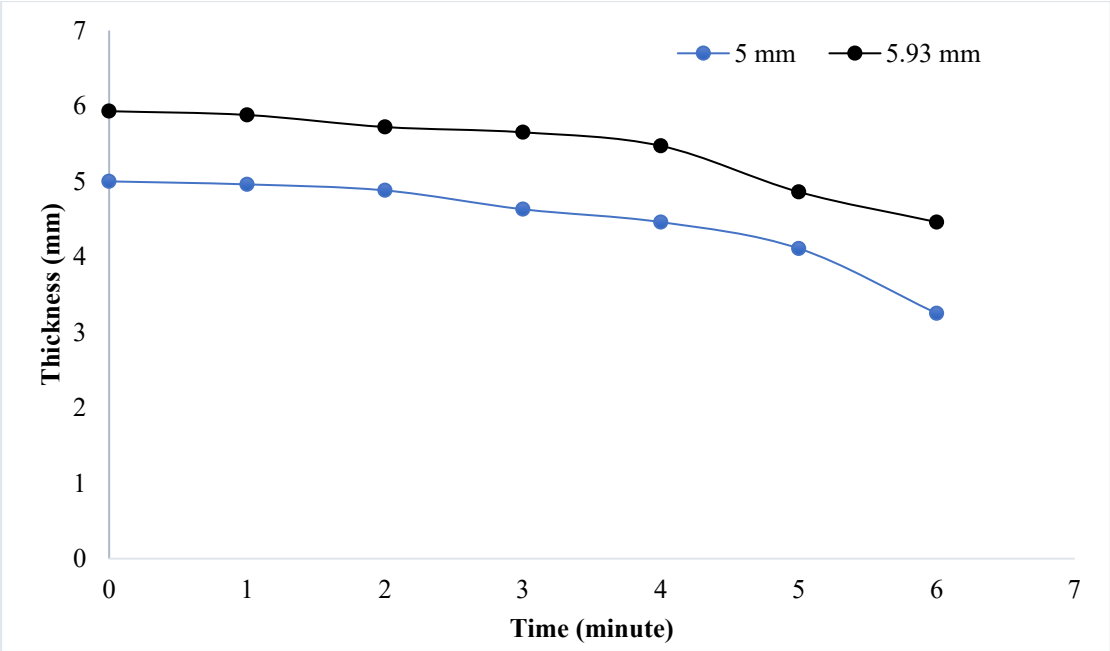

Figure 5.4 Reduction of sample thickness over the time under effect of water jet.

6. Applications

Additively manufactured parts have become integral to various industrial applications, with a subset of these products designed and produced using Fused Filament Fabrication (FFF) and PLA material. To validate the applicability of ultrasound measurements for such industrial applications, the A-scan ultrasound measuring technique is employed to gauge the thicknesses of these functional components. The obtained measurements are then compared with the nominal thicknesses, providing a comprehensive assessment of the precision and reliability of ultrasound testing in the context of additively manufactured functional parts, particularly those created through FFF with PLA material. This comparison serves as a crucial step in ensuring the efficacy and suitability of ultrasound measurement techniques for quality assurance in industrial utilization of additively manufactured components. To demonstrate applicability to industrial parts, a pipe, a heat exchanger and a gear mold were selected for evaluation of applicability of ultrasound testing.

6.1. Pipe

For some aerospace applications, some pipes are designed and printed by 3D printing techniques. To validate the ultrasound measurements for typical aerospace applications, pipes of 38.1 mm(1.5inches), used in vent and marine system, and 101.6 mm (four inches) diameter, used for drain purposes, are printed by white PLA and measured by ultrasound testing to verify their thickness [95], [96]. For each diameter pipe, samples were printed with 2.5mm wall thickness (suitable for transporting liquids and gases) and 3.5mm wall thickness (suitable for transporting fluid). The different pipe diameters are an opportunity to examine the influence of part curvature on the measurement process. As depicted in Figure 6.1 the peaks are clearer in the larger pipes of different thicknesses. This is to be expected since larger diameter pipes will have smaller curvatures, hence the outer surface on which ultrasound measurements are taken will be flatter and a better connection to the transducer is likely. The peaks in the 38.1 mm diameter pipe with 2.5 mm thickness are clearer than the peaks of the 3.5 mm thick pipe. This is to be expected since previous results demonstrated clearer peaks with thinner samples. This implies that small diameter pipes with relativity large thickness will tend to yield peaks that are not very clear and hence a digital filter should be used for such samples. To calculate the thickness of the pipes, half the time difference between peaks is multiplied by the speed of sound of white PLA (2100 m/sec) and compared with nominal thickness as shown in Table *6.1*.

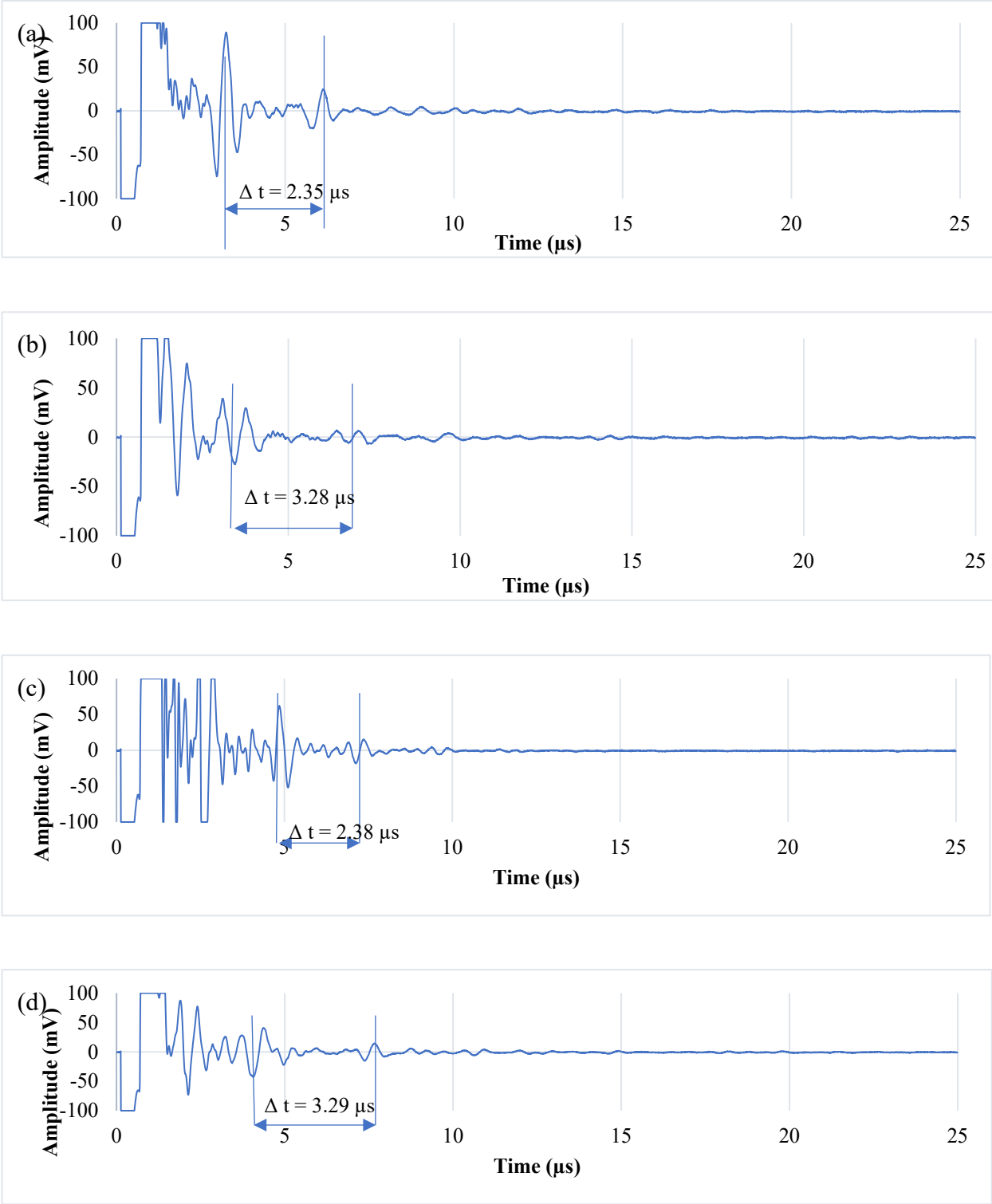

Figure 6.1 Time history of [⊥ :0/100%C/0] printed pipe test to show the time differences used to calculate the thicknesses (a) Time history of 38.1 mm pipe with 2.5 mm thickness; (b) Time history of 38.1 mm pipe with 3.5 mm thickness; (c) Time history of 101.6 mm pipe with 2.5 mm thickness; (d) Time history of 101.6 mm pipe with 3.5 mm thickness.

Table 6.1 Experimental calculation test based on the time differences of [⊥ :0/100%C/0] test of printed pipes with different diameters and thicknesses.

Sample measurement	Sample thickness (mm)			
	38.1 mm diameter pipe (1.5 inches)		101.6 mm diameter pipe (4 inches)	
Experimental calculation (mm)	2.47	3.45	2.5	3.45
Nominal thickness (mm)	2.50	3.5	2.5	3.5
Difference between nominal and experimental (mm)[%]	0.03[1.2%]	0.05[1.42%]	0.0[0%]	0.05[1.42%]

[%] =[(Nominal- Experimental)/Nominal × 100%]

6.2. Heat exchanger

To enhance the efficiency of a heat exchanger, efforts are being made to maximize the contact surface area with the working fluid. Achieving this goal requires the design of complex components within the heat exchanger, which can be challenging to fabricate using conventional manufacturing methods. In response to this challenge, 3D printing techniques are being utilized [97], [98]. One specific design involves a heat exchanger featuring a helical inner case within a cylindrical outer case. The nominal thickness of both the inner and outer cases is set at 3.5 mm, as shown in Figure 6.2. The exchanger is designed and printed by white PLA. Ultrasound testing could be used to check the thickness of the inner and outer cases, and this could be useful for monitoring the structure during operation to ensure the thickness remains within an allowable range. The data is extracted from the ultrasound testing as shown in Figure 6.3 and to calculate the thickness of the exchanger cases, half the time difference between peaks is multiplied by the speed of sound of white PLA (2100 m/sec) and compared with nominal thickness measured with calipers. Results are shown in Table 6.2.

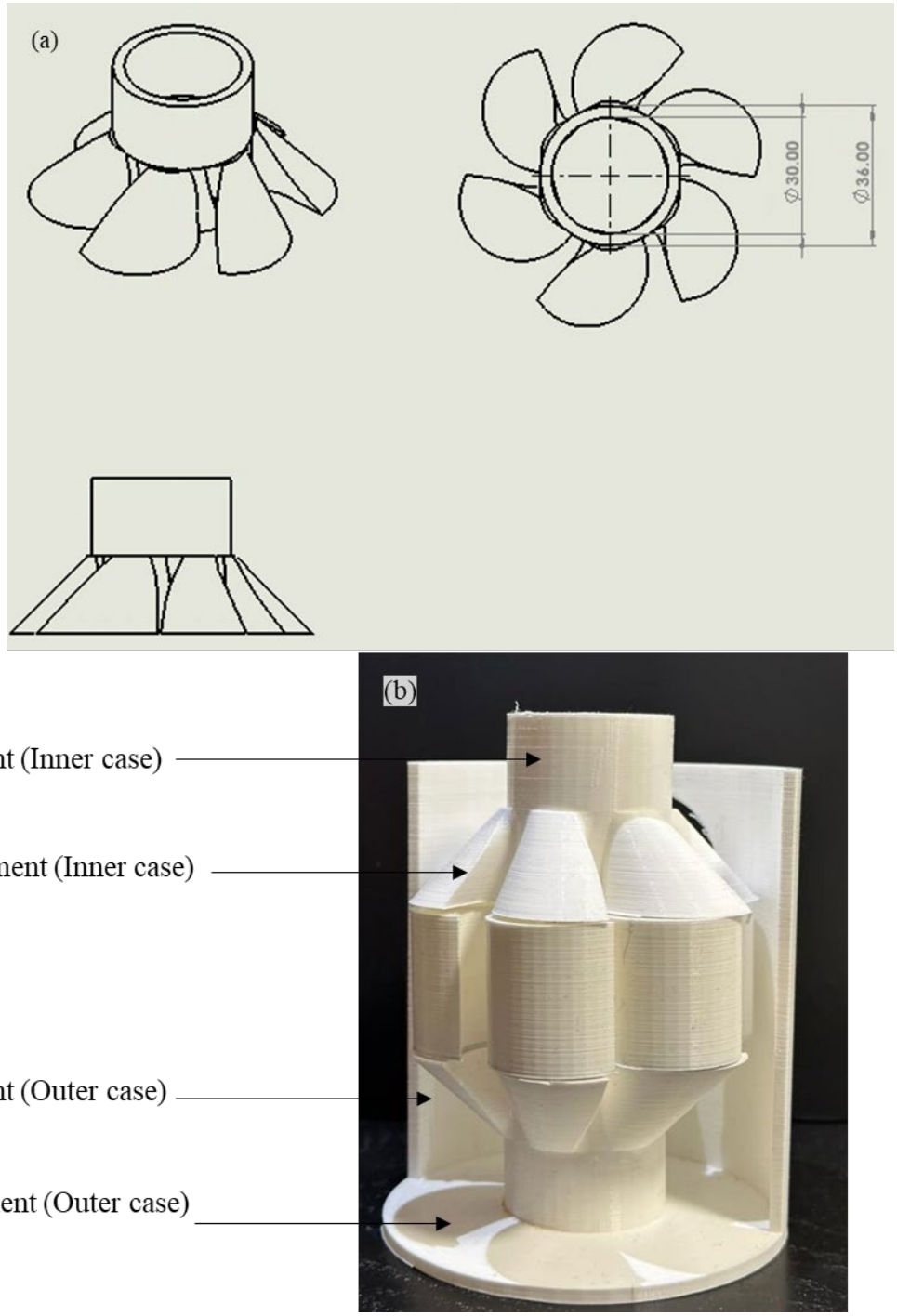

Figure 6.2 (a) 2D drawing of the inner case of heat exchanger; (b) FFF assembly of printed heat exchanger for ultrasound testing purposes.

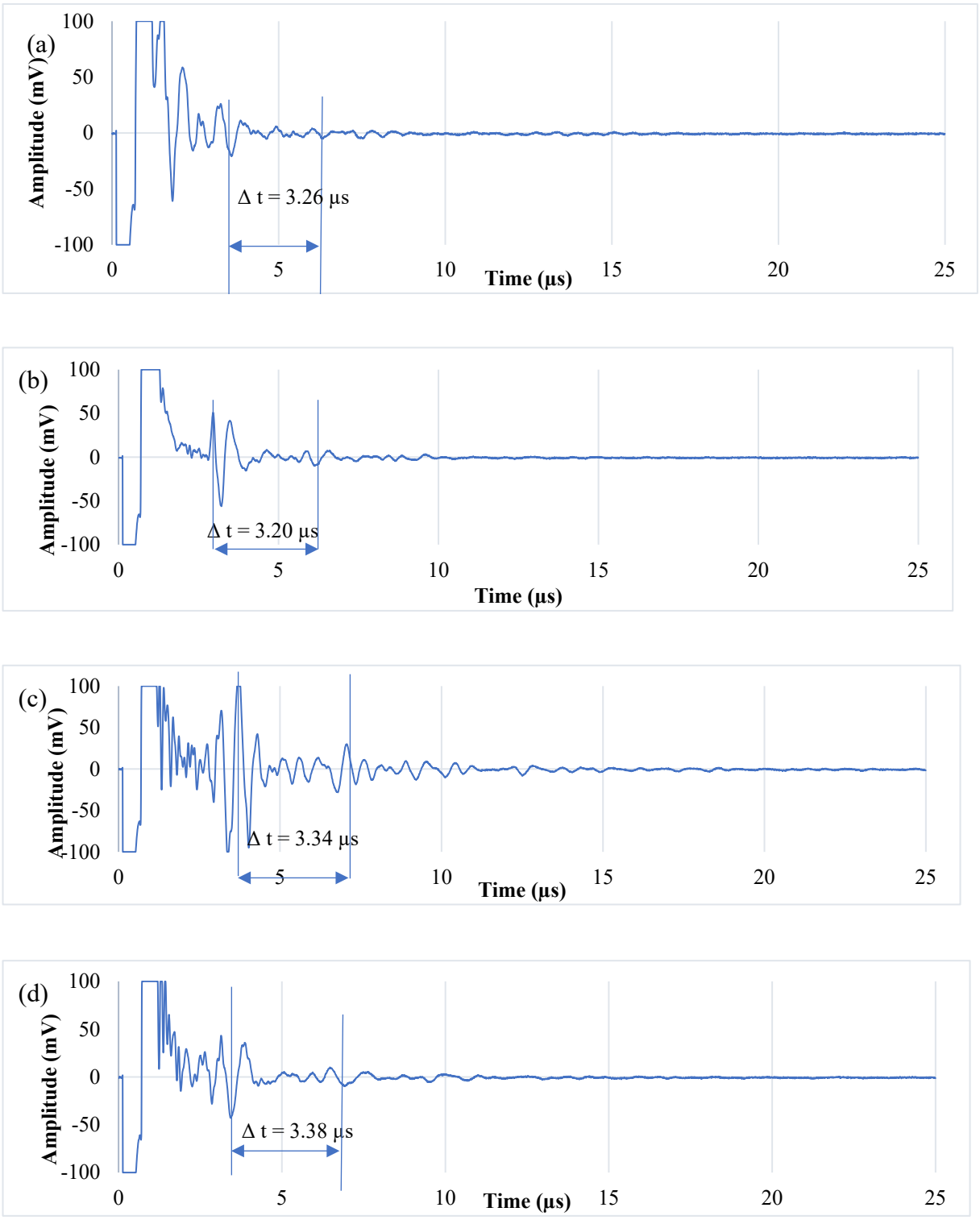

Figure 6.3 Time history of [⊥ :0/100%C/0] printed heat exchanger test to show the time differences used to calculate the thicknesses (a) Time history of pipe of the inner helical case [⊥: 0/100%C/0]; (b) Time history of inner helical case [⊥ :0/100%C/0] ; (c) Time history of side outer case [⊥ :0/100%C/0]; (d) Time history of bottom side outer case [‖ :0/100%C/0].

Table 6.2 Experimental calculation test based on the time differences of [0/100%C/0] test of printed heat exchanger from different positions.

Sample measurement	Sample thickness (mm)			
	Pipe of helical inner case	Helical inner case	Side outer case	Bottom of outer case
Experimental calculation (mm)	3.42	3.36	3.50	3.54
Nominal thickness (mm)	3.5	3.50	3.50	3.50
Difference between caliper and experimental (mm) [%]	0.08[2.3%]	0.14[4.0%]	0[0%]	0.31[-1.13%]

[%] = [(Nominal- Experimental)/Nominal × 100%]

The experimental calculations demonstrate that there is excellent agreement between the nominal (caliper measured) thickness and the ultrasound testing calculations. Notable that, at Figure 6.3 (a) the peaks are not very clear as others. This is matched with Figure 6.1 findings, which indicated that by increasing thickness of the high curved sample, the peaks will not be very clear.

6.3. Gear molds

Using 3D printing techniques allows for the production of complex shapes from different materials. As a form of mass production, products can be manufactured using injection molding with custom 3D printed molds [99]. Additive manufacturing can easily produce complex molds, which facilitates the mass production of products such as gears, Figure 6.4. Here, a gear mold is designed and printed based on a specified thickness. The mold is printed with blue PLA as the inner spur mold thickness is 3.5 mm and the outer case thickness is 7 mm. Ultrasound testing is then be used to verify the specifications of the mold by placing the transducer on the outer wall of the mold either in the middle to specify the inner spur thickness or on the sides to measure outer case thickness, which in turn helps to ensure the quality of the final part. Figure 6.5 shows the ultrasound results used to calculate the thickness of the mold. As before, half the time difference between peaks is multiplied by the speed of sound of white PLA (2100 m/sec), results are as shown in Table 6.3.

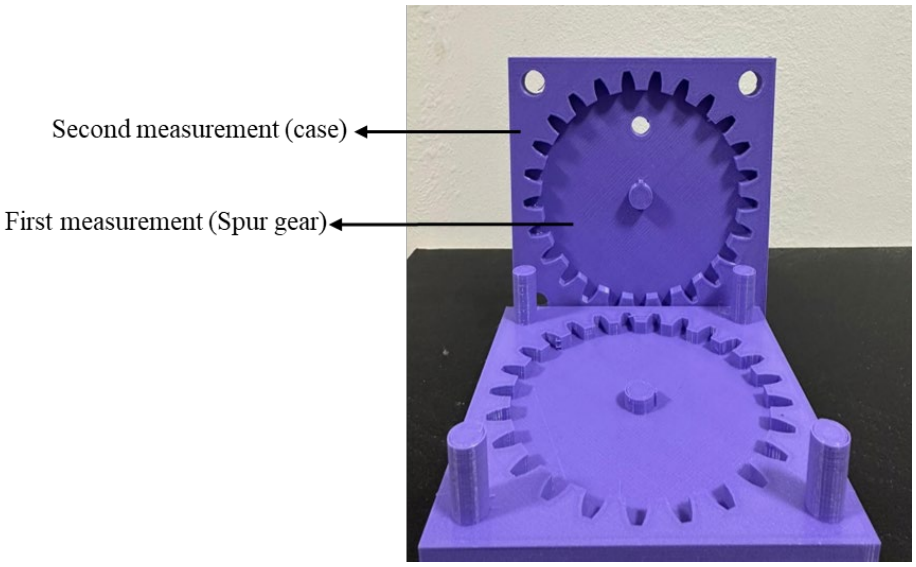

Figure 6.4 FFF assembly of printed gear mold for ultrasound testing purposes.

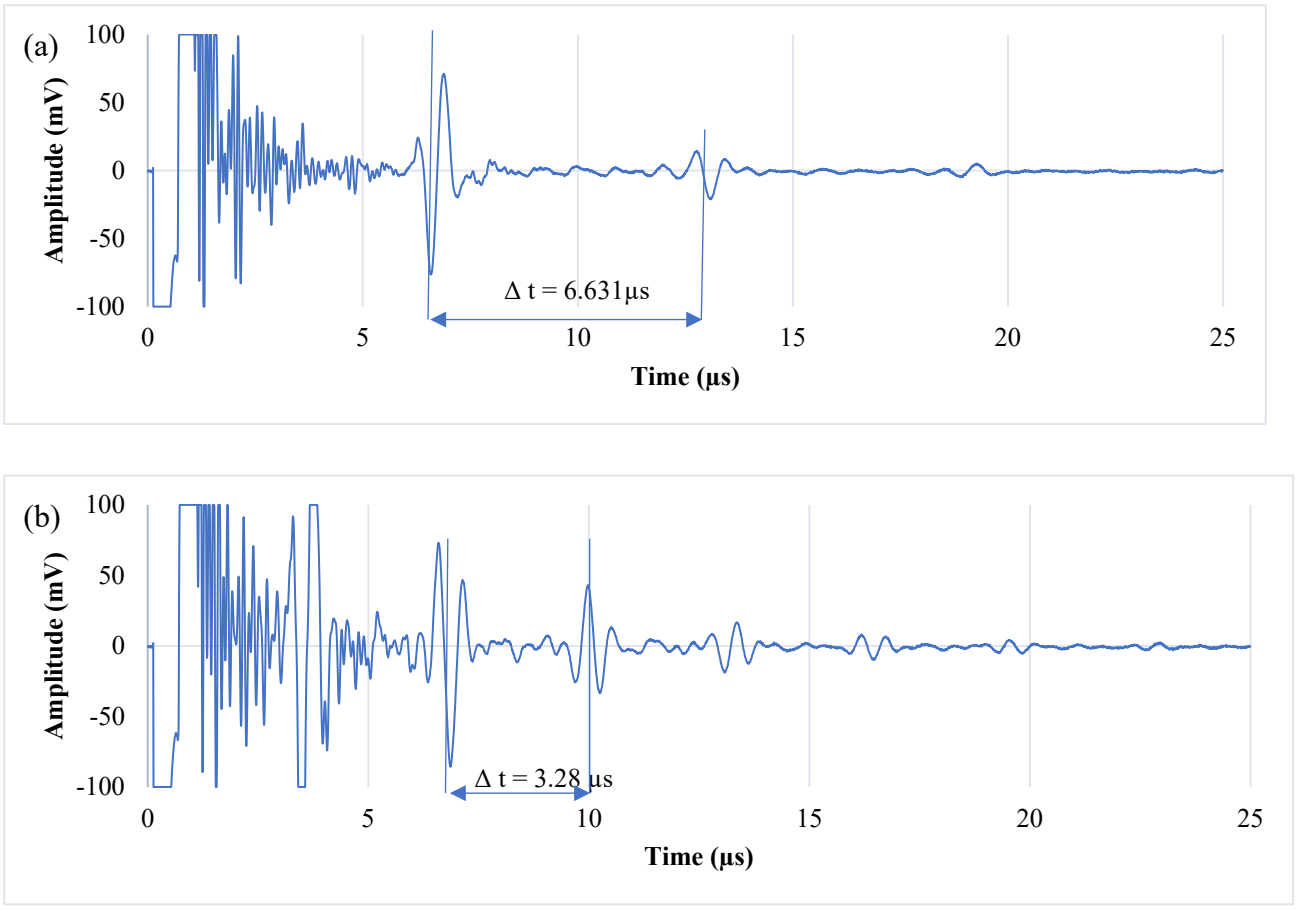

Figure 6.5 Time history [‖ :0/100%C/0] of printed gear mold test to show the time differences used to calculate the thicknesses (a) Time history of gear case; (b) Time history of spur.

The peaks are very clear with high amplitudes, Figure 6.5. This is to be expected since the transducer is oriented parallel to the printing axis.

Table 6.3 Experimental calculation test based on the time differences of [‖ :0/100%C/0]; test of printed gear mold from different positions.

Sample measurement	Sample thickness (mm)	
	Spur gear	Case
Experimental calculation (mm)	3.44	6.96
Nominal thickness (mm)	3.5	7.0
Difference between caliper and experimental (mm)[%]	0.06[1.71%]	0.04[0.57%]

[%] =[(Nominal- Experimental)/Nominal × 100%]

7. Summary and conclusions

7.1. Conclusion

In this thesis, we evaluated the application of a 10 MHz ultrasound contact transducer on the thickness measurement of parts fabricated by FFF. Results showed that ultrasound testing is very sensitive to 3D printing parameters such as infill pattern, sample thickness and orientation, etc. The 10 MHz transducer is sufficiently accurate for measuring the thickness of the FFF 3D printed parts (with nozzle diameter of 0.4 mm) up to 5 mm. However, for parts equal or thicker than 10 mm, there were noticeable differences between the caliper and ultrasound test readings, indicating a higher level of measurement error. Samples printed with all concentric infill pattern showed reliable results in both orientations of the transducer. We also studied the effect of transducer orientation, both parallel and perpendicular relative to the printing axis. It was observed that measurements taken perpendicular to the printing axis generally exhibited lower validity, particularly when a side wall was present.

An infill percentage study was also performed, and the results revealed that as the infill percentage decreases, the thickness measurement capability of the ultrasound testing decreases, leading to a loss of accuracy for thickness measurements. Through studying the effect of the infill patterns such as grid, triangle, and zig zag, it was demonstrated that all infill patterns with the presence of a top and bottom layer and with the transducer parallel to the printing axis measurements, were unreliable for measurements beyond 5 mm. Notably, parts printed with a zigzag infill pattern showed more consistent results with the presence of the top/bottom layer for parallel measurement and presence of side wall for perpendicular measurements. However, the ultrasound could not measure the thickness of samples printed with the all-triangle infill pattern and no side walls, with transducer perpendicular to the printing axis. The samples printed with the all-concentric infill pattern yields the most accurate results for both orientations of the transducer. Zigzag, triangle, and grid infill patterns demonstrated the same validity only with the transducer placed parallel to the printing axis. Among the different infill patterns, the concentric infill consistently provided the most reliable results.

Additionally, to evaluate the application of ultrasound testing in thickness monitoring in an industrial field, an erosion test was simulated, and ultrasound was used to measure the thickness of

3D printed samples in real time. Ultrasound testing was utilized to monitor the thickness loss due to slurry water erosion over time. This test demonstrated the ability for ultrasound measurement to monitor erosion in real time.

Finally, to evaluate the ultrasound thickness measurement in industrial applications, some functional parts were designed and printed. Results confirmed the observations made with the stepped gauge, demonstrating the wider interpretability of the stepped gauge results. Moreover, it was found that the curvature of the part had some effect on the ultrasound results. In particular, large curvatures combined with large thicknesses could be challenging for ultrasound. Under such circumstances, ultrasound measurement could be assisted by digital filtering techniques.

In summary, this study considered the application of ultrasound testing for assessing the thickness of the 3D printed parts, shedding light on factors such as infill patterns, thickness variations, and erosion-related thickness loss. The findings underscore the importance of considering these factors in the quality assurance of 3D printed components, particularly in industrial settings.

7.2. Future work

Future work in this area could concentrate on several promising directions.

First, there is potential for exploring the use of ultrasonic testing to differentiate between parts printed with different materials or using diverse infill patterns. Research could consider the development of specialized ultrasound testing techniques that can identify and assess variations in material properties or infill patterns within a 3D printed part. Such investigations would be valuable for quality control and material characterization purposes.

Second, ultrasound testing may be able to detect and quantify the presence of foreign materials within 3D printed parts or detect any defects. This research avenue would involve developing methodologies to determine the type and quantity of foreign substances or materials embedded within the printed components. This is particularly pertinent in applications where material purity and composition are critical, such as in medical or aerospace industries.

Another extension for this work would be to use lower frequency transducers for the ultrasound thickness measurement. The current transducer with 10 MHz frequency of its elements could be at

higher bound of a suitable transducer for this application. It would be useful to use 1 and 5 MHz transducers especially for thicker 3D printed samples.

In summary, future research endeavors could extend the utility of ultrasound testing in the realm of 3D printing by addressing the challenges associated with material differentiation, infill pattern identification, and foreign material detection. These advancements have the potential to enhance the quality assessment and material characterization capabilities of ultrasound testing in the context of 3D printing technology.

8. References

[1] T. Peng, K. Kellens, R. Tang, C. Chen, and G. Chen, 'Sustainability of additive manufacturing: An overview on its energy demand and environmental impact', *Additive Manufacturing*, vol. 21. Elsevier B.V., pp. 694–704, May 01, 2018. doi: 10.1016/j.addma.2018.04.022.

[2] J. Butt, 'Exploring the interrelationship between additive manufacturing and industry 4.0', *Designs*, vol. 4, no. 2. MDPI AG, pp. 1–33, Jun. 01, 2020. doi: 10.3390/designs4020013.

[3] R. Godina, I. Ribeiro, F. Matos, B. T. Ferreira, H. Carvalho, and P. Peças, 'Impact assessment of additive manufacturing on sustainable business models in industry 4.0 context', *Sustainability (Switzerland)*, vol. 12, no. 17, Sep. 2020, doi: 10.3390/su12177066.

[4] D. R. Eyers and A. T. Potter, 'Industrial Additive Manufacturing: A manufacturing systems perspective', *Comput Ind*, vol. 92–93, pp. 208–218, Nov. 2017, doi: 10.1016/j.compind.2017.08.002.

[5] M. Jiménez, L. Romero, I. A. Domínguez, M. D. M. Espinosa, and M. Domínguez, 'Additive Manufacturing Technologies: An Overview about 3D Printing Methods and Future Prospects', *Complexity*, vol. 2019, 2019, doi: 10.1155/2019/9656938.

[6] J. Deckers, J. Vleugels, and J.-P. Kruth, 'Title Additive Manufacturing of Ceramics: A Review Author names and affiliations'.

[7] 'Which Additive Manufacturing Process Is Right for You? | manufacturing.REPORT'. Accessed: Jun. 30, 2023. [Online]. Available: https://manufacturing.report/articles/which-additive-manufacturing-process-is-right-for-you

[8] O. Abdulhameed, A. Al-Ahmari, W. Ameen, and S. H. Mian, 'Additive manufacturing: Challenges, trends, and applications', *Advances in Mechanical Engineering*, vol. 11, no. 2, Feb. 2019, doi: 10.1177/1687814018822880.

[9] S. Singh, G. Singh, C. Prakash, and S. Ramakrishna, ‘Current status and future directions of fused filament fabrication’, *Journal of Manufacturing Processes*, vol. 55. Elsevier Ltd, pp. 288–306, Jul. 01, 2020. doi: 10.1016/j.jmapro.2020.04.049.

[10] M. Delic and D. R. Eyers, ‘The effect of additive manufacturing adoption on supply chain flexibility and performance: An empirical analysis from the automotive industry’, *Int J Prod Econ*, vol. 228, Oct. 2020, doi: 10.1016/j.ijpe.2020.107689.

[11] B. Shaqour, A. Samaro, B. Verleije, K. Beyers, C. Vervaet, and P. Cos, ‘Production of drug delivery systems using fused filament fabrication: A systematic review’, *Pharmaceutics*, vol. 12, no. 6. MDPI AG, pp. 1–16, Jun. 01, 2020. doi: 10.3390/pharmaceutics12060517.

[12] M. Al-Makky and D. Mahmoud, ‘The importance of additive manufacturing processes in industrial applications.’

[13] S. L. Rodríguez-Reyna, C. Mata, J. H. Díaz-Aguilera, H. R. Acevedo-Parra, and F. Tapia, ‘Mechanical properties optimization for PLA, ABS and Nylon + CF manufactured by 3D FDM printing’, *Mater Today Commun*, vol. 33, Dec. 2022, doi: 10.1016/j.mtcomm.2022.104774.

[14] ‘An investigation on PVDF piezoelectric elements and linear array transducers.’, 2017. [Online]. Available: www.akustik.lth.se

[15] B. Filipovic, F. Milkovic, M. Subasic, S. Loncaric, T. Petkovic, and M. Budimir, ‘Automated ultrasonic testing of materials based on C-scan flaw classification’, in *International Symposium on Image and Signal Processing and Analysis, ISPA*, IEEE Computer Society, Sep. 2021, pp. 230–234. doi: 10.1109/ISPA52656.2021.9552056.

[16] H. Yu, ‘Scanning acoustic microscopy for material evaluation’, *Applied Microscopy*, vol. 50, no. 1. Springer, Dec. 01, 2020. doi: 10.1186/s42649-020-00045-4.

[17] F. Bertocci, A. Grandoni, and T. Djuric-Rissner, ‘Scanning acoustic microscopy (SAM): A robust method for defect detection during the manufacturing process of ultrasound probes for medical imaging’, *Sensors (Switzerland)*, vol. 19, no. 22, Nov.

2019, doi: 10.3390/s19224868.

[18] R. J. M. Wolfs, F. P. Bos, and T. A. M. Salet, ‘Correlation between destructive compression tests and non-destructive ultrasonic measurements on early age 3D printed concrete’, *Constr Build Mater*, vol. 181, pp. 447–454, Aug. 2018, doi: 10.1016/j.conbuildmat.2018.06.060.

[19] P. Lawley and T. Letcher, ‘Applications of Ultrasonic Non-Destructive Testing in 3D Printing’, 2015. [Online]. Available: http://openprairie.sdstate.edu/jurAvailableat:http://openprairie.sdstate.edu/jur/vol13/iss1/4

[20] F. C. Cruz, E. F. Simas Filho, M. C. S. Albuquerque, I. C. Silva, C. T. T. Farias, and L. L. Gouvêa, ‘Efficient feature selection for neural network based detection of flaws in steel welded joints using ultrasound testing’, *Ultrasonics*, vol. 73, pp. 1–8, Jan. 2017, doi: 10.1016/j.ultras.2016.08.017.

[21] ‘Nondestructive Evaluation Techniques : Ultrasound’. Accessed: Nov. 18, 2023. [Online]. Available: https://www.nde-ed.org/NDETechniques/Ultrasonics/index.xhtml

[22] S. K. Dwivedi, M. Vishwakarma, and A. Soni, ‘Advances and Researches on Non Destructive Testing: A Review’, 2018. Accessed: Nov. 20, 2023. [Online]. Available: www.sciencedirect.comwww.materialstoday.com/proceedings

[23] ‘Nondestructive Evaluation Techniques : Ultrasound’. Accessed: Jun. 30, 2023. [Online]. Available: https://www.nde-ed.org/NDETechniques/Ultrasonics/EquipmentTrans/transducermodeling.xhtml

[24] ‘Nondestructive Evaluation Techniques : Ultrasound’. Accessed: Jun. 30, 2023. [Online]. Available: https://www.nde-ed.org/NDETechniques/Ultrasonics/EquipmentTrans/piezotransducers.xhtml

[25] P. Singh, ‘Investigation of slurry erosion in pipeline materials.’ [Online]. Available: https://www.researchgate.net/publication/343206733

[26] J. Zhang, J. Kang, J. Fan, and J. Gao, ‘Study on erosion wear of fracturing pipeline under the action of multiphase flow in oil & gas industry’, *J Nat Gas Sci Eng*, vol. 32, pp. 334–346, May 2016, doi: 10.1016/j.jngse.2016.04.056.

[27] L. Bartolomé and J. Teuwen, ‘Prospective challenges in the experimentation of the rain erosion on the leading edge of wind turbine blades’, *Wind Energy*, vol. 22, no. 1. John Wiley and Sons Ltd, pp. 140–151, Jan. 01, 2019. doi: 10.1002/we.2272.

[28] A. Bernatek-Jakiel and J. Poesen, ‘Subsurface erosion by soil piping: significance and research needs’, *Earth-Science Reviews*, vol. 185. Elsevier B.V., pp. 1107–1128, Oct. 01, 2018. doi: 10.1016/j.earscirev.2018.08.006.

[29] P. B. Nagy, F. Simonetti, and G. Instanes, ‘Corrosion and erosion monitoring in plates and pipes using constant group velocity Lamb wave inspection’, in *Ultrasonics*, Elsevier B.V., 2014, pp. 1832–1841. doi: 10.1016/j.ultras.2014.01.017.

[30] M. Xie and Z. Tian, ‘A review on pipeline integrity management utilizing in-line inspection data’, *Engineering Failure Analysis*, vol. 92. Elsevier Ltd, pp. 222–239, Oct. 01, 2018. doi: 10.1016/j.engfailanal.2018.05.010.

[31] M. Mehrpouya, A. Dehghanghadikolaei, B. Fotovvati, A. Vosooghnia, S. S. Emamian, and A. Gisario, ‘The potential of additive manufacturing in the smart factory industrial 4.0: A review’, *Applied Sciences (Switzerland)*, vol. 9, no. 18. MDPI AG, Sep. 01, 2019. doi: 10.3390/app9183865.

[32] N. Vidakis, M. Petousis, E. Velidakis, M. Liebscher, V. Mechtcherine, and L. Tzounis, ‘On the strain rate sensitivity of fused filament fabrication (Fff) processed pla, abs, petg, pa6, and pp thermoplastic polymers’, *Polymers (Basel)*, vol. 12, no. 12, pp. 1–15, Dec. 2020, doi: 10.3390/polym12122924.

[33] M. Jiménez, L. Romero, I. A. Domínguez, M. D. M. Espinosa, and M. Domínguez, ‘Additive Manufacturing Technologies: An Overview about 3D Printing Methods and Future Prospects’, *Complexity*, vol. 2019, 2019, doi: 10.1155/2019/9656938.

[34] Al-Makky, M., & Mahmoud, D. (2016). "The importance of additive manufacturing

processes in industrial applications." In: Proceedings of the 17th International AMME Conference, 19-21 April 2016, Military Technical College, Kobry El-Kobbah, Cairo, Egypt. 17th International Conference on Applied Mechanics and Mechanical Engineering (AMME)'.

[35] Gibson, I. "Ask Not What Additive Manufacturing Can Do for You...". Engineering Design and Innovation Centre, National University of Singapore, Singapore 117576, and Centre for Rapid & Sustainable Product Development, IP Leiria, Portugal.'.

[36] M. Mehrpouya, A. Dehghanghadikolaei, B. Fotovvati, A. Vosooghnia, S. S. Emamian, and A. Gisario, 'The potential of additive manufacturing in the smart factory industrial 4.0: A review', *Applied Sciences (Switzerland)*, vol. 9, no. 18. MDPI AG, Sep. 01, 2019. doi: 10.3390/app9183865.

[37] R. Prabhu, S. R. Miller, T. W. Simpson, and N. A. Meisel, 'The earlier the better? Investigating the importance of timing on the effectiveness of design for additive manufacturing education', 2018. [Online]. Available: https://proceedings.asmedigitalcollection.asme.org

[38] M. Delic and D. R. Eyers, 'The effect of additive manufacturing adoption on supply chain flexibility and performance: An empirical analysis from the automotive industry', *Int J Prod Econ*, vol. 228, Oct. 2020, doi: 10.1016/j.ijpe.2020.107689.

[39] J. Scott, N. Gupta, C. Weber, and T. Caffrey, 'Additive Manufacturing: Status and Opportunities', 2012.

[40] M. Al-Makky and D. Mahmoud, 'The importance of additive manufacturing processes in industrial applications.

[41] A. Uriondo, M. Esperon-Miguez, and S. Perinpanayagam, 'The present and future of additive manufacturing in the aerospace sector: A review of important aspects', *Proceedings of the Institution of Mechanical Engineers, Part G: Journal of Aerospace Engineering*, vol. 229, no. 11. SAGE Publications Ltd, pp. 2132–2147, Sep. 18, 2015. doi: 10.1177/0954410014568797.

[42] A. Dey, I. N. R. Eagle, and N. Yodo, ‘A review on filament materials for fused filament fabrication’, *Journal of Manufacturing and Materials Processing*, vol. 5, no. 3. MDPI AG, Sep. 01, 2021. doi: 10.3390/jmmp5030069.

[43] D. Fico, D. Rizzo, R. Casciaro, and C. E. Corcione, ‘A Review of Polymer-Based Materials for Fused Filament Fabrication (FFF): Focus on Sustainability and Recycled Materials’, *Polymers*, vol. 14, no. 3. MDPI, Feb. 01, 2022. doi: 10.3390/polym14030465.

[44] J. Steuben, D. L. Van Bossuyt, and C. Turner, ‘Design for Fused Filament Fabrication Additive Manufacturing.’, 2015. [Online]. Available: http://proceedings.asmedigitalcollection.asme.org/pdfaccess.ashx?url=/data/conferences/asmep/86609/

[45] X. Gao, S. Qi, X. Kuang, Y. Su, J. Li, and D. Wang, ‘Fused filament fabrication of polymer materials: A review of interlayer bond’, *Additive Manufacturing*, vol. 37. Elsevier B.V., Jan. 01, 2021. doi: 10.1016/j.addma.2020.101658.

[46] B. Brenken, E. Barocio, A. Favaloro, V. Kunc, and R. B. Pipes, ‘Fused filament fabrication of fiber-reinforced polymers: A review’, *Additive Manufacturing*, vol. 21. Elsevier B.V., pp. 1–16, May 01, 2018. doi: 10.1016/j.addma.2018.01.002.

[47] S. Singh, G. Singh, C. Prakash, and S. Ramakrishna, ‘Current status and future directions of fused filament fabrication’, *Journal of Manufacturing Processes*, vol. 55. Elsevier Ltd, pp. 288–306, Jul. 01, 2020. doi: 10.1016/j.jmapro.2020.04.049.

[48] S. Charlon, J. Le Boterff, and J. Soulestin, ‘Fused filament fabrication of polypropylene: Influence of the bead temperature on adhesion and porosity’, *Addit Manuf*, vol. 38, Feb. 2021, doi: 10.1016/j.addma.2021.101838.

[49] H. C. Wu and T. C. T. Chen, ‘Quality control issues in 3D-printing manufacturing: a review’, *Rapid Prototyp J*, vol. 24, no. 3, pp. 607–614, 2018, doi: 10.1108/RPJ-02-2017-0031.

[50] H. Kim, Y. Lin, and T. L. B. Tseng, ‘A review on quality control in additive

manufacturing', *Rapid Prototyping Journal*, vol. 24, no. 3. Emerald Group Publishing Ltd., pp. 645–669, 2018. doi: 10.1108/RPJ-03-2017-0048.

[51] T. Pereira, J. V. Kennedy, and J. Potgieter, 'A comparison of traditional manufacturing vs additive manufacturing, the best method for the job', in *Procedia Manufacturing*, Elsevier B.V., 2019, pp. 11–18. doi: 10.1016/j.promfg.2019.02.003.

[52] C. Dudescu and L. Racz, 'Effects of Raster Orientation, Infill Rate and Infill Pattern on the Mechanical Properties of 3D Printed Materials', *ACTA Universitatis Cibiniensis*, vol. 69, no. 1, pp. 23–30, Dec. 2017, doi: 10.1515/aucts-2017-0004.

[53] S. Hisham, S. Fenner Khan, and K. Kamarudin, 'Quality monitoring for Fused Filament Fabrication product: A review.', *International Journal of Research and Analytical Reviews*, 2022, [Online]. Available: www.ijrar.org

[54] J. Pernica, M. Sustr, P. Dostal, M. Brabec, and D. Dobrocky, 'Tensile Testing of 3D Printed Materials made by Different Temperature', *Manufacturing Technology*, vol. 21, no. 3, pp. 398–404, 2021, doi: 10.21062/mft.2021.039.

[55] N. Sathishkumar, A. S. M. Udayakumar, B. Vincent, and V. Ashok Kumar, 'Study and Analysis of 3D Printed FDM Components by Non-Destructive Testing Techniques', *International Journal of Research and Review (ijrrjournal.com)*, vol. 7, no. 5, p. 5, 2020.

[56] J. Butt, R. Bhaskar, and V. Mohaghegh, 'Non-Destructive and Destructive Testing to Analyse the Effects of Processing Parameters on the Tensile and Flexural Properties of FFF-Printed Graphene-Enhanced PLA', *Journal of Composites Science*, vol. 6, no. 5, May 2022, doi: 10.3390/jcs6050148.

[57] A. Wronkowicz, K. Dragan, and K. Lis, 'Assessment of uncertainty in damage evaluation by ultrasonic testing of composite structures', *Compos Struct*, vol. 203, pp. 71–84, Nov. 2018, doi: 10.1016/j.compstruct.2018.06.109.

[58] K. Peng, Y. Zhang, X. Xu, J. Han, and Y. Luo, 'Crack Detection of Threaded Steel Rods Based on Ultrasonic Guided Waves', *Sensors*, vol. 22, no. 18, Sep. 2022, doi:

10.3390/s22186885.

[59] Y. Liu, ‘Experimental Investigations on Transient Surface Water Transport and Ice Accreting Processes Pertinent to Aircraft Icing Phenomena Recommended Citation’.

[60] R. S. Dwyer-Joyce, B. W. Drinkwater, and C. J. Donohoe, ‘The measurement of lubricant-film thickness using ultrasound’, *Proceedings of the Royal Society A: Mathematical, Physical and Engineering Sciences*, vol. 459, no. 2032, pp. 957–976, Apr. 2003, doi: 10.1098/rspa.2002.1018.

[61] V. N. Kozlov, A. A. Samokrutov, and V. G. Shevaldykin, ‘Thickness measurements and flaw detection in concrete using ultrasonic echo method’, *Nondestructive Testing and Evaluation*, vol. 13, no. 2, pp. 73–84, 1997, doi: 10.1080/02780899708953020.

[62] Y. I. Oka and H. Hayashi, ‘Evaluation of erosion resistance for metal-ceramic composites and cermets using a water-jet testing apparatus’, *Wear*, vol. 271, no. 9–10, pp. 1397–1403, Jul. 2011, doi: 10.1016/j.wear.2010.11.040.

[63] Y. Jin, E. Walker, H. Heo, A. Krokhin, T. Y. Choi, and A. Neogi, ‘Nondestructive ultrasonic evaluation of fused deposition modeling based additively manufactured 3D-printed structures’, *Smart Mater Struct*, vol. 29, no. 4, 2020, doi: 10.1088/1361-665X/ab74b9.

[64] N.-M. Barkoula and J. Karger-Kocsis, ‘Review Processes and influencing parameters of the solid particle erosion of polymers and their composites’.

[65] L. Bartolomé and J. Teuwen, ‘Prospective challenges in the experimentation of the rain erosion on the leading edge of wind turbine blades’, *Wind Energy*, vol. 22, no. 1. John Wiley and Sons Ltd, pp. 140–151, Jan. 01, 2019. doi: 10.1002/we.2272.

[66] E. A. Valaker, S. Armada, and S. Wilson, ‘Droplet erosion protection coatings for offshore wind turbine blades’, in *Energy Procedia*, Elsevier Ltd, 2015, pp. 263–275. doi: 10.1016/j.egypro.2015.11.430.

[67] Y. Shida and Y. S. Sumitomo, ‘Water jet erosion behaviour of Ti-Ni binary alloys’,

1991. Accessed: Nov. 20, 2023. [Online]. Available: https://www.sciencedirect.com/science/article/pii/0043164891900642

[68] S. Hloch *et al.*, 'Effect of pressure of pulsating water jet moving along stair trajectory on erosion depth, surface morphology and microhardness', *Wear*, vol. 452–453, Jul. 2020, doi: 10.1016/j.wear.2020.203278.

[69] A. Dashtkar *et al.*, 'Rain erosion-resistant coatings for wind turbine blades: A review', *Polymers and Polymer Composites*, vol. 27, no. 8. SAGE Publications Ltd, pp. 443–475, Oct. 01, 2019. doi: 10.1177/0967391119848232.

[70] M. A. O. Alum, C. Nworah, and A. Omolegbe, 'SPE-172360-MS A Review of Erosion-Corrosion Monitoring and Inspection Techniques for Amenam High Pressure (HP) Header', 2014.

[71] 'Markforged Metal 3D Printer: The Metal X 3D Printing System-Siemens Additive Manufacturing'. Accessed: Nov. 19, 2023. [Online]. Available: Markforged Metal 3D Printer: The Metal X 3D Printing System

[72] H. Lipson, F. C. Moon, J. Hai, and C. Paventi, '3D-Printing the History of Mechanisms'. [Online]. Available: www.explore.cornell.edu

[73] J. M. Chacón, M. Á. Caminero, P. J. Núñez, E. García-Plaza, and J. P. Bécar, 'Effect of nozzle diameter on mechanical and geometric performance of 3D printed carbon fibre-reinforced composites manufactured by fused filament fabrication', *Rapid Prototyp J*, vol. 27, no. 4, pp. 769–784, 2021, doi: 10.1108/RPJ-10-2020-0250/FULL/XML.

[74] S. Singh, G. Singh, C. Prakash, and S. Ramakrishna, 'Current status and future directions of fused filament fabrication', *Journal of Manufacturing Processes*, vol. 55. Elsevier Ltd, pp. 288–306, Jul. 01, 2020. doi: 10.1016/j.jmapro.2020.04.049.

[75] M. L. Dezaki, M. K. A. M. Ariffin, A. Serjouei, A. Zolfagharian, S. Hatami, and M. Bodaghi, 'Influence of infill patterns generated by cad and fdm 3d printer on surface roughness and tensile strength properties', *Applied Sciences (Switzerland)*, vol. 11,

no. 16, Aug. 2021, doi: 10.3390/app11167272.

[76] M. Qamar Tanveer, G. Mishra, S. Mishra, and R. Sharma, 'Effect of infill pattern and infill density on mechanical behaviour of FDM 3D printed Parts- a current review', *Mater Today Proc*, vol. 62, pp. 100–108, Jan. 2022, doi: 10.1016/j.matpr.2022.02.310.

[77] M. Eryildiz, 'The effects of infill patterns on the mechanical properties of 3D printed PLA parts fabricated by FDM', *Ukrainian Journal of Mechanical Engineering and Materials Science*, vol. 7, no. 1–2, pp. 1–8, 2021, doi: 10.23939/ujmems2021.01-02.001.

[78] S. Ganeshkumar *et al.*, 'Investigation of Tensile Properties of Different Infill Pattern Structures of 3D-Printed PLA Polymers: Analysis and Validation Using Finite Element Analysis in ANSYS', *Materials*, vol. 15, no. 15, Aug. 2022, doi: 10.3390/ma15155142.

[79] 'Buildabong 3D Printed Water Tobacco Pipe - Cheap Water Tobacco Pipes Dot Com'. Accessed: Jul. 02, 2023. [Online]. Available: https://cheapwatertobaccopipes.com/product/buildabong-3d-printed-water-tobacco-pipe/

[80] H. Choi, J. Y. Yeom, and J. M. Ryu, 'Development of a multiwavelength visible-range-supported opto–ultrasound instrument using a light-emitting diode and ultrasound transducer', *Sensors (Switzerland)*, vol. 18, no. 10, Oct. 2018, doi: 10.3390/s18103324.

[81] C. T. M. Eneh, I. O. Afara, M. K. H. Malo, J. S. Jurvelin, and J. Töyräs, 'Porosity predicted from ultrasound backscatter using multivariate analysis can improve accuracy of cortical bone thickness assessment', *J Acoust Soc Am*, vol. 141, no. 1, pp. 575–585, Jan. 2017, doi: 10.1121/1.4973572.

[82] S. Y. Guan, L. Li, and X. K. Wang, 'Near-Surface Defects Identification in water immersion ultrasonic testing based on FFT and Phase Spectrum Difference', in

Proceedings of 2020 IEEE Far East NDT New Technology and Application Forum, FENDT 2020, Institute of Electrical and Electronics Engineers Inc., Nov. 2020, pp. 115–119. doi: 10.1109/FENDT50467.2020.9337546.

[83] M. Berson *et al.*, 'High frequency (20 MHz) ultrasonic devices: advantages and applications', 1999. [Online]. Available: www.elsevier.com/locate/ejultrasou

[84] C. C. Guyott, P. Cawley, and R. D. Adams, 'The Non-destructive Testing of Adhesively Bonded Structure: A Review', *J Adhes*, vol. 20, no. 2, pp. 129–159, 1986, doi: 10.1080/00218468608074943.

[85] R. Stramare *et al.*, 'Evaluation of finger joint synovial vascularity in patients with rheumatoid arthritis using contrast-enhanced ultrasound with water immersion and a stabilized probe', *Journal of Clinical Ultrasound*, vol. 40, no. 3, pp. 147–154, Mar. 2012, doi: 10.1002/jcu.21887.

[86] B. Klucinec, M. Scheidler, C. Denegar, E. Domholdt, and S. Burgess, 'Transmissivity of Coupling Agents Used to Deliver Ultrasound Through Indirect Methods', 2000. [Online]. Available: www.jospt.org

[87] C. L. Huang, Y. Bin Chen, Y. L. Lo, and Y. H. Lin, 'Development of chitosan/β-glycerophosphate/glycerol hydrogel as a thermosensitive coupling agent', *Carbohydr Polym*, vol. 147, pp. 409–414, Aug. 2016, doi: 10.1016/j.carbpol.2016.04.028.

[88] A. Mostavi, N. Kamali, N. Tehrani, S. W. Chi, D. Ozevin, and J. E. Indacochea, 'Wavelet based harmonics decomposition of ultrasonic signal in assessment of plastic strain in aluminum', *Measurement (Lond)*, vol. 106, pp. 66–78, Aug. 2017, doi: 10.1016/j.measurement.2017.04.013.

[89] M. Sheykholeslami, Y. Hojjat, M. Ghodsi, K. Kakavand, and S. Cinquemani, 'Investigation of δ e effect on vibrational behavior of giant magnetostrictive transducers', *Shock and Vibration*, vol. 2015, 2015, doi: 10.1155/2015/478045.

[90] F. Lavecchia, M. G. Guerra, and L. M. Galantucci, 'Chemical vapor treatment to improve surface finish of 3D printed polylactic acid (PLA) parts realized by fused

filament fabrication', *Progress in Additive Manufacturing*, vol. 7, no. 1, pp. 65–75, Feb. 2022, doi: 10.1007/s40964-021-00213-2.

[91] P. Yadav, A. Sahai, and R. S. Sharma, 'Strength and Surface Characteristics of FDM-Based 3D Printed PLA Parts for Multiple Infill Design Patterns', *Journal of The Institution of Engineers (India): Series C*, vol. 102, no. 1, pp. 197–207, Feb. 2021, doi: 10.1007/s40032-020-00625-z.

[92] M. Moradi, A. Aminzadeh, D. Rahmatabadi, and A. Hakimi, 'Experimental investigation on mechanical characterization of 3D printed PLA produced by fused deposition modeling (FDM)', *Mater Res Express*, vol. 8, no. 3, Mar. 2021, doi: 10.1088/2053-1591/abe8f3.

[93] A. Al Rashid and M. Koç, 'Numerical simulations on thermomechanical performance of 3D printed chopped carbon fiber-reinforced polyamide-6 composites: Effect of infill design', *J Appl Polym Sci*, vol. 139, no. 44, Nov. 2022, doi: 10.1002/app.53081.

[94] F. N. Mullaveettil, R. Dauksevicius, and Y. Wakjira, 'Strength and elastic properties of 3D printed PVDF-based parts for lightweight biomedical applications', *J Mech Behav Biomed Mater*, vol. 120, Aug. 2021, doi: 10.1016/j.jmbbm.2021.104603.

[95] P. K. Mishra and T. Jagadesh, 'Applications and Challenges of 3D Printed Polymer Composites in the Emerging Domain of Automotive and Aerospace: A Converged Review', *Journal of The Institution of Engineers (India): Series D*. Springer, 2022. doi: 10.1007/s40033-022-00426-x.

[96] B. Ergene, İ. ŞEKEROĞLU, Ç. Bolat, and B. Yalçın, 'An experimental investigation on mechanical performances of 3D printed lightweight ABS pipes with different cellular wall thickness', *Journal of Mechanical Engineering and Sciences*, vol. 15, no. 2, pp. 8169–8177, Jun. 2021, doi: 10.15282/jmes.15.2.2021.16.0641.

[97] L. Szabó and D. Fodor, 'The Key Role of 3D Printing Technologies in the Further Development of Electrical Machines', *Machines*, vol. 10, no. 5. MDPI, May 01, 2022. doi: 10.3390/machines10050330.

[98] A. Ahmad, A. Abbas, G. Hussain, O. Al-Abbasi, M. Alkahtani, and K. Altaf, ‘Performance evaluation of 3D printed polymer heat exchangers: influence of printing temperature, printing speed and wall thickness with consideration of surface roughness’, *International Journal of Advanced Manufacturing Technology*, vol. 128, no. 7–8, pp. 3627–3647, Oct. 2023, doi: 10.1007/s00170-023-12079-5.

[99] J. R. C. Dizon, A. D. Valino, L. R. Souza, A. H. Espera, Q. Chen, and R. C. Advincula, ‘3D printed injection molds using various 3D printing technologies’, in *Materials Science Forum*, Trans Tech Publications Ltd, 2020, pp. 150–156. doi: 10.4028/www.scientific.net/MSF.1005.150.